Title

Exoplanet Biosignatures: Understanding Oxygen as a Biosignature in the Context of Its Environment.

Journal

Astrobiology, 18(6)

ISSN

1531-1074

Authors

Meadows, Victoria S
Reinhard, Christopher T
Arney, Giada N
et al.

Publication Date

2018-06-01

DOI

10.1089/ast.2017.1727

Peer reviewed

ASTROBIOLOGY
Volume 18, Number 6, 2018
Mary Ann Liebert, Inc.
DOI: 10.1089/ast.2017.1727

Exoplanet Biosignatures: Understanding Oxygen as a Biosignature in the Context of Its Environment

Victoria S. Meadows,[1,2] Christopher T. Reinhard,[3,4] Giada N. Arney,[2,5] Mary N. Parenteau,[2,6] Edward W. Schwieterman,[2,4,7–9] Shawn D. Domagal-Goldman,[2,10] Andrew P. Lincowski,[1,2] Karl R. Stapelfeldt,[11] Heike Rauer,[12] Shiladitya DasSarma,[13,14] Siddharth Hegde,[15,16] Norio Narita,[17–19] Russell Deitrick,[1,2] Jacob Lustig-Yaeger,[1,2] Timothy W. Lyons,[4,7] Nicholas Siegler,[11] and J. Lee Grenfell[12]

Abstract

We describe how environmental context can help determine whether oxygen (O_2) detected in extrasolar planetary observations is more likely to have a biological source. Here we provide an in-depth, interdisciplinary example of O_2 biosignature identification and observation, which serves as the prototype for the development of a general framework for biosignature assessment. Photosynthetically generated O_2 is a potentially strong biosignature, and at high abundance, it was originally thought to be an unambiguous indicator for life. However, as a biosignature, O_2 faces two major challenges: (1) it was only present at high abundance for a relatively short period of Earth's history and (2) we now know of several potential planetary mechanisms that can generate abundant O_2 without life being present. Consequently, our ability to interpret both the presence and absence of O_2 in an exoplanetary spectrum relies on understanding the environmental context. Here we examine the coevolution of life with the early Earth's environment to identify how the interplay of sources and sinks may have suppressed O_2 release into the atmosphere for several billion years, producing a false negative for biologically generated O_2. These studies suggest that planetary characteristics that may enhance false negatives should be considered when selecting targets for biosignature searches. We review the most recent knowledge of false positives for O_2, planetary processes that may generate abundant atmospheric O_2 without a biosphere. We provide examples of how future photometric, spectroscopic, and time-dependent observations of O_2 and other aspects of the planetary environment can be used to rule out false positives and thereby increase our confidence that any observed O_2 is indeed a biosignature. These insights will guide and inform the development of future exoplanet characterization missions. Key Words: Biosignatures—Oxygenic photosynthesis—Exoplanets—Planetary atmospheres. Astrobiology 18, 630–662.

[1]Department of Astronomy, University of Washington, Seattle, Washington.
[2]NASA Astrobiology Institute, Virtual Planetary Laboratory Team, Seattle, Washington.
[3]School of Earth and Atmospheric Sciences, Georgia Institute of Technology, Atlanta, Georgia.
[4]NASA Astrobiology Institute, Alternative Earths Team, Riverside, California.
[5]Planetary Systems Laboratory, NASA Goddard Space Flight Center, Greenbelt, Maryland.
[6]NASA Ames Research Center, Exobiology Branch, Mountain View, California.
[7]Department of Earth Sciences, University of California, Riverside, California.
[8]NASA Postdoctoral Program, Universities Space Research Association, Columbia, Maryland.
[9]Blue Marble Space Institute of Science, Seattle, Washington.
[10]Planetary Environments Laboratory, NASA Goddard Space Flight Center, Greenbelt, Maryland.
[11]NASA Exoplanet Exploration Program, Jet Propulsion Laboratory/California Institute of Technology, Pasadena, California.
[12]German Aerospace Center, Institute of Planetary Research, Extrasolar Planets and Atmospheres, Berlin, Germany.
[13]Department of Microbiology and Immunology, School of Medicine, University of Maryland, Baltimore, Maryland.
[14]Institute of Marine and Environmental Technology, University System of Baltimore, Maryland.
[15]Carl Sagan Institute, Cornell University, Ithaca, New York.
[16]Cornell Center for Astrophysics and Planetary Science, Cornell University, Ithaca, New York.
[17]Department of Astronomy, The University of Tokyo, Tokyo, Japan.
[18]Astrobiology Center, NINS, Tokyo, Japan.
[19]National Astronomical Observatory of Japan, NINS, Tokyo, Japan.

1. Introduction

The search for life across interstellar distances is a scientific challenge that pushes the boundaries of observational astronomy and requires careful consideration of the signs of life that we will best be able to detect. These signs are known as ''biosignatures''—life's global impacts on the atmosphere and/or surface of a planetary environment.

The most useful biosignatures meet three criteria: reliability, survivability, and detectability, which together enhance the probability that the biosignature can be detected and interpreted as being due to life (*e.g.*, Domagal-Goldman *et al.*, 2011; Seager *et al.*, 2012; Meadows, 2017). The reliability criterion seeks to answer whether an observed feature of the planetary environment has a biological origin, and whether it is more likely to be produced by life than by planetary processes such as geology and photochemistry. The survivability criterion determines whether the candidate biosignature gas can avoid the normal sinks in a planetary environment and build up to detectable levels. These sinks include, but are not limited to, destruction by photolysis and photochemistry, reactions with volcanic gases and the surface, and (for soluble gases) dissolution in the ocean. Finally, the detectability criterion asks whether the gas is spectrally active and clear of overlap with other chemical species in the wavelength region to be observed, and whether it is accessible in high enough abundance and at appropriate regions in the planetary atmosphere to be observed by techniques such as transmission, secondary eclipse, phase curves, and direct imaging.

With these three criteria, Earth's abundant molecular oxygen (O_2) has been identified as the strongest biosignature for terrestrial planets and was also initially thought to be straightforward to interpret as having a biological origin. O_2 fulfills the three requirements of a biosignature in the following ways:

1.1. Reliability

It is the volatile byproduct of oxygenic photosynthesis—the metabolism driven by sunlight, which is the dominant source of energy on our planet's surface—and so clearly has a biological origin. Until recently, O_2 was considered to have little or no abiotic planetary sources, as the Sun's UV spectrum drives photochemistry that produces only trace amounts in Earth's atmosphere (*e.g.*, Walker, 1977; Hu *et al.*, 2012; Domagal-Goldman *et al.*, 2014; Harman *et al.*, 2015). O_2 also has no significant geological sources—unlike methane (CH_4) and carbon dioxide (CO_2), which are known to be produced by geological processes (Etiope and Sherwood-Lollar, 2013). Very early work considered O_2 to be an even stronger biosignature when seen along with gases such as CH_4 and nitrous oxide (N_2O) in chemical thermodynamic disequilibrium (*e.g.*, Lederberg, 1965; Lovelock, 1965; Hitchcock and Lovelock, 1967; Lovelock and Kaplan, 1975), although given Earth's negligible abiotic O_2 sources, its high abundance alone indicates a biological origin.

1.2. Survivability

With a strong, planet-wide photosynthetic source, and relatively weak sinks compared with early periods of Earth's history (and different stellar hosts), O_2 has risen over time to become the second most abundant gas in our atmosphere (at around 21% by volume). The atmosphere's more dominant gas, N_2—which may also be biologically mediated (Catling and Kasting, 2007; Johnson and Goldblatt, 2015)—is considered a much poorer biosignature because N_2 only exhibits strong absorption in the extreme ultraviolet (XUV; $0.01 < \lambda < 0.121\,\mu m$). In this wavelength region, several other common molecules also absorb H_2O, CO_2, CO, O_2, CH_4 and other hydrocarbons (Rothman *et al.*, 2013), and stars are much less luminous in the UV than in the visible regions, reducing the UV reflection or transmission signal from the planetary atmosphere. Sinks for O_2 include outgassing of reduced gases such as CH_4 and H_2, crustal oxidation, and photolytic destruction in the stratosphere.

1.3. Detectability

These factors lead to a high abundance and even mixing throughout the atmospheric column, making O_2 accessible to observation by transit spectroscopy. Depending on the observing geometry and atmospheric composition of a terrestrial (predominantly composed of silicate rocks and metals) planet, transmission spectroscopy may not reach the near-surface environment, instead probing the stratosphere and upper troposphere (Bétrémieux and Kaltenegger, 2013, 2014; Misra *et al.*, 2014b; Meadows *et al.*, 2018). This gives O_2 a significant advantage over other proposed, often more complex biosignature molecules, including methanethiol and dimethyl disulfide (Pilcher, 2003; Domagal-Goldman *et al.*, 2011; Seager and Bains, 2015), which are more susceptible to photolysis by UV radiation and so are confined largely to the lower troposphere, with significantly smaller concentrations in the stratosphere (Domagal-Goldman *et al.*, 2011).

O_2 is also one of the very few biogenic gases that absorbs strongly in the visible and near-infrared (NIR), likely wavelength regions to be covered by upcoming NASA missions and ground-based telescopes seeking to characterize extrasolar planets. O_2 has strong features at wavelengths $<0.2\,\mu m$, and a γ band at $0.628\,\mu m$, B-band at $0.688\,\mu m$, a strong A-band at $0.762\,\mu m$, and the $a\ ^1\Delta_g$ band at $1.269\,\mu m$ (Rothman *et al.*, 2013). O_2 could also be inferred from detection of its photochemical byproduct, ozone (O_3) (Ratner and Walker, 1972), which has strong bands in the UV (0.2–0.3 μm), visible (0.5–0.7 μm) and midinfrared (MIR) (9.6 μm) (Rothman *et al.*, 2013). O_2 at high abundance could be identified by collisionally induced absorption as O_2 molecules collide with each other or form the O_4 complex, which has strong bands in the visible (0.34–0.7 μm; Hermans *et al.*, 1999; Thalman and Volkamer, 2013) and in the NIR (at 1.06 μm, Greenblatt *et al.*, 1990; and at 1.27 μm, Maté *et al.*, 2000).

However, although O_2 is clearly a strong biosignature, recent research has indicated that its availability in a planetary atmosphere and its unique interpretation as a biological product may not be as straightforward as originally thought. These insights have come from exploration of the processes governing the long-term evolution of atmospheric O_2 on the early Earth, and advances in theoretical modeling of star–planet interactions for planets orbiting other stars. This research indicates that the picture is far more complex, with both significant false negatives—planetary processes that suppress the buildup of atmospheric O_2, despite the presence of biological production (Lyons *et al.*, 2014;

Planavsky *et al.*, 2014b; Reinhard *et al.*, 2017), and false positives—planetary processes that generate large (modern Earth-like) abundances of O_2 abiotically (*e.g.*, Wordsworth and Pierrehumbert, 2014; Luger and Barnes, 2015; Gao *et al.*, 2015; Harman *et al.*, 2015; Tian, 2015; see Meadows, 2017 for a review), being possible.

On the early Earth, it is likely that oxygenic photosynthesis was developed well in advance of the rise of O_2 to significant levels in our atmosphere, constituting a false negative. Isotope measurements point to transient low levels of O_2 in the early Earth's environment 3.0–2.65 Ga, which were likely generated by oxygenic photosynthesis (Czaja *et al.*, 2012; Crowe *et al.*, 2013; Planavsky *et al.*, 2014a; Riding *et al.*, 2014). Yet the irreversible, global accumulation of O_2 in the atmosphere, which was likely mediated by burial and removal of organic carbon from Earth's surface environment (Kasting, 2001; Lyons *et al.*, 2014), evidently occurred somewhat later, between 2.45 and 2.2 billion years ago (Ga; Farquhar, 2000; Bekker *et al.*, 2004; Canfield, 2005). Recent sulfur isotope data (Luo *et al.*, 2016) place this transition at 2.33 Ga. However, recent studies of Earth's carbon isotope record suggest that the record does not constrain the history of organic burial well enough to evaluate whether changes in fractional organic burial since 3.6 Ga can explain the rise of O_2 (Krissansen-Totton *et al.*, 2015). Other proposed mechanisms for oxygen's rise include hydrogen escape from the upper atmosphere (Catling *et al.*, 2001) and the long-term evolution of volcanic–tectonic processes at Earth's surface (Kump and Barley, 2007; Kasting, 2013; Lee *et al.*, 2016). Additional data suggest that the permanent rise of O_2 to high levels in Earth's atmosphere (>1% of the present atmospheric level (PAL)) may have been delayed even further, to 0.8 Ga (Planavsky *et al.*, 2014b), long after the advent of oxygenic photosynthesis.

This delay between the evolution of the biological source of O_2, photosynthesis, and the subsequent rise of abundant O_2 in our atmosphere is due to diverse geological sinks for O_2 in the environment effectively countering its biological production—ultimately resulting in a false negative. This example points to the importance of understanding a planetary environment to identify characteristics that may potentially reduce our ability to see a biosignature, even if a strong biological source exists.

Environmental context will also be extremely important for identifying the likelihood for false positives in a planetary environment—abiotic processes that could mimic a biosignature. O_2 was long considered the most robust biosignature possible, because in Earth's modern environment, there were no known false positives, such as geological processes and photochemistry, that could generate it. For example, on Earth, the abiotic production of O_2, principally by photolysis of water vapor, is at least a million times less than that produced by photosynthesis (Walker, 1977; Harman *et al.*, 2015).

However, recent modeling studies examining star–planet interactions, especially for exoplanets orbiting M dwarfs, have identified several mechanisms that could potentially lead to the abiotic production of significant amounts of O_2. These mechanisms ultimately rely on conditions that lead to the photolysis of CO_2 or H_2O, two O-bearing gases that are likely to be common on terrestrial planets in the habitable zone (HZ). One mechanism for O_2 buildup requires the vaporization of oceans, and the subsequent photolysis of water vapor and loss of H, for planets orbiting early, superluminous M dwarf stars (Luger and Barnes, 2015). A low noncondensable gas inventory in a planetary atmosphere can drive high stratospheric H_2O abundances by increasing the altitude of the tropospheric ''cold trap,'' leading to the photolysis of H_2O and the loss of H to space. Because the water loss is a strong function of the planet's atmospheric composition, this potential abiotic O_2 generation mechanism can affect planets orbiting any type of star (Wordsworth and Pierrehumbert, 2014). Finally, photolysis of CO_2 as a source of atmospheric O_2 may occur on planets orbiting M dwarfs. Whether photolytic O_2 is produced is dependent on both how well the UV spectrum of the star photolyzes CO_2 and the suppression of catalytic or other processes that would allow the CO and O to rapidly recombine (*e.g.*, Domagal-Goldman *et al.*, 2014; Tian *et al.*, 2014; Gao *et al.*, 2015; Harman *et al.*, 2015). Each of these mechanisms leaves telltale signs in the planetary environment that can point to the abiotic source of the O_2 (*e.g.*, Schwieterman *et al.*, 2015b, 2016).

Rather than demonstrating that O_2 is not suitable as a biosignature, our new and evolving understanding of false positives for O_2 *increases* its robustness (Meadows, 2017). The study of O_2 as a biosignature has taught us that by attempting to understand the environmental context, including the possibility for false positives and negatives, we will ultimately improve our interpretation of exoplanet observations and increase our confidence that they do indeed indicate the presence of life. Knowledge gained from the delayed rise of O_2 during the history of our own planet helps us identify environmental contexts for false negatives for O_2, and interdisciplinary modeling studies of exoplanets have helped us to explore and identify the stellar and planetary characteristics that are more likely to lead to O_2 false negatives. This knowledge can guide target selection for habitable planets, and can be used to design observations to search for the necessary environmental context to increase our confidence in the interpretation. Moreover, these studies serve as a template for future exoplanet biosignature development, and the lessons learned from our study of O_2 can help guide the development of a generalized framework for biosignature development and detection (see *e.g.*, Catling *et al.*, 2018).

In Section 2, we describe in more detail the evolution of O_2 throughout Earth's history, highlighting the ways in which the environment initially suppressed and then finally permitted its development as a detectable biosignature. In Section 3, we discuss the known potential false positive mechanisms for terrestrial exoplanets, and their likely observable environmental impact. In Section 4, we discuss the specific observational implementation for O_2 detection and how confidence in its biogenicity can be enhanced, including (1) characterization of planetary, stellar, and planetary system environmental context; (2) the search for O_2; and (3) the specific environmental characteristics that could be sought to help discriminate false negatives and positives. We describe the photometric and spectroscopic measurements required to execute these three steps for different near-term exoplanet observing facilities, including the James Webb Space Telescope (JWST), extremely large ground-based telescopes, and for proposed space-based direct imaging coronographic/starshade missions. In Section

5, we discuss and prioritize the most important discriminating measurements, and then discuss the robustness of any detection as a function of accessible wavelength range and other telescope characteristics. In Section 6, we present our conclusions.

2. The Coevolution of Life with Its Environment, False Negatives, and the Rise of Earth's O_2

There are tantalizing suggestions that life may have emerged very early during the 4.6 billion year evolution of our planet, but the development of photosynthesis, and the subsequent oxygenation of the atmosphere, likely occurred much later. Carbonaceous compounds enriched in ^{12}C (Mojzsis *et al.*, 1996; Rosing, 1999), potentially biogenic sedimentary structures (Nutman *et al.*, 2016), and purported microfossils (Dodd *et al.*, 2017) are present in the oldest sedimentary rocks on Earth. Furthermore, ^{12}C-enriched graphitic inclusions in recycled zircons have been suggested to date the emergence of life to before the earliest sedimentary rocks, at $\sim$4.1 Ga (Bell *et al.*, 2015). These observations are consistent with a biological origin, but in all cases are somewhat equivocal (see, for example, Lepland *et al.*, 2002; van Zuilen *et al.*, 2002; McCollom and Seewald, 2006). Nevertheless, strong isotopic evidence for the presence of important microbial metabolisms such as methanogenesis (Ueno *et al.*, 2006) and dissimilatory sulfate reduction (Shen *et al.*, 2001; Ueno *et al.*, 2009) is observable by at least $\sim$3.5 Ga, suggesting that although the precise timing of biochemical steps remains to be elucidated, key landmarks in evolution of life—the emergence of life from prebiotic chemistry, the development of cellularity, and the development of metabolism—likely occurred relatively soon after Earth's formation.

Photosynthesis, the ability to harvest the Sun's energy to support life, may have also evolved early in our planet's history, with multiple geological and geochemical lines of evidence suggesting that anoxygenic phototrophs were present on Earth by at least 3.3 Ga (Westall *et al.*, 2011) and possibly as far back as 3.5–3.7 Ga (Buick, 1981; Nutman *et al.*, 2016). These early anoxygenic phototrophs used strong reductants such as hydrogen or hydrogen sulfide to donate electrons to a single photosystem (PSI) that harvested light (Olson and Pierson, 1986). Volcanism could have produced these reductants at sufficient concentrations to drive photosynthesis, but only in relatively limited environments. Consequently early Earth's anoxygenic phototrophs would have been challenging to detect remotely, as their productivity would have been limited by the spatial restriction of their reductants, with a resultant relatively small impact on Earth's globally averaged characteristics (*e.g.*, Canfield *et al.*, 2006). These phototrophs are also not known to produce gaseous byproducts.

The evolution of oxygenic photosynthesis to use globally abundant water was arguably one of the most important biological innovations on Earth. Oxygenic photosynthesis uses energy from the Sun to convert CO_2 and liquid water to glucose, with O_2 as a byproduct:

$$6CO_2 + 6H_2O \rightarrow C_6H_{12}O_6 + 6O_2. \quad (1)$$

There are competing theories on the antiquity of oxygenic photosynthesis, and more specifically water oxidation, as some researchers believe that this metabolic capability may have arisen very soon after the origin of life (*e.g.*, Cardona, 2015, 2016, 2017). However, recent phylogenetic analyses examining the origins of oxygenic photosynthesis in cyanobacteria have found that microbes basal to the cyanobacterial lineage (*Melainabacteria* and *Sericytochromatia*) lack photosynthetic machinery. This suggests that photosynthesis arose late in cyanobacteria, and that these genes were acquired by horizontal gene transfer from more primitive anoxygenic phototrophs (Soo *et al.*, 2017).

Because H_2O, CO_2, and sunlight are globally available components of the habitable terrestrial environment, they allow oxygenic photosynthesis to dominate large fractions of the planetary surface (Kiang *et al.*, 2007a; Léger *et al.*, 2011). The subsequent oxygenation of the atmosphere and oceans significantly impacted Earth's global environment, and ultimately allowed for biological (Knoll *et al.*, 2006) and mineralogical diversification (Hazen *et al.*, 2008). Oxygenic photosynthesis maintains much of the living biomass on our planet today (Falkowski *et al.*, 2000), and its dominance in our biosphere and its global distribution have also made photosynthesis more detectable on a planetary scale. However, whether O_2 rises to detectable levels in a planetary atmosphere will depend on the balance between sources and sinks for O_2 in surface environments, and in particular whether planetary processes, such as geological burial of organic carbon (*e.g.*, Des Marais *et al.*, 1992), atmospheric escape of hydrogen (Catling *et al.*, 2001), or changes in reductant fluxes to the surface (Kasting, 2013) can support the buildup of biologically generated O_2 in the atmosphere on long timescales.

In this section, we discuss the evolution of oxygenic photosynthesis in an environmental and geochemical context, including the suppression and eventual rise of atmospheric O_2, and the interplay between biological production of O_2 and its consumption by sinks present in early Earth surface environments. Ultimately, we wish to understand the environmental selective pressures driving the evolution of water oxidation and O_2 production on the early Earth, so they can be generalized and extrapolated to rocky habitable exoplanets.

2.1. The evolution of oxygenic photosynthesis

Much research has been directed at understanding the evolutionary transition between anoxygenic and oxygenic photosynthesis, and this article is not intended to be an exhaustive review of the various schools of thought. There is a difference in the complexity of photosynthetic machinery between oxygenic and anoxygenic phototrophs. The light reactions of oxygenic photosynthesis in cyanobacteria, algae, and plants use two linked photosystems: photosystems I (PSI) and II (*PS*II). PSII and the oxygen-evolving complex allow for the extraction of electrons from water molecules, which have a very positive redox potential (O_2/H_2O pair; $E_0' = +0.87$ V) (see overview in Schwieterman *et al.*, 2018). The photosynthetic machinery of anoxygenic phototrophs is different. These primitive phototrophs use a single photosystem, which can be classified into one of two families—type I reaction centers, including PSI in chloroplasts, cyanobacteria, green sulfur bacteria, heliobacteria, and phototrophic acidobacteria, and type II reaction centers, such as *PS*II in

chloroplasts, cyanobacteria, purple bacteria, and green nonsulfur bacteria (Allen and Williams, 1998; Bryant *et al.*, 2007). Rather than using chlorophyll pigments that absorb light at wavelengths in the visible range, anoxygenic phototrophs utilize a diversity of bacteriochlorophyll pigments that absorb in the NIR (Senge and Smith, 1995).

The evolution of photosynthesis may have been driven, in part, by the redox potential of electron donors or reductants within an environmental context, with a step-wise increase in the redox potentials of reductants donating electrons to *PS*II (Pierson and Olson, 1989; Olson, 2006). The most ancient form of anoxygenic photosynthesis uses strong reductants such as H_2 or H_2S to donate electrons to a single photosystem (Olson and Pierson, 1986), but the limited availability of these volcanogenic compounds may have provided evolutionary pressures to develop a second photosystem, which could use weaker but more abundant reductants, such as Fe(II) and water (Olson, 1970, 1978).

Modern cyanobacteria produce O_2 resulting from the extraction of electrons from water, but there is a large difference in the redox potentials between the O_2/H_2O pair ($E_0' = +0.87$ V) of oxygenic photosynthesis and the S_0/HS^- pair ($E_0' = -0.27$ V) commonly used by anoxygenic photosynthesis. Researchers have speculated that an intermediate reductant, such as Fe(II) ($E_0' = +0.30$ V at circumneutral pH) or Mn(II) ($E_0' = \sim +0.60$ V), could have bridged the gap and acted as a transitional electron donor before water (Pierson and Olson, 1989; Olson, 2006). The widespread abundance of reduced iron (and potentially reduced manganese) on the early Earth would have made it particularly suitable as an electron donor for photosynthesis. Pierson *et al.* (1993) pointed out that the oxidized iron products of this type of photosynthesis would have provided substantial protection from UV radiation for surface-dwelling phototrophs before the development of an O_3 shield.

Due, in part, to the wide availability of water as an electron donor compared with the limited availability of volcanogenic reductants, oxygenic phototrophs spread easily and dominated aquatic and terrestrial habitats. Indeed, the evolution of oxygenic photosynthesis would ultimately result in a radical restructuring of Earth surface environments, with significant impacts on all major biogeochemical cycles. The so-called Great Oxidation Event, which occurred at $\sim$2.3 Ga (Bekker *et al.*, 2004; Luo *et al.*, 2016), set the stage for the evolution of more complex life-forms dependent on O_2. Consequently, O_2 is not only a promising biosignature, but it may also indicate an environment in which multicellularity, and even intelligence, can be supported (*e.g.*, Catling *et al.*, 2005).

It is of course difficult to estimate the likelihood that oxygenic photosynthesis would evolve on an exoplanet. The availability of carbon sources (CO_2 and/or reduced carbon) must be considered, and in the case of CO_2 fixation, the availability of reductants or electrons must also be factored in. In speculating about the evolution of photoautotrophy on an exoplanet, volcanism—a common geological process on terrestrial habitable planets—can supply CO_2 and other reduced species such as H_2. The possibility may exist that the same evolutionary selective pressures based on electron donor availability that gave rise to oxygenic photosynthesis on the early Earth could play out on an exoplanet, leading to the same metabolic outcome.

If photosynthesis did evolve on an exoplanet, it would likely coevolve with its environment to develop light-harvesting pigments that make use of the available stellar spectrum at the surface of the planet. Previous work suggested that chlorphyll *a* evolved to absorb the peak solar photon flux onto the planetary surface (Kiang *et al.*, 2007a, 2007b), which could potentially be predicted for different star–planet combinations. The peak photon flux will be the result of the interplay between the incident solar spectrum and subsequent absorption by molecules in the atmosphere, as well as efficiency considerations for NIR radiation, which may be too low in energy to drive photosynthesis efficiently beyond a limiting wavelength (Kiang *et al.*, 2007a, 2007b). On Earth, O_3 absorption in our atmosphere drives the Sun's incident peak photon flux near 600 nm redward. The peak photon flux at the surface is at 688 nm, where the principal photosynthetic pigment, chlorophyll *a*, absorbs (Kiang *et al.*, 2007b). However, on the early Earth, without abundant O_3, the peak photon flux at the surface may have been different, but potentially also pushed redward by strong blue absorption from hydrocarbon haze. Such hazes may have been present during early periods of Earth's history when the atmosphere was more reducing (Arney *et al.*, 2016).

In the case of exoplanets, the spectrum of the host star will be well known in the visible range, and the planetary atmospheric composition may be constrained by spectral observations. These observations will allow radiative transfer models to predict photon fluxes at the planetary surface, and potentially help identify the most likely spectral region for photosynthetic pigment absorption. However, it should be noted that the Kiang *et al.* (2007a, 2007b) supposition that phototrophs evolved to absorb the maximum photon flux (which was developed when considering vegetation) does not hold up when applied to cyanobacteria and anoxygenic phototrophs. Photosynthesis in these microbes is often inhibited by high light levels, and maximum photosynthetic activity can sometimes be observed at only 10–20% of the maximum solar irradiation (*e.g.*, Murata *et al.*, 2007; Trouwborst *et al.*, 2007).

2.2. The suppression, and ultimate rise, of O_2 on the early Earth

Although the evolution of oxygenic photosynthesis represented a critical evolutionary innovation, it was not a sufficient condition for appreciable and persistent planetary oxygenation, which may not have happened until as recently as 0.8 Ga (Lyons *et al.*, 2014). Understanding oxygen's late rise in our atmosphere requires a basic discussion of the factors modulating Earth's global O_2 cycle (Fig. 1). Oxygenic photosynthesis on the modern Earth fixes carbon (*i.e.*, converts atmospheric CO_2 into organic carbon) at a net rate of $\sim$100 Pg (10^{15} g) of carbon per year, distributed roughly evenly between the marine and terrestrial photosynthetic biospheres (Field *et al.*, 1998). For every mole of carbon fixed into biomass by oxygenic photosynthesis, one mole of free O_2 is released to the environment.

However, the vast majority of this O_2 is consumed very rapidly through aerobic respiration in surface environments, with only a very small fraction of the organic carbon initially produced by oxygenic photosynthesis (less than 1%) escaping respiration and becoming buried in marine and

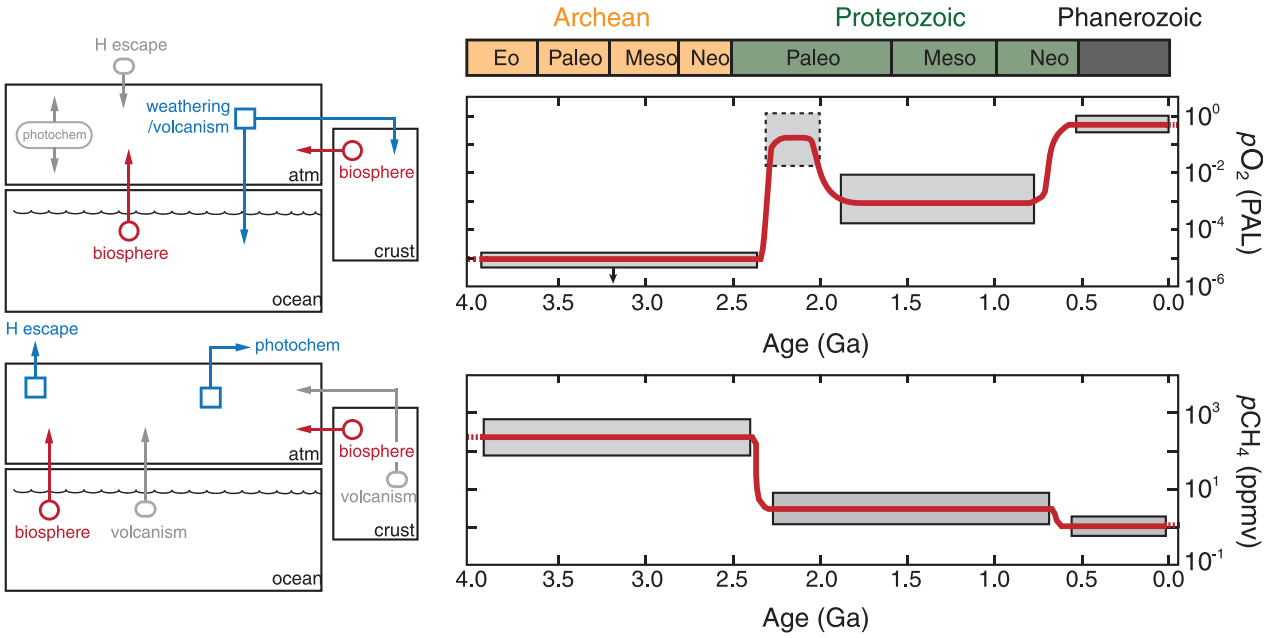

FIG. 1. Overview of the major processes controlling atmospheric O_2 and CH_4 levels (left panels). Red circles/arrows denote net biogenic sources (*e.g.*, after accounting for biological consumption), gray ovals/arrows denote potential abiotic sources, and blue squares/arrows denote net sink fluxes. Schematic depiction of the evolution of atmospheric O_2 and CH_4 throughout Earth's history (right panels). Using results from Reinhard *et al.* (2017), shaded boxes show ranges based on geochemical proxy or model reconstructions, whereas red curves show possible temporal trajectories through time. (Credit: Chris Reinhard)

terrestrial sediments (Berner, 1982). This relatively slow ''leak'' of organic carbon into Earth's upper crust represents a net source of O_2 to Earth's atmosphere. In addition, a fraction of photosynthetically produced organic matter that escapes burial will be consumed by microbial sulfate reduction, which essentially transfers electrons from organic matter to sedimentary pyrite (FeS_2), the burial of which similarly results in a net release of O_2 to surface environments. These fluxes are augmented by the irreversible escape of H to space, which scales with the total abundance of H-bearing reduced gases at the homopause (*e.g.*, CH_4 and H_2; Hunten, 1973). Although this represents a very small flux on the modern Earth, it is critical to consider as a mechanism of secular oxidation on timescales of planetary evolution (Catling *et al.*, 2001). Input fluxes of O_2 are ultimately balanced on long timescales by O_2 consumption during the uplift and oxidative weathering of reduced mineral phases in Earth's crust (including previously buried organic carbon and pyrite sulfur) and through reaction with volcanic and metamorphic reductants (Kasting and Canfield, 2012).

Whether a planet develops a biogenic O_2-rich atmosphere will thus depend not only on the evolution of oxygenic photosynthesis but also on the long-term balance between sources and sinks of O_2 at the surface (*e.g.*, Gebauer *et al.*, 2017). The accumulation and stability of large biogenic O_2 inventories in a planetary atmosphere will, in turn, depend on how input/output fluxes scale with atmospheric O_2 levels (if at all) and on secular changes in planetary degassing, differentiation, and atmospheric escape. An important consequence of this is that the evolution of oxygenic photosynthesis cannot, on its own, be expected to yield a remotely detectable oxidizing atmosphere. The planetary environment also plays a crucial role.

Earth's history provides an instructive example. Constraints from stable isotopes and trace element proxies indicate the evolution of oxygenic photosynthesis on Earth by at least $\sim$3.0 Ga (Planavsky *et al.*, 2014a) and perhaps much earlier (Rosing and Frei, 2004). However, complementary isotopic constraints indicate that Earth's atmosphere was pervasively reducing until $\sim$2.5 Ga (Farquhar *et al.*, 2001; Pavlov and Kasting, 2002; Zahnle *et al.*, 2006). There thus appears to have been a very significant period on Earth during which oxygenic photosynthesis was present but large amounts of O_2 did not accumulate in Earth's atmosphere. In addition, there is some evidence that after the initial accumulation of O_2 in Earth's atmosphere at $\sim$2.3 Ga, atmospheric O_2 levels remained relatively low for much of the subsequent $\sim$2 billion years (Planavsky *et al.*, 2014b; Cole *et al.*, 2016; Tang *et al.*, 2016), during which biogenic O_2, although clearly present, may have been challenging to detect remotely given current technology (Reinhard *et al.*, 2017).

In sum, the emergence of a biogenic O_2-rich atmosphere will depend on both the evolution of oxygenic photosynthesis and geochemical dynamics at the planetary surface that are favorable for the long-term accumulation of a large atmospheric O_2 inventory; if planetary conditions are not favorable, then a false negative will occur. These dynamics will, in turn, depend on a series of planetary factors that may be challenging to constrain observationally or from first principles. For example, heat flux from a planetary interior (as constrained by radiogenic element inventory and planet size), O_2 fugacity of the planetary mantle (as constrained by

both initial chemistry and long-term recycling of materials from the surface), the degree of crustal differentiation (as constrained by both overall heat fluxes and planetary rheology), and ocean chemistry can interact to buffer atmospheric O_2 to low levels despite the presence of oxygenic photosynthesis. The ability to constrain these contextual variables through observations of the planet and star, or through modeling, may ultimately form a critical component of diagnosing false negatives for O_2 on living planets. Similarly, they lay the foundation for critical thinking on the nature and use of contextual information for other proposed biosignatures as well.

2.3. Earth's history of oxygen's companion biosignatures CH_4 and N_2O

The role of the environment in enhancing or suppressing the atmospheric accumulation of biogenic gases also applies to other species, such as CH_4 and N_2O, and the detection of these gases could be used to strengthen confidence that the observed O_2 in an exoplanet atmosphere is indeed biogenic (*e.g.*, Hitchcock and Lovelock, 1967). Atmospheric levels of these gases will be a function of production at the surface (whether biological or abiotic), but will also depend strongly on sink fluxes due to biological recycling, geological processes, and photochemistry in the atmosphere. For example, N_2O is photochemically unstable in reducing atmospheres (Roberson *et al.*, 2011), as these atmospheres lack the O_2, O_3, or CO_2 of more oxidizing atmospheres, which shields N_2O from UV photolysis to N_2. Consequently, in more reducing atmospheres, it is difficult to sustain high atmospheric levels of N_2O without large surface fluxes. The abundance of N_2O in planetary atmospheres also depends on the spectrum of the host star, and many M dwarfs are less able to directly photolyze N_2O, allowing longer lifetimes and higher abundances for the same surface flux (Segura *et al.*, 2005; Rauer *et al.*, 2011; Rugheimer *et al.*, 2013, 2015). However, in general, unless the atmosphere is already oxidizing, whether due to the action of oxygenic photosynthesis, or stellar-driven atmospheric evolution to high-O_2 or high-CO_2 states (*e.g.*, Meadows *et al.*, 2018; Luger and Barnes, 2015), relatively high N_2O fluxes will be required to maintain elevated atmospheric N_2O levels. These kinetic constraints on biogenic gas abundance in planetary atmospheres have led to approaches that emphasize the magnitude of chemical disequilibrium between species (*e.g.*, O_2/O_3 and CH_4), and this approach can potentially provide more specific information about the magnitude of production/consumption fluxes compared with the abundance of a single biogenic gas (Lovelock and Kaplan, 1975; Kasting *et al.*, 2013; Krissansen-Totton *et al.*, 2016a).

The evolution of atmospheric chemistry on Earth, as described hereunder, illustrates how searching for secondary gases to strengthen confidence in oxygen's biogenic origin may be both challenging and illuminating (Fig. 3).

2.3.1. The Archean ($\sim$4.0–2.5 Ga)–low O_2, high CH_4.

During most of the Archean Eon, background atmospheric O_2 levels were vanishingly low (likely less than $\sim 10^{-7}$ times PAL; Zahnle *et al.*, 2006), with peak O_3 levels correspondingly low (Kasting and Donahue, 1980). Theoretical models predict that under such reducing atmospheric conditions, and with relatively low oxidant levels in the ocean (*e.g.*, dissolved O_2, NO_3^-, and SO_4^{2-}), atmospheric CH_4 levels may have been $\sim$2–3 orders of magnitude above those of the modern Earth (Fig. 3; Pavlov *et al.*, 2003). Indeed, new isotopic tools are emerging for fingerprinting the photochemical impacts of much higher atmospheric pCH_4 and its modulation by Earth's biosphere (*e.g.*, Izon *et al.*, 2017). Although there is now firm evidence for transient increases in atmospheric O_2 levels during the late Archean (Anbar *et al.*, 2007; Kendall *et al.*, 2010), the magnitude and duration of these O_2 pulses are not well constrained at present. Thus, for much of Archean time, Earth's atmosphere was characterized by very low O_2/O_3 but elevated CH_4.

2.3.2. The Paleoproterozoic ($\sim$2.2–2.0 Ga)–higher O_2, low CH_4, possible N_2O.

After the first large-scale oxygenation of the ocean–atmosphere system after $\sim$2.3 Ga, there was a period of the Paleoproterozoic during which atmospheric O_2/O_3 levels may have risen to (or even exceeded) modern levels for perhaps 100–200 million years or more (Fig. 3; Lyons *et al.*, 2014). This increase in atmospheric O_2 would, in all likelihood, have led to a corresponding drop in atmospheric CH_4 levels, and may have UV shielded and photochemically stabilized N_2O for the first time in Earth's history.

2.3.3. The mid-Proterozoic ($\sim$1.8–0.8 Ga)–lower O_2, low CH_4.

Atmospheric O_2/O_3 levels appear to have dropped markedly and remained at relatively low background levels for much of the mid-Proterozoic (Lyons *et al.*, 2014; Planavsky *et al.*, 2014b; Cole *et al.*, 2016; Reinhard *et al.*, 2016; Tang *et al.*, 2016). At the same time, recent Earth system modeling of the CH_4 cycle under mid-Proterozoic conditions as inferred from the geochemical proxy record (*e.g.*, atmospheric pO_2 and marine SO_4^{2-} levels) implies that atmospheric CH_4 may also have been rather low, on the order of $\sim$1–10 ppmv (Olson *et al.*, 2016).

2.3.4. The late Proterozoic ($\sim$800–550 million years ago [Ma])–higher O_2, low CH_4, higher N_2O.

The geochemical record indicates another series of significant shifts in ocean–atmosphere redox during the late Proterozoic, after which atmospheric O_2/O_3 levels may have ultimately stabilized at roughly modern levels. Atmospheric pO_2 subsequently varied between $\sim$0.25 and 1.5 PAL over the past $\sim$500 million years (Berner *et al.*, 2006). Earth's atmosphere during this period has been characterized by correspondingly low atmospheric CH_4 (Fig. 3) and possibly relatively high N_2O production (Buick, 2007) and atmospheric N_2O.

One striking implication of this history is that throughout Earth's evolution, either O_2 or CH_4, or neither, dominated the atmosphere, and so the canonical O_2–CH_4 disequilibrium biosignature may have been challenging to observe in the atmosphere over most of Earth's history. This is despite the fact that oxygenic photosynthesis has been present at Earth's surface for at least $\sim$3 billion years (Planavsky *et al.*, 2014a), and methanogenesis has been extant for $\sim$3.5 billion years (Ueno *et al.*, 2006). The source–sink relationships for the coupled O_2 and CH_4 cycles throughout Earth's history may thus have led to a persistent false negative signal, during which major biogenic gases were being

produced and consumed at potentially high rates, but did not coaccumulate in the atmosphere at potentially detectable levels (Reinhard *et al.*, 2017). Possible exceptions include relatively high O_2/O_3 during the Paleoproterozoic and during the past ~500 million years, and potentially detectable O_3 during the mid-Proterozoic (Reinhard *et al.*, 2017). However, the possibility remains that Earth's surface biosphere, definitively established by at least ~3.5 billion years ago, may not have been detectable by using biosignature gases until relatively recently in Earth's geological history.

2.4. Secondary photosynthetic biosignatures

Earth also demonstrates alternative ways in which our photosynthetic biosphere has impacted the environment beyond the abundant O_2 that eventually rose in our atmosphere. These secondary biosignatures include surface reflectivity signatures from light harvesting (Kiang *et al.*, 2007a, 2007b) and other pigments developed for nonphotosynthetic purposes by phototrophs (Hegde *et al.*, 2015; Schwieterman *et al.*, 2015a), as well as the strong jump in reflectivity longward of chlorophyll *a* at 0.7 μm, from the red edge of vegetation (Gates *et al.*, 1965; Kiang *et al.*, 2007a). Another secondary biosignature of photosynthesis in globally averaged spectra of our planet is the seasonal variations in the abundance of CO_2 (Meadows, 2008) due to growth and decay of vegetation on land, which imparts a ~2% seasonal variation in CO_2 abundance (Keeling, 1960; Hall *et al.*, 1976; Keeling *et al.*, 1976). Earlier in Earth's history before the permanent rise of O_2, small amounts of biogenic O_2 may also have shown seasonal variation (see Schwieterman *et al.*, 2018, for a review; Reinhard *et al.*, 2016).

Either a corroborative surface or temporal signature may be sought as a secondary confirmation of a photosynthetic origin for any detected O_2 in a planetary atmosphere. The vegetation red edge has likely been widespread on Earth since about 0.46 Ga (Carroll, 2001; Igamberdiev and Lea, 2006), corresponding with the rise of land plants, and may be coincident with the rise of O_2 to near-modern levels. However, in false negative situations wherein planetary processes are suppressing the rise of photosynthetically generated O_2, surface reflectivity biosignatures from photosynthetic and nonphotosynthetic pigments produced by phototrophs may have been the only way to detect photosynthesis (Schwieterman *et al.*, 2015a).

3. Star–Planet Interactions, and the Generation of False Positives for O_2 in Exoplanetary Environments

Although false negatives may reduce the atmospheric signal and so preclude the detectability of biosignatures, false positives complicate the interpretation of any O_2 that is observed. False positives for O_2 on uninhabitable planets have been postulated for decades (Schindler and Kasting, 2000; Selsis *et al.*, 2002; Des Marais *et al.*, 2002 and references therein), but were considered more likely to occur for planets outside the habitable zone, and so were anticipated to be easy to identify and exclude. However, several plausible O_2 false positive scenarios for planets in the habitable zone have since been identified (*e.g.*, Wordsworth and Pierrehumbert, 2014; Luger and Barnes, 2015; Tian, 2015; Harman *et al.*, 2015; see Meadows, 2017 for a more detailed review). These mechanisms rely primarily on conditions that lead to the photolysis of H_2O and/or CO_2 in a terrestrial planet atmosphere, and in some cases stabilize the photolytic byproducts of CO_2 from recombination by suppressing the photolytic formation of catalysts from other atmospheric gases. Rather than weakening oxygen's role as a biosignature, knowledge of false positives allows us to identify observable characteristics of the stellar or planetary environment that indicate the mechanisms that most likely generate them. Each potential false positive mechanism that is ruled out by observations increases the robustness of a biogenic interpretation for O_2. Hereunder we summarize some of the most significant false positive mechanisms for planets in the habitable zone.

3.1. Low noncondensable gas inventories

The possible abiotic O_2 generation mechanism that will likely be the most difficult to observationally recognize and preclude involves photolysis of water—and subsequent hydrogen loss—from terrestrial atmospheres that are depleted in noncondensable gases such as N_2 (Wordsworth and Pierrehumbert, 2014). This mechanism may produce Earth-like quantities of O_2 on an ocean-bearing world. To work, the effectiveness of the ''cold trap''—the rapid reduction in temperature with altitude that causes rising water vapor on Earth to condense and thereby remain trapped in the troposphere—must be weakened. This occurs when the atmospheric temperatures are high, or when the total inventory of noncondensable gases—for example, N_2, O_2, or CO_2—is low (Wordsworth and Pierrehumbert, 2014). Because this mechanism to allow water into the stratosphere relies primarily on a planetary property, a low inventory of gases that do not condense at typical habitable zone terrestrial planetary temperatures and pressures, it may work for planets orbiting stars of any spectral type, including Sun-like stars. With a low inventory of noncondensable gases, water is able to rise higher into the atmosphere before it condenses, and it is more vulnerable to photolysis by incident stellar UV radiation at these higher altitudes. The water's H atoms escape, leaving abiotic O_2 to build up in the atmosphere. This continues until O_2, itself a noncondensable gas, overwhelms surface sinks to reach a sufficiently high atmospheric abundance that it can establish a cold trap, and halt the loss of water vapor. For an abiotic planet that is largely Earth-like except for the N_2 inventory, Wordsworth and Pierrehumbert (2014) calculate that this proposed mechanism could result in planets with a very Earth-like O_2 partial pressure (~0.15 bars), while losing significant amounts of water.

3.2. Enhanced M dwarf premain sequence stellar luminosity

Another mechanism that may be capable of generating thousands of bars of abiotic O_2 explores the impact of the premain sequence, super-luminous phase of young M dwarf stars on terrestrial planet environments (Luger and Barnes, 2015). The extended contraction phase of premain sequence young stars makes them significantly more luminous (*e.g.*, Baraffe *et al.*, 1998) than they will be when they enter the main sequence hydrogen burning phase. Consequently, planets that form in what will become the main sequence

habitable zone are subjected early on to very high levels of radiation (Lissauer, 2007). This super-luminous phase is longer for lower mass M dwarfs than other stellar spectral types, and can extend for up to 1 billion years (Gyr: Baraffe *et al.*, 1998). Modeling suggests that this super-luminous phase can drive the loss of up to several Earth ocean equivalents of water for an M dwarf HZ terrestrial planet (Luger and Barnes, 2015; Tian, 2015). The resultant water-rich atmosphere will be susceptible to photolysis and hydrogen escape, and may produce hundreds or thousands of bars of O_2 (Luger and Barnes, 2015; photolysis of an Earth ocean of water can produce $\sim$240 bars of O_2 on an Earth-like planet, Kasting, 1997).

The amount of O_2 generated in this scenario is a strong function of stellar spectral type, XUV flux, original water inventory, planetary mass, and the position of the planet in the habitable zone. Planets in the outer regions of the habitable zone of M0–M3V stars are less likely to generate significant amounts of abiotic O_2 (Luger and Barnes, 2015), as are planets orbiting M0–M3V dwarfs with lower stellar XUV, as slower water loss may preclude O_2 generation and buildup (Tian, 2015). However, for planets orbiting later type M dwarfs (M4V and later) depending on the planet's original water inventory, mass, stellar parameters, and the strength of surface sinks (Rosenqvist and Chassefière, 1995; Schaefer *et al.*, 2016), up to several hundreds of bars of photolytically produced O_2 could build up in the atmosphere (Luger and Barnes, 2015). For the recently discovered Proxima Centauri b, orbiting an M5.5V star, estimates of ocean loss during the 169 ± 13 Myr (Barnes *et al.*, 2018) before the planet enters the habitable zone are sensitive to the assumed form of the XUV evolution. Results for global water loss range from less than one ocean (<250 bars O_2 generated), assuming a constant XUV flux for the host star for the first 3 Gyr (Ribas *et al.*, 2016), up to 3–10 Earth ocean equivalents lost (750–2500 bars of O_2 generated), assuming that the XUV scales with the decreasing bolometric luminosity (Barnes *et al.*, 2018).

For terrestrial planets, if substantial CO_2 is also outgassed over time, and the planet has little or no surface ocean in which to sequester CO_2, then these types of worlds could sustain atmospheres with large quantities of both CO_2 and O_2 (Meadows *et al.*, in press). Over time the O_2 may be lost and CO_2 may continue to accumulate. Although we have evidence that Venus lost a global ''ocean'' that was at least 3 m deep (de Bergh *et al.*, 1991), any abiotic O_2 generated was subsequently lost to surface or interior sinks (Rosenqvist and Chassefieré *et al.*, 1995; Hamano *et al.*, 2013; Schaefer *et al.*, 2016) or top-of-atmosphere loss processes. The latter may include the recently discovered ''electric wind'' surrounding Venus, which can strip O_2 ions from the planet (Collinson *et al.*, 2016).

3.3. Stellar spectrum driven photochemical production

Abiotic O_2 and its proxy, O_3, can also be formed through planetary photochemistry of CO_2. Each photochemical reaction requires photons that exceed a threshold energy level—or equivalently, photons at wavelengths shorter than a threshold wavelength—to be absorbed by and split the molecule undergoing photolysis. Planetary photochemistry is strongly sensitive to the UV spectral energy distribution of the parent star (*e.g.*, Segura *et al.*, 2003, 2005, 2010; Grenfell *et al.*, 2007, 2014; Rugheimer *et al.*, 2013, 2015), and in particular the ratio of shorter to longer wavelength UV radiation, which can split molecules and drive reactions that change the composition of the atmosphere, without relying on atmospheric escape.

The ultimate composition of the planetary atmosphere will then depend on the sources and sinks for photochemical reactions provided by the planetary environment. For example, photochemical abiotic O_2 production will depend strongly on the source of O atoms, which is primarily controlled by the abundance and photolysis rates of atmospheric CO_2, SO_2, H_2O, and other O-bearing gases. The atmospheric sink will depend on the availability of H atoms in the atmosphere from H_2, H_2S, and hydrocarbons. Although water vapor can be sourced from a planetary ocean, the availability of other gases, such as CO_2, SO_2, and reducing (H-bearing) gases, is governed by the planet's volcanic outgassing rates, which can be sustainable on long geological timescales.

In particular, CO_2 is likely a common atmospheric gas on terrestrial planets. In the Solar System, CO_2 dominates the atmospheric composition of Venus and Mars, and was likely a significant component of the early Earth's atmosphere as well (Kasting *et al.*, 1993; Sheldon *et al.*, 2006; Sleep, 2010; Driese *et al.*, 2011). The key reactions to produce O_2 from CO_2 photolysis include $CO_2 + h\nu \rightarrow CO + O$, and the collisional recombination reaction $O + O + M \rightarrow O_2 + M$, where M is a third molecule that carries away excess energy to stabilize the collisional product. The yield of O_2 from this process depends on how efficiently the back reaction to regenerate CO_2 can occur. This, in turn, depends on the atmospheric abundance of catalysts such a HO_x (*e.g.*, from water vapor; Tian *et al.*, 2014) or NO_x (*e.g.*, from cosmic rays; Grenfell *et al.*, 2012) (c.f. Yung and DeMore, 1999; Stock, *et al.*, 2017).

Aqueous reactions may also remove atmospheric O_2, especially if the planet supports a surface ocean, and these reactions are also important for our understanding of abiotic O_2 generation. For example, the rate of reaction of dissolved CO and O_2 to reform CO_2, and thereby draw down atmospheric O_2, is poorly understood, but is crucial to understanding the final balance of O_2 in the atmosphere (Harman *et al.*, 2015). Similarly, weathering of surface crust (*e.g.*, Anbar *et al.*, 2007), and the sequestration of O_2 into the planetary mantle (*e.g.*, Hamano *et al.*, 2013; Schaefer *et al.*, 2016) are key processes that control O_2 draw down, and could result in abiotic O_2 buildup if slow. Conversely, if these processes are aggressive enough, they could produce a false negative for biologically produced O_2 by scrubbing photosynthetically generated O_2 from a planetary atmosphere, as likely happened over Earth's history, and discussed in Section 2.

Several groups have identified potential photochemical mechanisms to generate abiotic O_2 and O_3 on terrestrial planets in the habitable zone (Domagal-Goldman and Meadows, 2010; Hu *et al.*, 2012; Domagal-Goldman *et al.*, 2014; Tian *et al.*, 2014; Gao *et al.*, 2015; Harman *et al.*, 2015). However, the amounts of abiotic O_2 and O_3 generated in these simulations differ, in part, due to different assumptions about the abundance of available catalysts to drive recombination of CO_2, or destruction of O_2 and O_3, which can be affected by the availability of H_2O and the spectrum of the star, as well as the efficiency of the CO and O_2 reaction in seawater. The mechanism that could produce

the largest signal from CO_2 photolysis requires a desiccated, cold, H-poor atmosphere. This water-poor atmosphere cannot support photolytic generation of the OH catalyst that accelerates CO_2 recombination (Gao *et al.*, 2015). In this scenario, a catalytic cycle feedback with O_3 formation combines with the suppression of CO_2 recombination, and photochemical models predict stable atmospheric fractions of O_2 near 15%.

In another proposed mechanism, recombination of photolyzed CO_2 can be slowed by a parent star (typically an M dwarf) with a higher far-ultraviolet (FUV; $0.122 < \lambda < 0.2$ μm) to mid-ultraviolet (MUV; $0.2 < \lambda < 0.3$ μm) and near-ultraviolet (NUV; $0.3 < \lambda < 0.44$ μm) ratio when compared with the Sun. The higher FUV photolyzes CO_2, but the lower MUV–NUV radiation inhibits the photolysis of water and other HO_x chemistry that would drive recombination (Tian *et al.*, 2014; Harman *et al.*, 2015). For the cases considered for this mechanism, atmospheric O_2 abundances as high as 0.2% to 6% are predicted, with higher values corresponding to little or no O_2 sinks in the planetary environment (Harman *et al.*, 2015). When more realistic sinks are included, abiotic O_2 abundances are reduced by many orders of magnitude (*e.g.*, Harman *et al.*, 2015).

As another possible abiotic mechanism for O_2 buildup, Léger *et al.* (2011) discussed the efficacy of known surface catalysts for abiotic photogeneration of O_2 from water splitting, but concluded that it was highly unlikely that sufficient catalysis could occur on a habitable planet to generate a false positive. However, a subsequent study argued that this may be possible for a planet with shallow oceans, strong NUV, and significantly large areas of surface TiO to produce Earth-like quantities of O_2 from the splitting of water >1 billion years (Narita *et al.*, 2015).

O_3 can often serve as a proxy for O_2, especially in the MIR where O_2 does not have spectral features (*e.g.*, Des Marais *et al.*, 2002). However, abiotic O_3 could also be formed through photolysis of the abiotic O_2 generated by ocean loss, with calculated values ranging from 1% of PALs of O_3 up to values comparable with Earth's current O_3 abundance for planets orbiting in the HZ of M dwarfs, depending on whether liquid water remains (Meadows *et al.*, 2018). However, the spectral slope of the UV radiation of the star could also photochemically generate O_3, even without buildup of O_2. FUV radiation can favor the generation of O_3 through photolysis of CO_2 (and O_2), whereas MUV or NUV radiation photolytically destroys O_3. Consequently, abiotic O_3 could accumulate—even without significant generation of O_2—for stars with the highest FUV to MUV ratios. O_3 was produced at 10% of Earth's current O_3 column abundance in the simulations of Domagal-Goldman *et al.* (2014) for M dwarf planets, without appreciable buildup of abiotic O_2.

Although the mechanisms that generate abiotic O_2 and O_3 are driven primarily by the interaction of the incident stellar spectrum with the planetary atmosphere, they can be balanced by the destruction or sequestration of O_2 and O_3 in the planetary environment. These losses could be through photolysis, catalysis, catalytic recombination into CO_2, or interaction with the planetary surface and ocean, if present. The net atmospheric accumulation of O_2 and O_3 is highly sensitive to these boundary conditions, which include weathering rates and aqueous sinks for CO, all of which are currently poorly understood.

3.4. Summary of false positives

Recent research indicates that there are several mechanisms that could produce abiotic O_2 and O_3 in a planet's atmosphere, with each presenting a potential false positive to different degrees. A summary of key components of this information is presented in Figure 2. Two of the mechanisms allow water to enter a planet's stratosphere where it is photolyzed, and the H atoms lost to space, resulting in O_2 buildup in the planet's upper atmosphere. Water entering the stratosphere is either enabled by loss of an ocean in a runaway greenhouse process (Luger and Barnes, 2015)—a mechanism that is most effective for late-type (*i.e.*, less massive) M dwarfs—or through lack of noncondensable gases in the planetary atmosphere, which could affect planets orbiting stars of any spectral type (Wordsworth and Pierrehumbert, 2014). The runaway mechanism could produce an O_2-dominated atmosphere of hundreds of bars, and the lack of noncondensable gases could potentially result in atmospheres that are $\sim$15% O_2. Earth-like quantities of O_2 have also been proposed to be generated by the splitting of liquid water by a surface TiO photocatalyst (Narita *et al.*, 2015).

The other major class of processes that build up abiotic O_2 relies on the photolysis of CO_2 and circumstances that inhibit CO_2 recombination from CO and O_2 (Hu *et al.*, 2012; Tian *et al.*, 2014; Gao *et al.*, 2015; Harman *et al.*, 2015). For photochemical production without atmospheric escape, O_2 abundances as high as 0.2% to 6% are predicted, with higher values corresponding to little or no O_2 sinks in the planetary environment. More realistic modeling of sinks can reduce these estimates by orders of magnitude (*e.g.*, Domagal-Goldman *et al.*, 2014; Harman *et al.*, 2015). Finally O_3 may be considered a proxy for O_2 in a planetary atmosphere, and large abundances of abiotic O_3 may build up in the massive O_2-rich atmospheres possible after ocean loss (Meadows *et al.*, 2018), although in these cases large amounts of O_2 will also be present. Domagal-Goldman *et al.* (2014) were not able to generate large abundances of O_2 from CO_2 photolysis for habitable planets orbiting M dwarfs, but did produce potentially detectable O_3 column abundance as high as 10% of Earth's modern abundance.

In most cases, however, the mechanism for abiotic production of O_2 or O_3 leaves a ''tell,'' an impact on the planetary environment that may be detectable. These indications can range from the presence of collisionally induced absorption from O_2 molecules that collide more frequently in dense, O_2-rich postocean-loss atmospheres (Schwieterman *et al.*, 2016; Meadows *et al.*, 2018), CO from the photolysis of CO_2 (Schwieterman *et al.*, 2016), lack of water vapor (Gao *et al.*, 2015), lack of collisionally induced absorption from N_2 (Schwieterman *et al.*, 2015b), to the absence of reducing gases (Domagal-Goldman *et al.*, 2014). In the following section we describe the observations needed to search for O_2 in a terrestrial planetary atmosphere and to discriminate whether that O_2 is abiotic or biological in origin based on characteristics of the parent star and the planetary environment.

4. Observational Requirements for Detecting and Discriminating O_2 From Potential False Positives

Exoplanet observing techniques required to characterize an exoplanet environment and search for life include time- and

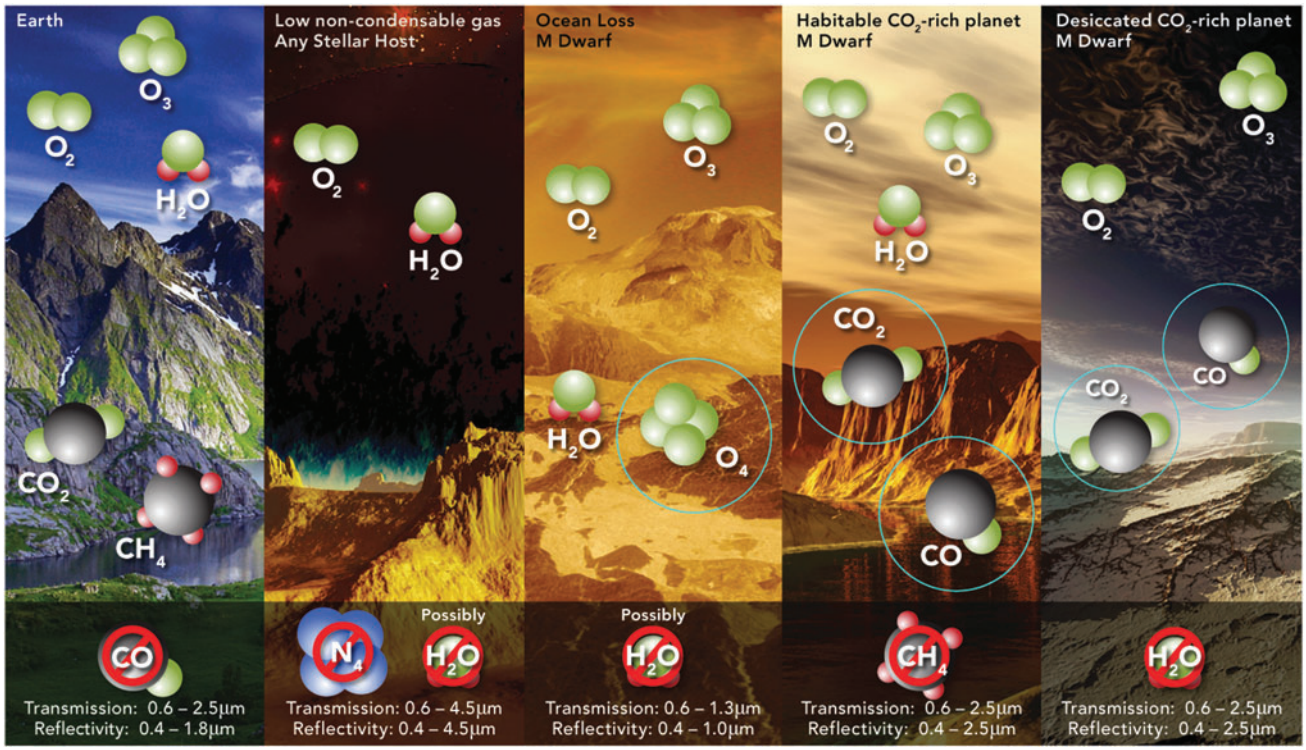

FIG. 2. Potential false positive mechanisms for O_2. This cartoon summarizes the atmospheric mechanisms by which O_2 could form abiotically at high abundance in a planetary atmosphere (Meadows, 2017). The extreme left panel is Earth, the four panels to the right show the different mechanisms and their observational discriminants. Circled molecules, if detected, would help reveal a false positive mechanism, a lack of detection of the ''forbidden'' molecules in the bottom shaded bar would also help to reveal the false positive mechanism. For example, the presence of CO and CO_2, and the absence of CH_4, is a strong indicator for a photochemical source of O_2 from the photolysis of CO_2 on a habitable CO_2-rich M dwarf planet (Figure credit: Ron Hasler).

wavelength-dependent photometry, phase-dependent photometry, and spectroscopy. Time-resolved information is valuable because it can show planetary rotation and changing cloud patterns (Cowan and Strait, 2013), and measurements taken over the course of a planetary orbit may reveal seasonality. Seasonal changes may be biologically driven (*e.g.*, Keeling *et al.*, 1976) and so may be valuable as a separate metric from the presence of abundant O_2 for detecting life on an exoplanet. Phase-dependent observations, that is, those taken when the exoplanet is at different points in its orbit and may be seen at different illumination phases, can reveal interesting features such as ocean glint or the presence of forward-scattering clouds, which may be water (Robinson *et al.*, 2010). At thermal wavelengths, phase-dependent observations can be used to search for planetary day–night temperature differences and atmospheric molecular absorption (Meadows *et al.*, 2018).

Spectra, meanwhile, open the door to detailed characterization and quantification of surface features and atmospheric gas abundances. Atmospheric gas abundances derived from spectra would then be used as inputs to atmospheric photochemical–climate models to predict the gas surface fluxes required to sustain the observed abundance; quantifying these surface fluxes may aid in distinguishing true biosignatures from abiotic processes (Domagal-Goldman *et al.*, 2011). Three main observational techniques will be used to obtain spectra of exoplanets in the next two decades—transmission spectroscopy, high-contrast direct imaging spectroscopy, and high-resolution spectroscopy. In this section, we discuss the pros and cons of different exoplanet observing techniques, factors affecting target selection considerations, and which measurements will be the most valuable for characterizing terrestrial exoplanet environments and searching for life.

Transmission spectroscopy with the JWST, scheduled for launch in early 2019, will likely be our first opportunity to search for O_2 in the atmosphere of one to three habitable zone Earth-sized planets (Cowan *et al.*, 2015). Transmission spectroscopy, where a spectrum of the planetary atmosphere is taken when a planet transits in front of and is ''backlit'' by its parent star, offers advantages and disadvantages for exoplanet characterization. This technique is most likely to succeed for habitable zone planets orbiting M dwarfs, where a stronger signal from the planet can be obtained because a terrestrial-sized planet can block out a more significant fraction of the small M dwarf's light, and the proximity of the planet to the star results in many more transits in a given time span. The longer path length through the backlit planetary atmosphere enhances the impact of higher altitude aerosols and trace gases on the transmission spectrum (Fortney, 2005) when compared with the downward-looking observations of reflected light from the planet expected from direct imaging. Because the atmosphere is ''backlit'' by the star, the decrease in signal-to-noise (S/N) ratio with increasing wavelength is less problematic than in reflected

light observations, where the planet becomes less reflective at longer wavelengths.

However, a number of processes can limit the ability of transmission observations to probe a planet's troposphere. These processes include refraction (Bétrémieux and Kaltenegger, 2013, 2014; Misra *et al.*, 2014b), condensates/aerosols (Kreidberg *et al.*, 2014; Misra and Meadows, 2014; Morley *et al.*, 2015), and the optical depth contributed by atmospheric constituents (Meadows *et al.*, 2018). Transmission cannot observe the planetary surface, and the accessible regions of the atmosphere of a habitable planet will likely be water-poor layers above the water-preserving cold trap, potentially making it more difficult to detect atmospheric water vapor by using this technique (Meadows *et al.*, 2018). However, several O_2, O_3, and O_4 bands may be accessible.

Direct imaging requires telescopes with sufficient spatial resolution, and instrumentation that can suppress the star's brightness, so that the much fainter planet can be imaged. This allows the planet to be studied through either photometry or spectroscopy. Angular/spatial resolution for a telescope scales with 1/D, where D is the diameter of the telescope. Larger telescopes provide smaller spatial resolution, and so can separate planets that are closer to their star. High-performing technologies to suppress light from the central star include internal occulters to block or redirect the star's light after it enters the telescope (coronagraphs; Stapelfeldt *et al.*, 2015), or external occulter spacecraft that fly between the telescope and the star (starshades; Seager *et al.*, 2015). Direct imaging can potentially probe the entire atmospheric column and even retrieve information on the planetary surface for clear sky scenes. This technique is, therefore, less sensitive to aerosols, and more sensitive to the deeper, near-surface atmosphere than transmission spectroscopy (Arney *et al.*, 2016, 2017).

The first space-based direct imaging mission to be launched will be the Wide Field Infrared Survey Telescope (WFIRST) in the mid-2020s, but this coronagraph-enabled 2.4 m telescope is unlikely to be able to detect and characterize terrestrial planets (Robinson *et al.*, 2016). However, the 2020 Astronomy Decadal Survey will review the potential for WFIRST to have a ''rendezvous'' with an external occulter (Seager *et al.*, 2015), which may provide the starlight suppression suitable for discovering rocky worlds.

Development is currently underway for more capable direct imaging mission concepts such as the Habitable Exoplanet Imaging Mission (HabEx) and the Large Ultra-Violet Optical Infrared Surveyor (LUVOIR), one of which could be launched in the mid-2030s. Such a mission could enable observations of smaller Earth-sized targets, and search for O_2 and other atmospheric constituents in their spectra (Postman *et al.*, 2010; Bolcar *et al.*, 2015; Dalcanton *et al.*, 2015; Rauscher *et al.*, 2015; Seager *et al.*, 2015; Stapelfeldt *et al.*, 2015; Mennesson *et al.*, 2016).

Complementary to these space-based telescopes, future 30–40 m ground-based observatories (extremely large telescopes, ELTs; *e.g.*, Kasper *et al.*, 2008), coming on line in the mid-late 2020s, will also offer the capability to detect and measure the spectra of perhaps 10 or more terrestrial exoplanets in the habitable zones of M dwarfs (Crossfield, 2016), depending on the occurrence rate of M dwarf HZ planets (*e.g.*, Dressing and Charbonneau, 2015). Transmission spectroscopy of later-type M dwarf exoplanets using high-spectral resolution spectrographs could obtain some of the earliest ground-based ELT measurements (Szentgyorgyi *et al.*, 2016), and search for O_2 in exoplanet atmospheres (Rodler and López-Morales, 2014). By combining coronagraphs and adaptive optics with high-resolution spectrographs (*e.g.*, Lovis *et al.*, 2017), and employing template-matching techniques to disentangle exoplanet spectral lines from Earth's own atmospheric absorption features (*e.g.*, Snellen *et al.*, 2015), spectra of nontransiting exoplanets may also be possible. Ground-based direct imaging observations at 3–10 μm for planets orbiting in the habitable zones of F, G, and K stars (Brandl *et al.*, 2014; Snellen *et al.*, 2013; Quanz *et al.*, 2015; Crossfield, 2016) are also anticipated for the late 2020s.

Direct imaging observations are constrained by inner- and outer-working angles (IWAs and OWAs)—the smallest and largest planet–star separations over which the observatory is capable of achieving adequate starlight suppression to reveal the planet. For coronagraphs, these angles scale with λ/D, the telescope's resolution element, where λ is the wavelength of the observations and D is the telescope mirror diameter. Desirable IWAs on coronagraphs are typically 2–3 λ/D and largely determined by the effectiveness and stability of the coronagraph working in conjunction with its telescope and spacecraft; the OWA is determined by the format size of the coronagraph's deformable mirrors. For starshades, the IWA depends on the geometric ratio between the size of the starshade and the separation distance between the starshade and its telescope. Because its IWA is independent of the telescope aperture, the starshade can allow observations of close-in planets (improved IWA) with relatively smaller telescope apertures. However, the telescope must still be at least large enough to have the requisite spatial resolution to separate the planet and the star, and to collect sufficient light from the planet in a reasonable amount of exposure time.

The IWA will tend to make observations of planets in the habitable zone of M dwarfs difficult, because these stars are intrinsically faint, and the habitable zone is 20 times closer to the star than it would be for a G dwarf. For instance, the Earth-sized planet orbiting in the habitable zone of the M dwarf star Proxima Centauri is only 0.0485 AU away from its parent star (Anglada-Escudé *et al.*, 2016), which at the Sun—Proxima Centauri distance corresponds to a planet–star angular separation on the sky of 37 milliarcseconds at maximum elongation. Therefore, although direct imaging of Earthlike planets orbiting the closest M dwarfs may be possible for larger observatories like the 16-m diameter LUVOIR concept, and LUVOIR may have as many as 8% of its accessible targets orbiting M dwarfs, direct imaging space missions tend to focus primarily on planets orbiting F, G, and K stars for which the planet–star angular separations are larger.

4.1. Target selection

Careful target selection may help reduce the likelihood of false positive O_2, although the stellar and planetary properties most likely to result in false positive O_2 are still being explored. Several of the proposed false positive mechanisms for O_2 production are more likely to occur for planets around later type M dwarfs, which may be more susceptible to early ocean loss and buildup of O_2 from subsequent H loss (Baraffe *et al.*, 1998; Luger and Barnes, 2015). In

contrast, planets in the habitable zones of F, G, and K stars will not experience a super-luminous host star for a significant period of time. M dwarfs may also have NUV/FUV flux ratios that are more favorable for photochemical production of O_2 or O_3 (Domagal-Goldman *et al.*, 2014; Tian *et al.*, 2014; Harman *et al.*, 2015). Systems older than a few Gyr may be preferred, to allow time for biologically generated O_2 to overwhelm sinks and rise in the atmosphere, and to increase the probability that abiotic O_2 generated during the star's super-luminous premain sequence phase has been depleted through sequestration in the planetary environment (Schaefer *et al.*, 2016) or lost to space (Collinson *et al.*, 2016; Ribas *et al.*, 2016; Airapetian *et al.*, 2017; Dong *et al.*, 2017; Garcia-Sage *et al.*, 2017).

When searching for biosignatures, it would, therefore, be advantageous to select older F, G, K, or earlier type M dwarf targets (M0–M3), where the habitable zones are likely safer from a false positive for O_2 through premain sequence ocean loss (Luger and Barnes, 2015). It will also be important to have measurements, or proxies, to estimate the UV spectrum of the M dwarf host star. However, some of these false positive mechanisms are less dependent on the host star, and are instead tied to planetary properties such as a lack of noncondensable gas species in the planetary atmosphere (Wordsworth and Pierrehumbert, 2014) or an abundance of surface TiO (Narita *et al.*, 2015). In these cases, abiotic O_2 production could occur for planets with suitable characteristics orbiting stars of any spectral type. Target selection for detailed follow-up will instead be informed by characterization of the planet's environment, and specifically a census of bulk gases such as N_2, O_2, and CO_2. More theoretical work is needed to better understand the factors that affect habitability so that the planets most likely to be able to support life are chosen for detailed follow-up.

We are now entering a new era wherein the first observations to constrain the nature of terrestrial exoplanet atmospheres are being taken (*e.g.*, de Wit *et al.*, 2016), potentially providing some of the first empirical information relevant to habitability and false positive processes. Early observations of exoplanets with high levels of incident starlight such as GJ1132b (Berta-Thompson *et al.*, 2015) and the inner TRAPPIST-1 planets (Gillon *et al.*, 2016, 2017) may reveal key characteristics of their planetary environments that shape abiotic O_2 generation and persistence, and even provide an observational test for the limits of the habitable zone.

4.2. Key measurements of environmental characteristics that provide context for O_2 detection

Should a promising candidate planet be identified, there are several key observations that can help place detection of atmospheric O_2 into context, and help discriminate between biological and abiological sources. The first of these is detailed knowledge of the parent star, including its spectral type, metallicity, age, observed or inferred UV to infrared spectrum, and a measure of its activity levels, including the amplitude and frequency of stellar flares. The spectral type and age help to identify the likely stellar evolutionary path of the star (Baraffe *et al.*, 1998), which drives planetary evolution, including atmospheric loss processes, which may produce false positives. The spectrum of the star is needed as input to atmospheric climate and photochemistry models, which will be used to determine atmospheric temperature, and the efficiency of photochemical production and destruction of O_2 and O_3.

Basic properties of the planet are also important, such as radius, orbit, and mass. Radius is most readily determined for transiting exoplanets where the fractional dimming of the star during the transit is a direct consequence of the planet's size, or more explicitly, its cross-sectional area. However, only a small fraction of habitable zone planets will transit (from 0.5% to 1.5% for G to M dwarf host stars). For nontransiting planets, determining a planetary radius is more challenging, as a size–albedo degeneracy exists in reflected light, as a planet could have a given measured brightness either because it is small but reflective, or because it is larger and less reflective. The range of plausible albedos for a terrestrial planet could easily span 0.06 to 0.9, potentially generating a factor of 7 uncertainty in the estimated size of the planet. Observations at MIR wavelengths—wherein emissivities for most terrestrial planetary surfaces are close to 1—may be used to infer planetary radius, especially if a color temperature can be derived from the shape of the MIR spectrum. JWST MIR thermal observations of Proxima Centauri b at different points in its orbit (a thermal phase curve) may reveal day–night temperature differences (Kreidberg and Loeb, 2016; Turbet *et al.*, 2016; Meadows *et al.*, 2018), whereas future ELTs may have the ability to image terrestrial planets in the habitable zones of a small sample of M dwarfs at wavelengths near 10 μm (*e.g.*, Quanz *et al.*, 2015). If the planet can be directly imaged at multiple epochs in its orbit, then the relative astrometry of the star and planet can be used to derive the orbital parameters. This can be done in either reflected light or in thermal emission, but the better angular resolution available at shorter wavelengths favors the use of reflected light imaging.

If the planet is not directly imaged, then its orbit may be determined indirectly—by measuring its dynamical influence on the host star or other planets in the system. The planetary mass and orbit, including its inclination, can be determined with sufficiently precise stellar astrometry to measure the reflex motion of the star induced by the planet. Stellar radial velocity (RV) measurements can determine all the orbital elements except for inclination, the angle of orientation of the planet's orbital plane to the observer. Since RV measures only the radial component of the star's orbital velocity, without knowing the orbital plane orientation, these measurements provide only a lower limit on the planetary mass (*e.g.*, Anglada-Escudé *et al.*, 2016).

For nontransiting planets, this RV orbital inclination ambiguity can be resolved by combining RV with imaging detections at more than one epoch and over a significant fraction of the planet's orbit, or through observations of emitted or reflected light from the planet in high-resolution spectroscopy. With the latter technique, the spectral shift in planetary atmospheric atomic or molecular lines reveals the RV of the planet itself (*e.g.*, Snellen *et al.*, 2015), and since the planetary orbital velocity is known from the stellar RV period, the inclination can be derived. Terrestrial planets will be extremely challenging to observe this way, and may have to await second- or third-generation instruments on ground-based ELTs. However, searching for emission from visible light aurorae on planets orbiting M dwarfs may

help improve the contrast for planetary RV measurements (Luger *et al.*, 2017). In the special case of transiting planets in multiplanet systems, the perturbations of one planet by another can sometimes be measured as changes in the timing of successive transits (transit timing variations) and allow the planetary masses to be derived (*e.g.*, Gillon *et al.*, 2017).

Another key planetary characteristic needed to interpret an observation of O_2 in a planetary atmosphere is the presence of water, which could be in the form of atmospheric gas, condensed clouds, and/or a surface ocean. Although the possibility that the planet can support liquid water is more likely for an Earth-like planet within the surface liquid water habitable zone (Kasting *et al.*, 1993; Kopparapu *et al.*, 2013), it is not guaranteed, as water may not have been delivered to the planet during its formation (Lissauer, 2007; Raymond *et al.*, 2007), or it may have been subsequently lost (Luger and Barnes, 2015; Airapetian *et al.*, 2016; Ribas *et al.*, 2016; Barnes *et al.*, 2018).

If water is present, it can help rule out several of the false positive mechanisms that rely on water loss (Luger and Barnes, 2015) or photochemistry in an extremely water-poor atmosphere (Gao *et al.*, 2015). Knowledge of the water vapor profile—and the detection of condensate clouds that form at the water vapor cold trap—would rule out another false positive mechanism associated with high-altitude photolysis in atmospheres without a cold trap (Wordsworth and Pierrehumbert, 2014). However, if residual water persists after water loss from either early ocean loss or lack of noncondensable gases, then abiotic O_2 and water vapor may both be seen in the spectrum (Meadows *et al.*, 2018). Absorption features for water occur throughout the visible (0.65, 0.7, 0.73, 0.8, and 0.95 μm), NIR (1.1, 1.4, and 1.8–2.0 μm), and MIR (6.3 and 18–20 μm) (Rothman *et al.*, 2013).

Observing liquid surface water itself may be challenging and will likely only be possible for reflected light observations of nearby planets with an optimal orbital plane orientation. Observing liquid surface water is a less ambiguous habitability indicator than observations of gaseous water spectral features, which could be present in uninhabitable steam atmospheres. One such method to detect liquid surface water is ocean glint, caused by specular reflection off a smooth surface (Cox and Munk, 1954). Glint has been used to detect the presence of hydrocarbon seas on the surface of Saturn's moon Titan (Stephan *et al.*, 2010) and water oceans in spacecraft views of Earth (Robinson *et al.*, 2014).

Previously, Robinson *et al.* (2010, 2014) used a sophisticated 3D spectral Earth model to show that the spectral behavior of Earth deviates strongly from Lambertian (*i.e.*, isotropic) scattering behavior toward crescent phases when specular reflection would be most apparent. Forward scattering from glint may mimic forward scattering behavior of clouds, but Robinson *et al.* (2010) showed that ocean glint even in the presence of realistic clouds (covering ~50% of the planet) is up to a factor of 2 brighter than forward scattering from clouds and a nonglinting (*i.e.*, Lambertian) ocean. Glint is most readily observed at phase angles within about 60°of new phase and for orbital plane inclinations that are no more than 30° from edge on to the observer. Glint from Earth's surface is most detectable at wavelengths near 0.8–0.9 μm where Earth's atmosphere is relatively transparent (although it may also be observed in the continuum between the longer 1.1, 1.4, and 1.9 μm water vapor bands).

Terrestrial exoplanet glint measurements are not possible in transmission, and outside the realm of feasibility for JWST phase curve measurements, even for the exoplanet orbiting the closest star (Proxima Centauri b; Anglada-Escudé *et al.*, 2016). In the case of Proxima, measurement precision for detecting glint in an NIR phase curve would need to be smaller than 10^{-8} (Meadows *et al.*, 2018), but this is significantly smaller than typical JWST noise floor estimates, which are on the order of 10^{-5} (Greene *et al.*, 2016), and so unachievable. However, these measurements may be achievable for future ELTs and for nearby habitable zone targets observed by large space-based exoplanet characterization missions such as LUVOIR (Meadows *et al.*, 2018).

Tectonic activity is critical to the long-term habitability of planets, as it both recycles elements required for life (*e.g.*, Berner, 2004; Wordsworth, 2016) and serves as a global thermostat that regulates climate over geological timescales (Walker *et al.*, 1981). Direct observations of tectonic activity will be extremely challenging, but observable impacts of tectonics on the planetary environment may be more accessible. A heterogeneous distribution of surfaces seen in maps generated by using time-resolved photometry (Cowan *et al.*, 2009) may suggest the presence of continents. Gases released from volcanic eruptions could also be sought (Kaltenegger and Sasselov, 2009; Kaltenegger *et al.*, 2010), but the resulting formation and accumulation of aerosols in the upper atmosphere would likely provide larger, time-variable signals (Hu *et al.*, 2013; Misra *et al.*, 2015). The ''ingredients'' for tectonic activity could also be inferred based on the elemental composition of the system. Planetary mass and radius, informed by the Fe, Si, and Mg abundance of the host star, could be used to constrain the interior composition and structure and the likelihood that a planet is tectonically active (Young *et al.*, 2014; Dorn *et al.*, 2015).

Additional contextual information to guide interpretation of a planet's habitability can come from atmospheric pressure. Rayleigh scattering could be used to indicate pressure above the visible surface (Benneke and Seager, 2012; von Paris *et al.*, 2013), whether that be the planetary surface or a cloud or haze layer, as is the case for Venus. However, interpretation of these measurements can be compromised by a surface that strongly absorbs or scatters in the blue, as is the case for Mars and Earth, respectively. Rayleigh scattering will be less useful for planets orbiting M dwarfs, as the host star produces little radiation at the blue end of the visible spectrum wherein Rayleigh scattering dominates, significantly lowering the S/N at these wavelengths (Meadows *et al.*, 2018).

Collision-induced features that are more sharply dependent on atmospheric pressure may provide an even more sensitive measurement of atmospheric pressure. For example, N_4 or O_4 features (N_2–N_2 or O_2–O_2) seen in the NIR could be used to indicate higher pressures (Misra *et al.*, 2014a; Schwieterman *et al.*, 2015b). N_4 absorbs strongly near 4.15 μm, just shortward of the strong 4.3 μm CO_2 band, and creates a strong spectral effect for abundances of $pN_2 >$ 0.5 bar (Schwieterman *et al.*, 2015b). The location of this strongly diagnostic feature in the infrared creates challenges for direct-imaging missions currently under study due to IWA and thermal background limitations to much shorter wavelengths. However, it remains perhaps the only feature capable of directly confirming large quantities of N_2 in an atmosphere (Schwieterman *et al.*, 2015b).

Finally, a census of atmospheric gases should be performed to inform planetary composition, chemistry, and climate. The composition of the atmosphere will be important for assessing the potential of the planet to generate photochemical false positives and for calculating surface fluxes required to maintain O_2 and O_3 in the planetary atmosphere. It will also help identify potential sources of nutrients and energy for life at the surface. The atmospheric composition, and in particular knowledge of greenhouse gas abundances and distributions, when combined with information on the incoming stellar flux, can also be used to model the climate of the planet and its potential surface habitability.

However, to determine the planet's atmospheric composition, we will need not only good observations, but also robust techniques for spectroscopic retrieval that can maximize information content from low spatial- and spectral-resolution data of poor sensitivity (*e.g.*, Irwin *et al.*, 2008; Madhusudhan and Seager, 2009; Benneke and Seager, 2012; Line *et al.*, 2014; Waldmann *et al.*, 2015). The observation type (*e.g.*, transmission, emission, and direct), wavelength coverage, and spectral resolution (among other factors) affect how complete a spectral search for atmospheric gases will be.

Degeneracies between physical parameters can also complicate inferences of the atmospheric composition. Such degeneracies have been described between the following: gas mixing ratios and temperature in secondary eclipse (Waldmann *et al.*, 2015); mixing ratios, planetary radius, and reference pressure in transit (Benneke and Seager, 2012; Heng and Kitzmann, 2017); mixing ratios and cloud coverage in transit (Barstow *et al.*, 2013); spectrally inactive gases (Benneke and Seager, 2012); and patchy clouds and mean molecular weight in transit (Line and Parmentier, 2016) to name a few. These degeneracies tend to arise as a result of low S/N observations that cover a narrow wavelength range. Consequently, many degeneracies can be lifted by using multiple instruments that together cover a wide wavelength (von Paris *et al.*, 2013b; Barstow *et al.*, 2015).

However, more work is needed to assess biases that arise due to the choice of parameterization in simple forward models (c.f. Feng *et al.*, 2016), as well as how additional information on the star, planet, and entire system of interest may help to enable a more complete understanding of the atmospheric composition in the event of continued exoplanet spectrum limitations.

4.3. Detecting the O_2 signal from a photosynthetic biosphere

On our own Earth, O_2 is abundant and evenly mixed throughout the atmosphere. The principal means of detecting O_2 is through its spectral features in the visible and NIR spectra at 0.69 (B-band), 0.76 (A-band), and 1.27 μm. On Earth-like exoplanets, it may be accessible to both transmission spectroscopy, which will likely probe above most of the deep atmosphere, and direct imaging, which can potentially sample the atmosphere all the way to the planetary surface. A spectral resolution of 70 would be needed to resolve the A-band at Earth-like abundances (Robinson *et al.*, 2016). The O_4 collisionally induced absorption features in the visible and NIR spectra may also be used as proxies for O_2, and may help constrain its concentration (Misra *et al.*, 2014a). They are weakly present in Earth's direct imaging spectrum (Tinetti *et al.*, 2006) but become much stronger when seen in transmission (Pallé *et al.*, 2009) or in denser O_2 atmospheres (Misra *et al.*, 2014a). O_2 is accessible to planned transmission spectroscopy and direct imaging at 0.76 and 1.27 μm, if the telescope and star will support it. But the 1.27 μm O_2/O_4 band may produce a stronger signal for planets orbiting late-type M dwarfs that have low output at wavelengths shortward of 0.8 μm, and so induce low planetary transmission or reflected light signals. Ground-based high-resolution spectroscopy may be able to detect O_2 on some habitable zone terrestrial planets orbiting M dwarfs by using the B- and A-bands in the visible spectrum (Snellen *et al.*, 2015; Lovis *et al.*, 2017).

Although obtaining well-constrained abundances for these O_2-bearing molecules may be challenging with first-generation observatories, observations of even the presence or absence of different bands of these molecules may help constrain O_2 abundances. The strong dependence of O_3 and O_4 features on O_2 concentrations could also be highly diagnostic of both chemistry and pressure. This combination of features can allow, for example, discrimination between atmospheres that contain 1% O_2, 20% O_2, and 90% O_2 (Section 4.4).

O_3 features in the UV could also point to the presence of O_2 in atmospheres with lower levels of O_2, when O_2 itself is not detectable. Figure 3 shows Proterozoic Earth with 0.01 bar of CO_2, 0.0003 bar of CH_4 and 0.1% the PAL of O_2, as suggested by recent studies of chromium isotopes in geological samples from the mid-Proterozoic (~1.8–0.8 Ga; Planavsky *et al.*, 2014b). O_2 itself is extremely weak in the spectrum, and is not discernable in this plot, but O_3 produces a relatively strong UV (Hartley) band from 0.2 to 0.3 μm that is not saturated, unlike the present Earth's, and so there is still a relatively high signal in the bottom of the band. Consequently, obtaining an accurate measurement of the flux level at the bottom of the band, needed to quantify abundance, is potentially easier than for current Earth-like conditions.

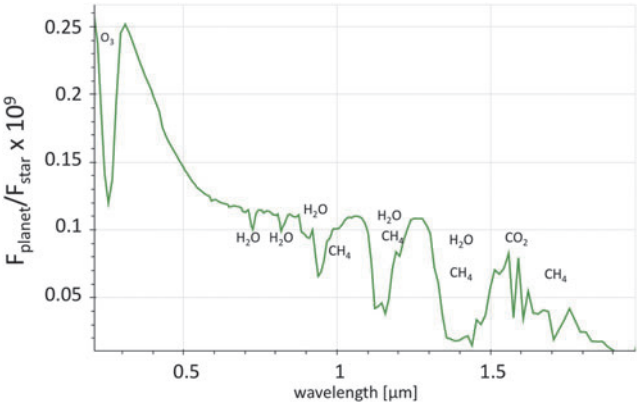

FIG. 3. Reflectance spectrum of the Proterozoic Earth assuming 0.1% PAL O_2 (Planavsky et al., 2014b), generated using the *Atmos* coupled climate-photochemical model (Arney *et al.*, 2016). Note the absence of strong O_2 features, but its photochemical byproduct O_3 produces a relatively strong feature in the UV from 0.2 to 0.3 μm. This figure was generated using the LUVOIR simulator available at https://asd.gsfc.nasa.gov/luvoir and described in Robinson *et al.*, (2016). LUVOIR, Large UltraViolet Optical Infrared Surveyor. (Credit: G. Arney)

Searching for O_2 in the atmosphere of Proxima Centauri b with ground-based telescopes may be possible in the next 5 years. Perhaps the most rapid path to this goal was suggested by Lovis *et al.* (2017), who proposed upgrades and the development of a coupling interface between the SPHERE high-contrast imager and the new ESPRESSO high-resolution spectrograph on the 8.2 m very large telescope. The combined high-contrast/high-resolution technique would provide the desired angular separation and contrast sensitivity of 10^{-7} in reflected light. This would make it possible to probe the O_2 bands at 0.63, 0.69, and 0.76 μm, along with water vapor at 0.72 μm and CH_4 at 0.75 μm. Lovis *et al.* (2017) calculated that a ~4-sigma detection of O_2 on an Earth-like Proxima Cen b could be made in about 60 nights of telescope time, spread over 3 years to observe the planet at maximum separation from the star. Even better results for the M dwarf habitable zone planets within 8 pc are likely possible with the ELTs slated for first light in the mid-to-late 2020s (*e.g.*, Rodler and López-Morales, 2014).

Future large space telescopes are being designed to detect O_2 for exoplanets orbiting F, G, and K stars. The design requirements for the HabEx and LUVOIR observatory concepts include the ability to detect O_2 in the atmospheres of neighboring Earth-like exoplanets (*e.g.*, Dalcanton *et al.*, 2015; Mennesson *et al.*, 2016). Whether a planet's O_2 spectral features are in practice detectable with these observatories will depend on several parameters, including the planet's O_2 abundance and the distance of the planet–star system to Earth. For example, an Earth-like exoplanet orbiting a Sun-like star at 20 pc would require integration times exceeding hundreds of hours to detect the O_2 A-band with sufficient S/N for even a 6.5 m (JWST-sized) optical telescope with 2 λ/D IWA coronagraphic capability. For planet–star systems farther than about 20 pc, this important spectral feature would be unobservable. A larger telescope (12.7 m) could detect O_2 out to about 40 pc given the same IWA—although, again, requiring very long integration times. Figure 4 shows the integration time as a function of wavelength centered on the O_2 A-band required for a 15 m LUVOIR-class telescope to obtain $S/N = 10$ for a planet identical to modern Earth orbiting a solar twin at a distance of 10 pc. The spectral resolution assumed here is 150. For these assumptions, 10 s of hours are required to obtain $S/N = 10$ across most of the wavelength ranges shown. Figure 5 shows the spectrum for the planet that could be obtained across the UV-VIS-NIR wavelength range in 30 h per coronagraphic bandpass for this same observatory. The significant increase in the size of the error bars at longer wavelengths is due to thermal emission from the telescope, which is assumed to be heated to 270 K. The spectral resolutions assumed for the UV-VIS-NIR channels for both Figures 4 and 5 are $R = 20$ for the UV ($\lambda < 0.4$ μm), $R = 150$ for the visible ($0.4 < \lambda < 0.85$), and $R = 100$ in the NIR ($\lambda > 0.85$). Both were simulated by using a coronagraph noise model based on the one described in Robinson *et al.* (2016).

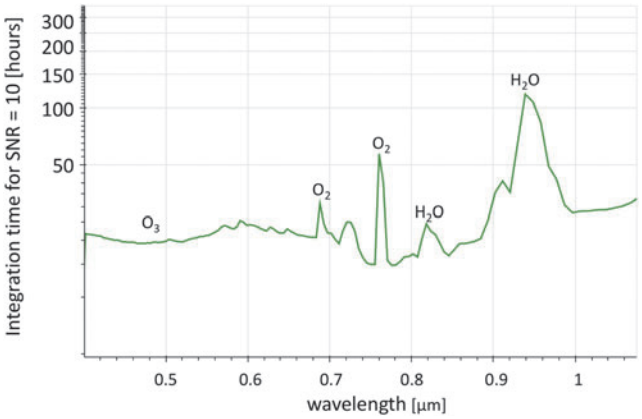

FIG. 4. The integration time as a function of wavelength required to obtain an S/N = 10 for the modern Earth orbiting a star at 10 pc for a 15 m LUVOIR-class telescope. The spectrum is roughly centered on the O_2 0.76 μm A-band. Spectral resolution = 150 in the visible region. S/N = 10 can be obtained in 10 s of hours at most wavelengths. This figure was generated using the LUVOIR simulator available at https://asd.gsfc.nasa.gov/luvoir and described in Robinson *et al.* (2016) (credit: G. Arney).

4.4. Discriminating false positives

Once O_2 is detected in a planetary spectrum, searching for additional observed environmental features to place the O_2 in context will aid in discriminating false positive O_2 from true biological O_2. Hereunder we describe currently known methods for observational discriminants for abiotic and biological O_2.

4.4.1. Identifying O_2 buildup from ocean loss. A proposed discriminant of the massive O_2-rich atmosphere produced by the loss of oceans of water during the premain sequence phase of the host star is the appearance of O_4 collisional complexes in the planet's spectrum (Schwieterman *et al.*, 2016); these features are caused by collision-induced O_2–O_2 absorption and are highly sensitive to atmospheric density. O_4 features occur at 0.345, 0.36, 0.38, 0.445, 0.475, 0.53, 0.57, and 0.63 μm in the visible and at 1.06 and 1.27 μm in the NIR (Greenblatt *et al.*, 1990; Hermans *et al.*, 1999; Maté *et al.*, 1999; Richard *et al.*, 2012; Schwieterman *et al.*, 2016). These strong O_4 features would indicate a O_2 atmosphere that is likely too massive to be biologically produced (Schwieterman *et al.*, 2016). In transmission observations, the NIR O_4 bands at 1.06 and 1.27 μm would be the best diagnostic spectral indicators of very high O_2 buildup ($pO_2 > 1$ bar; Misra *et al.*, 2014a; Schwieterman *et al.*, 2016). Figure 6 shows a simulated transmission spectrum of a high O_2 atmosphere with prominent O_4 bands. These longer wavelength bands are not as badly affected by the increase in Rayleigh scattering as their counterparts at shorter wavelengths.

Using the photon-limited JWST instrument model of Deming *et al.* (2009), Schwieterman *et al.* (2016) found that JWST/NIRISS could detect the 1.06 and 1.27 μm bands with an S/N of ~3, assuming 65-h integrations (10 transits) of an Earth-like planet around a star like GJ 876 (M4V; $R = 0.39$ $R_\odot$) (Fig. 7). However, other, more conservative estimates suggest that no features in any high-molecular weight atmosphere could be detected by JWST due to a systematic noise floor (*e.g.*, Greene *et al.*, 2016). For direct imaging observations, the shorter wavelength O_4 bands in the visible spectrum are now prominent against the Rayleigh scattering

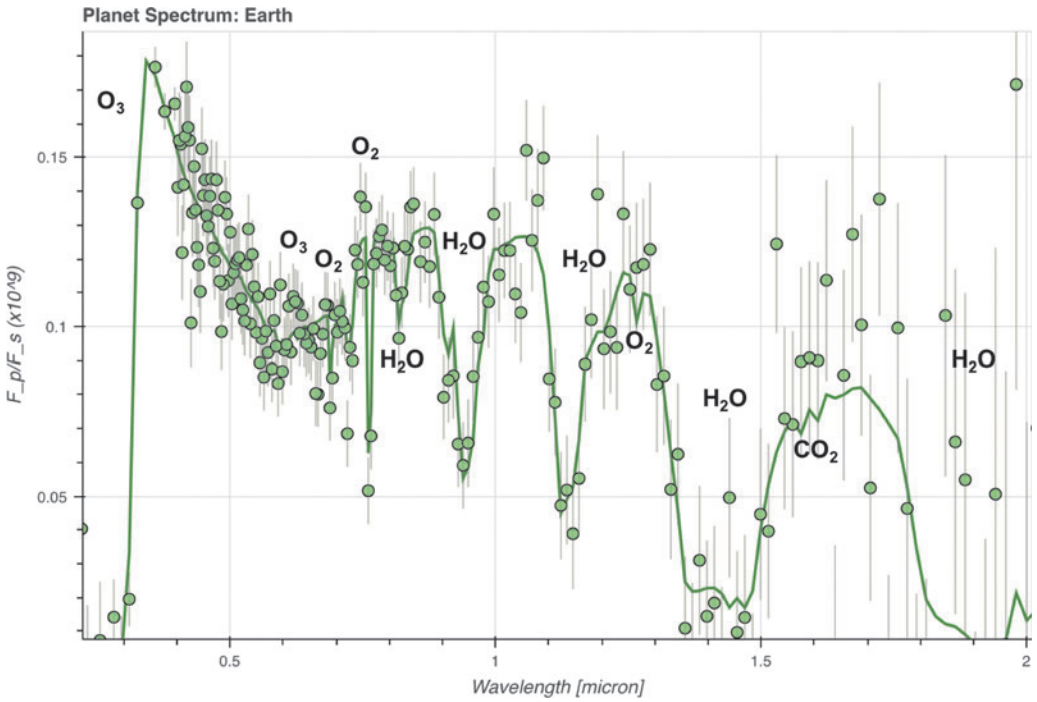

FIG. 5. The reflectance spectrum obtainable in 30 h by a 15 m space-based telescope observing modern Earth orbiting a Sun-like star at 10 pc. The gray bars denote the noise level, which increases significantly at wavelengths longward of 1.8 μm due to thermal radiation from the telescope, which is assumed to be heated to 270 K. This figure was generated using the LUVOIR simulator available at https://asd.gsfc.nasa.gov/luvoir and described in Robinson *et al.* (2016) (credit: G. Arney).

slope (Fig. 8). These bands can be obtained even within the shorter wavelength range constrained by the IWA for more distant targets, or for planets that are closer to their star as is the case for M and K habitable zone planets.

4.4.2. Identifying abiotic O_2/O_3 from CO_2 photolysis. An atmosphere with abiotic O_2 produced by CO_2 photolysis is more likely to have three additional features as follows: (1) a sufficient UV flux from the host star, (2) high CO_2 abundances in the atmosphere, and (3) photochemically produced CO (Hu *et al.*, 2012; Domagal-Goldman *et al.*, 2014; Tian *et al.*, 2014; Harman *et al.*, 2015; Gao *et al.*, 2015). A caveat to this scenario is the possible presence of catalysts that could accelerate the destruction of abiotically generated O_2—producing lower and potentially undetectable abiotic O_2 concentrations (Harman *et al.*, 2017). However, if these catalysts are not present, strong CO features in the presence of abundant O_2 and CO_2 could signal a false positive scenario (Schwieterman *et al.*, 2016; Meadows, 2017; bottom panels of Figs. 6 and 8). CO_2 exhibits strong spectral features near 1.65, 2, and 4.3 μm, and weaker bands occur near 0.78, 0.87, 1.05, and 1.2 μm (Rothman *et al.*, 2013). CO absorbs strongly near 2.35 and 4.6 μm. In practice, for exoplanet direct imaging space observatories that are not cryogenically cooled to lower than room temperature, simulations show that wavelengths longer than about 1.8 μm may be effectively unobservable, except for the brightest targets, due to the overwhelming thermal background of the telescope itself (Fig. 5). In this case, only the weaker 1.65 μm CO_2 band and none of the CO bands would be available. In addition, the NIR spectrograph channel may not extend to long enough wavelengths to access these features. This would make it challenging to identify this false positive in direct imaging. However, these longer wavelengths may be accessible to JWST. Assuming the most productive scenario known for abiotic O_2 generation from CO_2 photolysis ($pO_2 = 0.06$ bars) for an Earth-like M-dwarf HZ planet with a prebiotic N_2–CO_2–H_2O atmosphere (Harman *et al.*, 2015), CO and CO_2 bands shortward of 4.6 μm could be detected with an S/N ~ 3. This assumes a 65-h (10 transit) observation by JWST NIRISS (0.6–2.9 μm) and NIRSPEC (2.9–5.0 μm) and photon-limited noise (Fig. 9; Schwieterman *et al.*, 2016). As mentioned, the CO_2 and CO bands are the strongest features in the simulated spectrum. CO_2 may also be accessible at 15 μm by using thermal phase curve measurements of 10 to 100 s of hours on JWST, even for nontransiting planets, provided there is adequate day–night temperature difference (Meadows *et al.*, 2018).

4.4.3. Constraining abiotic O_2 from low N_2 inventories. The abiotic O_2 mechanism posited by Wordsworth and Pierrehumbert (2014) suggests that low noncondensing gas inventories on Earth-like planets could lead to abiotic O_2 buildup by lifting the tropospheric cold trap, allowing water to reach the stratosphere where it could be photolyzed. Atomic hydrogen would escape, leaving atomic oxygen behind to potentially build up in the atmosphere as O_2. However, this scenario could be ruled out if the noncondensing gas abundance could be directly constrained. Throughout Earth's long 4.5-billion-year history, the dominant noncondensable gas has been N_2. The N_4 (N_2–N_2; collision-induced absorption) feature overlaps with the 4.3 μm CO_2 band (Fig. 10), but absorbs over a much broader

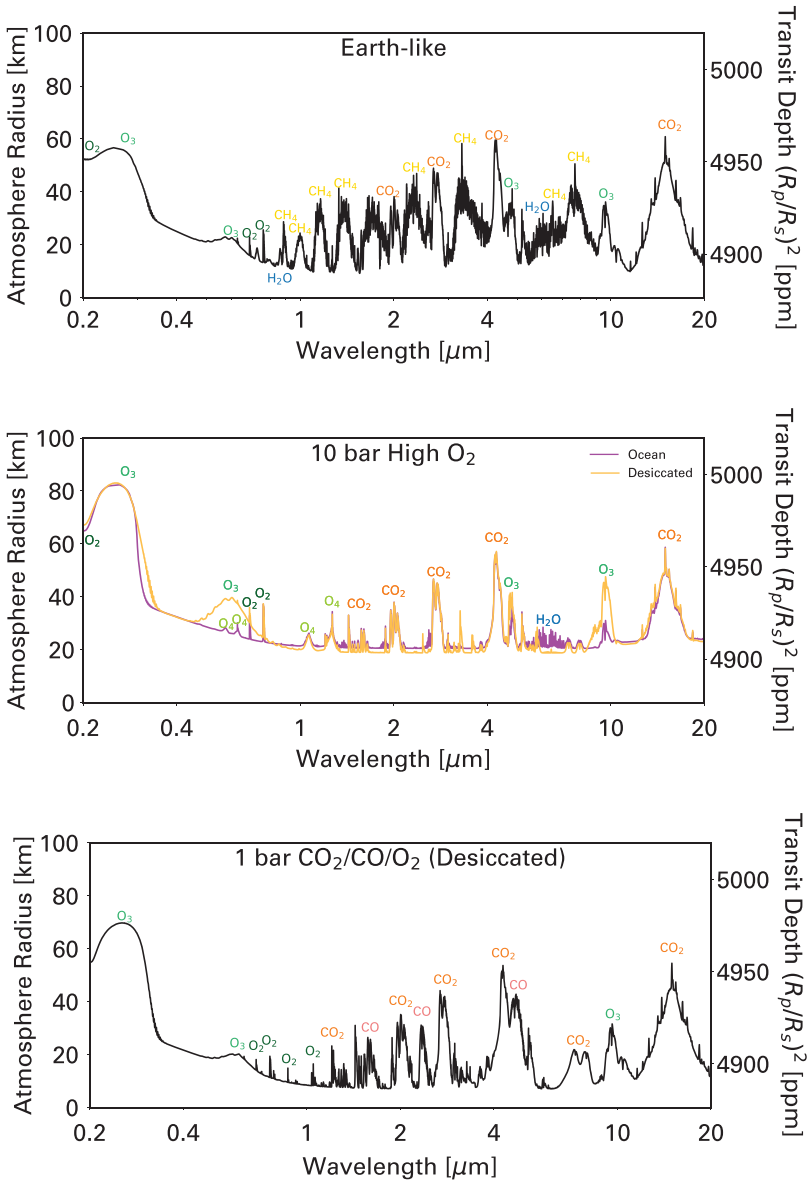

FIG. 6. Transit transmission spectra of potential planetary environments with different O_2 abundances for planet orbiting the M5.5V star Proxima Centauri (Meadows *et al.*, 2018). Illustrating spectral features that can help distinguish photosynthetic from abiotically generated O_2 in a planetary atmosphere. From top to bottom: self-consistent Earth-like atmosphere with 50% cloud cover (21% O_2); 10 bar abiotic O_2 (95% O_2) atmosphere produced by early ocean loss with ocean remaining (purple) and desiccated (orange); 1 bar desiccated CO_2/CO/O_2 atmosphere that has reached a kinetic–photochemical equilibrium between the photolysis rate of CO_2 and kinetics-limited recombination (15% O_2). Effective atmospheric radius in kilometers is on the left *y* axes and transit depth is shown on the right *y* axes. The photosynthetic source for O_2 in the Earth-like case is made more likely by the presence of O_2/O_3, water, and methane. High O_2 cases with and without water are distinguished by the presence of O_4, and the behavior of the 0.5–0.7 µm Chappuis band that is sensitive to tropospheric O_3, which is more abundant in the desiccated case. The desiccated chemical equilibrium atmosphere is easily distinguished by its high levels of CO.

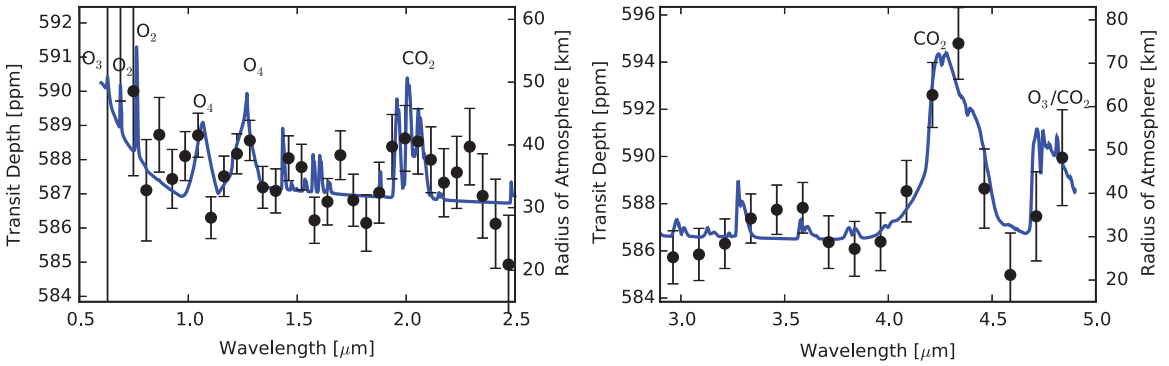

FIG. 7. Synthetic transmission spectrum of high O_2 atmosphere with NIR O_4 features at 1.06 and 1.27 µm. The model atmosphere is a hypothetical 100 bar O_2 atmosphere left behind by massive H escape during premain sequence evolution (Luger and Barnes, 2015). Data and error bars (1σ) for simulated JWST-NIRISS (left) and JWST-NIRSpec (right) were calculated with the noise model of Deming *et al.* (2009) assuming 65 h integrations (10 transits of an Earth-size planet around GJ876) and photon-limited noise. Figure adapted from Schwieterman *et al.* (2016). JWST, James Webb Space Telescope; NIR, near-infrared.

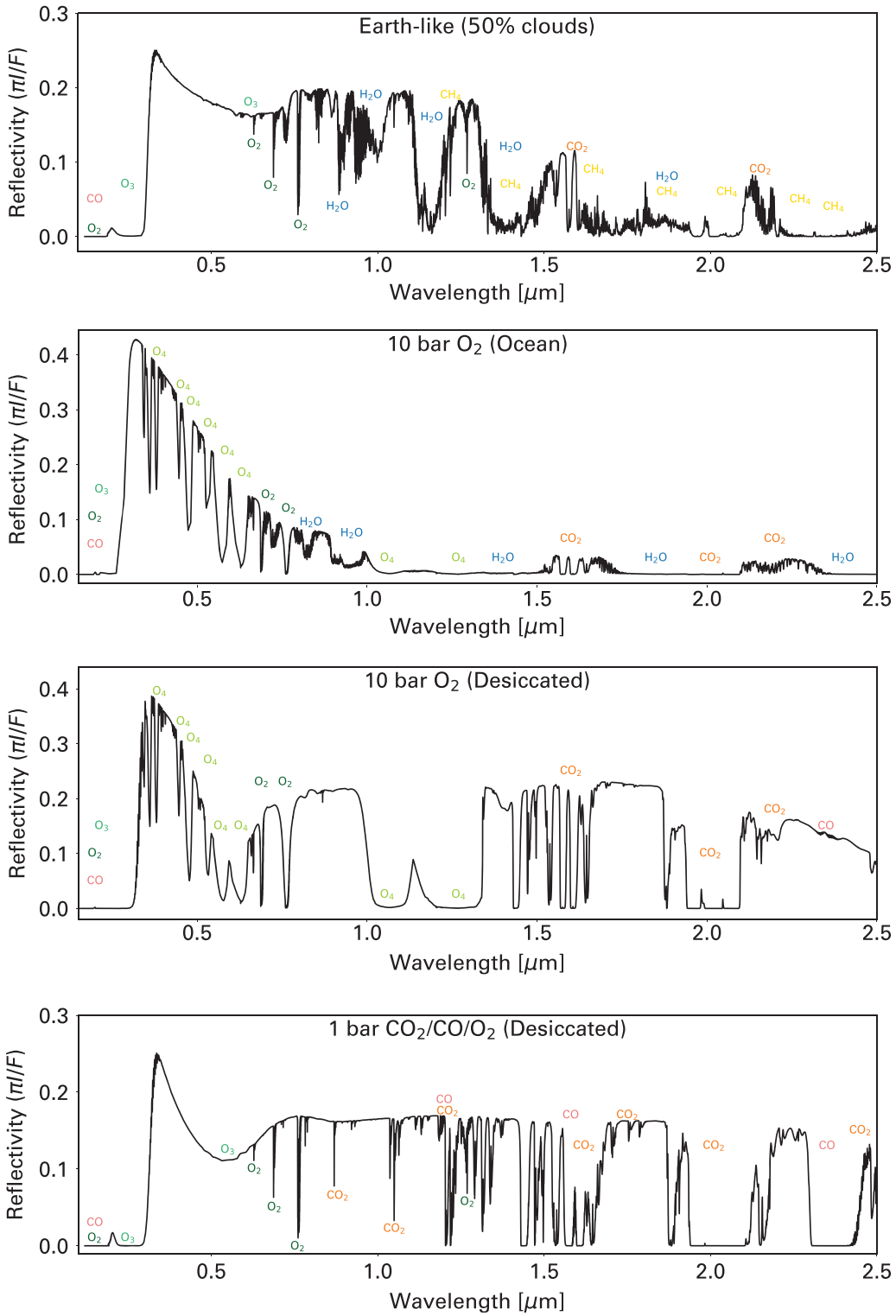

FIG. 8. Reflected light spectra of potential Proxima Centauri b climates from top to bottom: self-consistent Earth-like atmosphere with 50% cloud cover, 10 bar abiotic O_2 atmosphere with ocean, 10 bar desiccated O_2 atmosphere, 1 bar desiccated CO_2/CO/O_2 atmosphere in kinetic–photochemical equilibrium (see Meadows *et al.*, 2018). The O_2 content in these atmospheres is produced from very different mechanisms: Earth O_2 is biological, the 10 bar abiotic O_2 atmospheres result from the super-luminous premain sequence evolution of the planet's M dwarf host star, and the last atmosphere is a 1 bar CO_2 atmosphere that has <1 ppm hydrogen, resulting in a slow CO_2 recombination timescale compared with its photolysis rate and Earth-like levels of O_2. However, because hydrogen is also required to destroy ozone (O_3), this atmosphere exhibits more O_3 and a stronger Chappuis O_3 band at $\sim$0.6 µm. The 10 bar O_2 atmospheres are easily distinguished from Earth-like atmospheres by their deep, wide O_2–O_2 (O_4) collision-induced absorption bands. Moist versus desiccated abiotic O_2 cases are distinguished primarily by the presence or absence of water features. Around M dwarf stars, Earth-like planets with biological and geophysical sources of methane result in longer atmospheric lifetimes and correspondingly deep, observable methane features (Segura *et al.*, 2005; Rugheimer *et al.*, 2015).

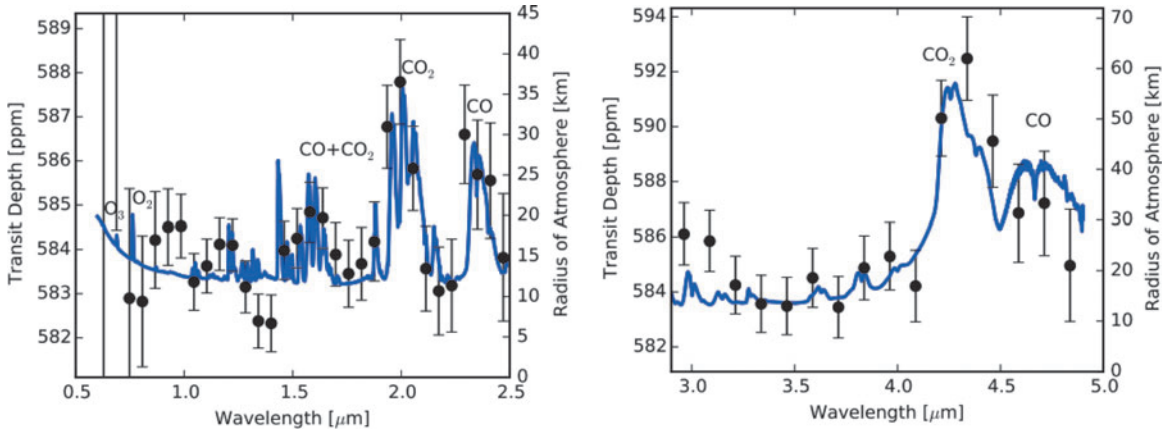

FIG. 9. Synthetic transmission spectrum with photochemical O_2 and CO features. Model prebiotic atmosphere in photochemical equilibrium around GJ876 from Harman *et al.* (2015) containing ∼6% abiotic O_2 and ∼1% CO. Data and error bars (1σ) for simulated JWST-NIRISS (left) and JWST-NIRSpec (right) were calculated with the noise model of Deming *et al.* (2009), assuming 65 h integrations (10 transits of an Earth-size planet around GJ876) and photon-limited noise. Figure adapted from Schwieterman *et al.* (2016).

region (Lafferty *et al.*, 1996; Schwieterman *et al.*, 2015b). In reflected light spectra, the influence of N_4 on the 4.1 μm region is strongly dependent on N_2 abundance beyond $P_0 = 0.5$ bars (see Fig. 9; Schwieterman *et al.*, 2015b). There is also a much weaker harmonic N_4 band at 2.1 μm (Shapiro and Gush, 1966), seen in the reflectance spectra of nitrogen ices on outer solar system bodies (Grundy and Fink, 1991), but this band is currently poorly characterized and probably too weak to create a measurable impact on plausible planetary atmospheres.

The spectral transmission depths due to N_4 will vary, depending on the abundance of CO_2 and the overall mean molecular weight of the atmosphere, but it can reach 10 ppm for an N_2-dominated atmosphere for an Earth-size planet transiting an M5V ($R = 0.2\ R_\odot$) star. Larger transmission depths may be possible for atmospheres with a significant low-molecular weight component such as H_2 (Schwieterman *et al.*, 2015b).

4.5. Considerations for super-Earths

The majority of the mentioned discussion assumed that the habitable planet being observed was close to Earth size, but terrestrial planets may have radii up to 1.5 times that of Earth (Weiss and Marcy, 2014; Rogers, 2015; Fulton *et al.*, 2017). These super-Earth atmospheres may be less Earth-like, as the larger masses of terrestrial super-Earths increase their ability to retain lighter molecules, such as H_2, and/or to produce substantial outgassing of heavier gases such as H_2O and CO_2. However, if their atmospheres are more Earth-like, the increased radius and gravity of larger planets will affect the detectability of O_2 (c.f. Rauer *et al.*, 2011) and false

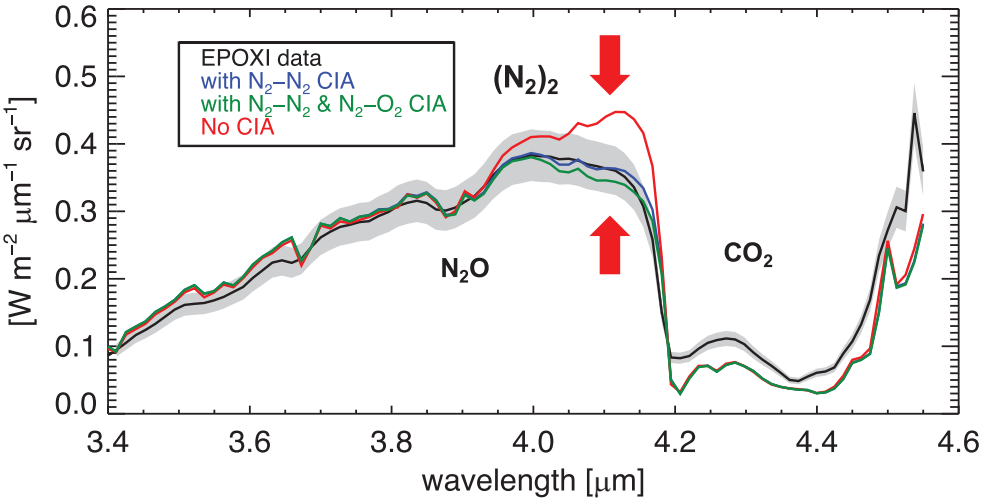

FIG. 10. The impact of N_4 absorption in Earth's disk-averaged NIR spectrum. This plot shows the spectral differences between the cases with N_4 absorption (blue and green) and the case without it (red), when compared with the EPOXI observations of the Earth in this wavelength range (black). N_4 is clearly required to match the observed spectrum of the Earth near 4.1 μm. The gray band shows the calibration uncertainty for the EPOXI data (Klassen *et al.*, 2008). Figure adapted from Schwieterman *et al.* (2015b).

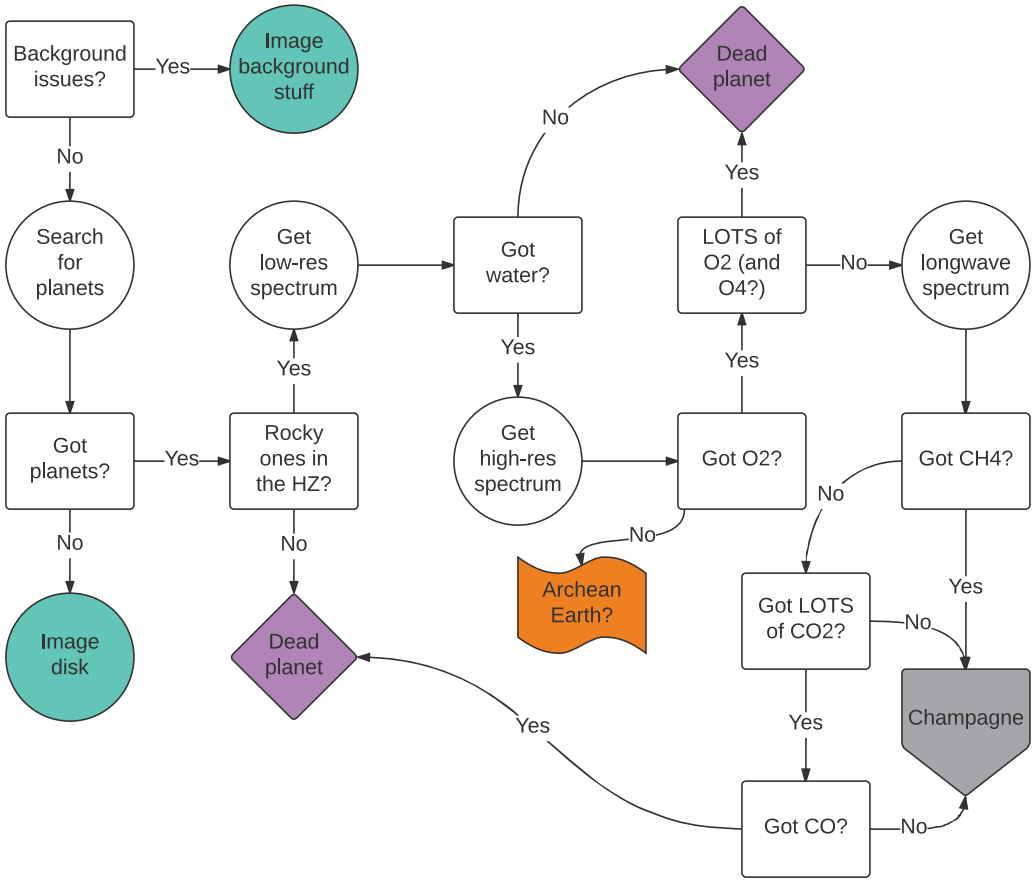

FIG. 11. A flowchart cartoon of possible steps to be taken in searching for a photosynthetic biosphere on an extrasolar planet, and in interpreting detection or nondetection of O_2. The process starts with a survey of the background, and includes searching not only for the biosignature O_2 but also for other atmospheric molecules such as CH_4, which may support the biological interpretation of any O_2 observed, and CO_2 and O_4, which may indicate abiotic processes that could be producing O_2 without life. This flowchart also shows how observations of molecules other than O_2 can be used to classify environments like the early Earth's, thereby identifying potentially habitable, but anoxic environments. (Credit: Shawn Domagal-Goldman).

positive discriminators to different degrees. For direct imaging, a larger planet will require smaller integration times for detection of spectral features, roughly proportional to $1/R_p^2$ such that a 1.5 Earth radius super-Earth needs a little less than half the exposure time of an Earth radius planet. Enhanced gravity will decrease the scale height of the planetary atmosphere, as scale height H is proportional to 1/g. This may allow a planet to emit to space at a higher temperature (Kopparapu *et al.*, 2014) potentially increasing detectability at thermal wavelengths, but will not affect the observability of features at nonthermal wavelengths, assuming the overall surface pressure of the atmosphere remained constant.

For transmission, however, the decrease in scale height due to enhanced gravity would decrease the size of molecular features in the spectrum and, therefore, their detectability. However, the increase in planet radius partially acts to offset this effect. After the scaling relationship for the size of molecule features observed in transmission (Winn, 2010), it can be shown that the size of molecular features in the atmosphere of a super-Earth scales inversely with the ratio of the density of the super-Earth to Earth. If we again assume a super-Earth with a 1.5 Earth's radius, and a mass of 4 Earth masses, then the size of molecular features in the transmission spectrum would be 84% that of an Earth-sized planet of similar atmospheric composition.

5. An Integrated Observing Strategy for Finding and Identifying an Oxygenic Photosynthetic Biosphere

The broad steps in a potential observing strategy to identify O_2-bearing, inhabited terrestrial planets include detecting the planet in the presence of astronomical noise sources, preliminary characterization of the planet, detection of O_2, the search for false positives, and using the combination of planetary environmental characteristics and the results of the false positive searches to discriminate between biotic and abiotic sources for O_2. These steps for a space-based direct imaging telescope are illustrated in Figure 11, including discriminating an O_2-bearing world from a habitable, but anoxic, world like the early Earth. For these steps, we specifically assume that spatially resolved spectra over the field of view are possible, and that the mission can observe in the UV–NIR wavelength range. Other observing strategies may be more appropriate for observatories without these capabilities. Although this strategy will be most

appropriate for a telescope concept such as LUVOIR or HabEx, a similar or complementary approach to characterizing planetary environmental context and searching for biosignatures could be developed for MIR-FIR direct imaging, or for transit spectroscopy.

Note that we assume that the target stars are well characterized before the planet search, including, if possible, measurements of UV radiation and stellar activity, especially if the mission is not capable of obtaining stellar characterization measurements itself. For missions with UV spectroscopic capabilities, observations of the star bracketing the exoplanet observations would also be particularly valuable for interpretation of the planet's photochemistry, and its biosignatures (*e.g.*, Segura *et al.*, 2005, 2010).

It is also important to note that a large direct imaging telescope that will observe nearby (<20 pc) habitable zone Earth-sized planets predominantly orbiting F–K dwarfs will have to search for planetary targets as part of the initial mission activities. This is because nearby nontransiting planets orbiting more Sun-like stars have yet to be found by existing observations and surveys. Instead, these surveys have either found Earth-sized planets transiting distant (800–1000 pc) stars (*e.g.*, *Kepler*), or orbiting nearby late type M dwarfs (ground-based surveys, *e.g.*, Berta-Thompson *et al.*, 2015), where the discovered planets may be far too close to their star to be observed in direct imaging (*e.g.*, TRAPPIST-1; Gillon *et al.*, 2017). The space-based astrometric *Gaia* mission does not have the precision to detect terrestrial planets (Sozzetti, 2014). Finding nontransiting Earth-sized planets around nearby stars with current ground-based RV searches is extremely challenging, and also favors M dwarf candidates, with the most promising discovery so far being Proxima Centauri b (Anglada-Escudé *et al.*, 2016).

For upcoming missions, the transiting exoplanet survey satellite (Ricker *et al.*, 2015) may also find $\sim$10 nearby planets transiting nearby planets transiting M dwarfs (Sullivan *et al.*, 2015), and the ESA PLATO mission will search for transiting planets orbiting G and K dwarfs (Rauer *et al.*, 2014). However, the probability of finding a transiting Earth around a G dwarf is 1 in 200, and there are only 20 G dwarfs within 10 pc. So although there may be a handful of suitable targets for direct imaging (most likely orbiting K dwarfs) found by transit or RV observations before the launch of large direct imaging telescopes, the majority of habitable zone planets characterized by large direct-imaging telescopes will have also been discovered by these missions in their first 1–2 years of operation.

5.1. Planet detection

As discussed, one of the first challenges will be to detect the planet and discriminate it from potential background sources, which include ''exozodiacal dust'' (''exozodi'') from the planetary system dust disk, and background stars and galaxies. This could be done either with multiepoch photometric observations—revisits to the planetary system spread out over a longer time period—or with multiwavelength imaging in a single visit. Multiepoch observations will acquire the position of the planet against the background sky, which will more robustly discriminate the planet from background sources. These observations will constrain the planet's orbit and help determine mass and orbital parameters such as semimajor axis and eccentricity (Stapelfeldt *et al.*, 2015), which are crucial for determining whether the planet is in the habitable zone of its parent star. An alternative, potentially faster method of planet detection would be to use a single visit with multiwavelength imaging to look for point sources near the star. Additional information could then be used to determine whether these sources are more or less likely to be planets or background objects. For example, point sources detected within the exo-zodi are more likely to be planets than sources detected outside the disk. During this detection phase, photometric colors—or low-resolution spatially resolved spectra across the field of view—could enhance our ability to discriminate planets from astrophysical noise sources such as stars, brown dwarfs, and galaxies (Seager *et al.*, 2015), but a definitive determination of whether the planet is in the HZ would not be possible with a single visit.

5.2. Preliminary characterization

If the planet is detected in a single visit, then planetary photometric colors could be used to not only discriminate planets from background noise sources but also to attempt to discriminate between different types of terrestrial or more volatile rich (*e.g.*, mini-Neptune) planets. However, planetary environments are rich and complex, especially terrestrial planets that may display inhomogeneous surfaces, volatiles in multiple phases, and a broad diversity of atmospheric compositions. Colors would, therefore, provide only a possibly ambiguous initial classification (*e.g.*, Crow *et al.*, 2011; Livengood *et al.*, 2011; Hegde and Kaltenegger, 2013), because strong degeneracies in environment types that fit a given region of the color–color diagram likely exist (Krissansen-Totton *et al.*, 2016b), and the overlying atmosphere and clouds can modify surface colors (Schwieterman *et al.*, 2015a). Therefore, a potentially more valuable initial method of discriminating between planetary targets would be to obtain low-resolution ($R \sim 10$) spectra to search for molecules with broad absorption features, such as water vapor and O_3 in the visible and NIR spectra. Although neither the H_2O nor the O_3 Chappuis band would be uniquely diagnostic of oceans or life, respectively, the detection of either of these gases would be consistent with habitability and biology. Water vapor features are present near the O_2 A-band at 0.72 and 0.85 μm, and at increasing strength at 0.95, 1.14, and 1.4 μm.

If multiepoch photometric/astrometric observations are used for detection, then the initial characterization could include determining the planet's orbit and, therefore, semimajor axis and eccentricity. These parameters will help determine the planet's insolation, which will constrain climate models of the planet, and indicate whether or not the planet is in the habitable zone. Mass determination may be done by using or combining any follow-up or existing RV data with the observed position of the planet. The orientation of the dust disk may also help break the RV degeneracy between mass and inclination of the planetary system, although an orbital solution for the planet will do this also. At this stage, direct constraints on planetary radius will only be possible if the planet transits, or if ground- or space-based MIR observations are able to observe the target (*e.g.*, Quanz *et al.*, 2015). Size or mass may help indicate planets that are

more likely to be terrestrial (Rogers, 2015; Fulton *et al.*, 2017), and size and mass will constrain its density.

Time-resolved, multiwavelength photometry, even in the limited wavelength range of a single 20% coronagraphic bandpass, and for a single visit, could be used to map the planet and search for surface inhomogeneities that may indicate a terrestrial planet (Cowan *et al.*, 2009; Kawahara and Fujii, 2010; Lustig-Yaeger *et al.*, 2017). This mapping could also take advantage of time-resolved segments of a long-exposure spectroscopic observation whose primary purpose is to search for atmospheric constituents (Lustig-Yaeger *et al.*, 2017). For multiepoch observations, photometry at NIR wavelengths (optimally at 0.8–0.9 μm, and/or between water bands in the 1.0–1.4 μm region) comparing brightness at different points in the planet's orbit near gibbous and crescent phases could be used to search for ocean glint (Robinson *et al.*, 2010, 2014). Glint observations may be challenging; observing the planet when half-illuminated produces a maximum separation between star and planet, but the crescent phase occurs at a close apparent separation between star and planet, when the planet is, therefore, more likely to be interior to the IWA. In addition, the inclination of the orbit of the planet to the observer must be closer to edge-on than face-on, otherwise glint will not be observed. Even so, LUVOIR-class missions with 16 m mirrors may be able to search for glint for a subset of their terrestrial planets (Meadows *et al.*, 2018). Detection of any of these planetary characteristics—terrestrial mass or size, interesting maps, glint, or hints at the presence of water or O_3—would be enough to motivate further observations at higher spectral resolutions ($R \sim 150$).

5.3. The search for an oxygenic photosynthetic biosphere with high-resolution spectroscopy

Once a promising target has been identified, significant time could be invested in obtaining a high-resolution spectrum. At an R of $\sim$150, individual features from many molecules can be detected. O_2 should be sought, and if detected, deeper observations should be taken to constrain its concentration. The O_2 A-band at 0.76 μm is a narrow but deep feature at Earthlike concentrations, and the wavelength range and spectral resolution of potential future direct imaging observatories such as HabEx and LUVOIR will be designed to detect it in the atmospheres of our exoplanetary neighbors. Detecting the O_3 UV Hartley band (0.2–0.3 μm) may reveal the presence of O_2 when O_2 concentrations are otherwise too low to produce observable spectral features. This may be the case for planets like the Proterozoic Earth, where its 0.1% PAL O_2 is likely not detectable in reflected light in the visible–NIR spectra with currently anticipated instrumentation, but the O_3 Hartley band produces a deep feature for λ <0.3 μm (Fig. 3). As stars are fainter in the UV spectrum, longer integration times, wider bandpasses, or both, will be required to obtain high S/N observations of UV absorption features. The 30-h observation of an Earth twin planet at 10 pc with a 15 m telescope shown in Figure 6 returned adequate S/N in the UV, but for a spectral resolution of 20, significantly lower than the $R = 150$ assumed for the visible channel. If O_2 or O_3 is not detected, but H_2O is, this may not indicate a lifeless planet, but rather one with a different dominant metabolism (*e.g.*, methane-producing), or an environment that leads to a false negative, as would have been the case for the early Earth.

5.4. Further characterization and elimination of false positives

Other molecules should be sought to characterize the planetary environment, including O_3, O_4, CO, CO_2, and CH_4, as well as clouds and aerosols. The presence of O_4, especially for a planet orbiting a late-type M dwarf, may indicate that any O_2 present is the result of ocean loss and H escape due to H_2O photolysis (Luger and Barnes, 2015; Schwieterman *et al.*, 2016). In direct imaging, the strong O_4 collision-induced absorption features in the visible region (0.34–0.7 μm) would likely be detectable in the same observations required to detect the O_2 (0.76 μm), and could potentially be in the same coronagraphic bandpass. However, for transmission observations, O_4 bands in the NIR at 1.06 and 1.27 μm would be more detectable than those in the visible, as they are less affected by the increase in atmospheric opacity engendered by Rayleigh scattering at shorter wavelengths. Note also that ground-based high-resolution spectroscopy will not be able to observe the broad features of O_4 collisionally induced absorption, and so this false positive discriminator is not available to this technique.

If abundant CH_4 is observed with O_2, this would make most photochemical false positives less likely, as CH_4 is a sink for photochemically generated O_2. It is also less likely to build up to detectable levels in the massive O_2 atmospheres of ocean loss planets. Thus, detection of CH_4 in an atmosphere with O_2 features would make ocean loss and photochemical false positives less likely, and suggest a high O_2 replenishment rate and a likely biogenic source of the O_2. However, CH_4 features may be challenging to observe at modern Earth-like concentrations because methane's strongest features are longward of 2.5 μm, where telescopic thermal emission and IWA issues may preclude observation. Weaker bands in the visible region (0.7–0.9 μm) would require abundances of CH_4 in excess of those seen in Earth's atmosphere today, but are within the wavelength ranges anticipated for direct imaging spacecraft and ground-based high-resolution spectroscopy (Lovis *et al.*, 2017). Indeed, as described in section 2.2, there may have been no period in Earth's history wherein both O_2 and CH_4 coexisted in high abundance (Olsen *et al.*, 2016; Reinhard *et al.*, 2017).

Photochemical generation of O_2 and/or O_3 from CO_2 photolysis (Hu *et al.*, 2012; Domagal-Goldman *et al.*, 2014; Gao *et al.*, 2015; Harman *et al.*, 2015) should be associated with high amounts of CO_2 and CO in the planetary atmosphere. CO_2 has a weak band near 1.6 μm, which is undetectable on modern Earth but would likely have a strong feature for atmospheres with enough CO_2 to produce O_2 or O_3 photochemically (Domagal-Goldman *et al.*, 2014). CO_2 has a much stronger band at 4.2 μm, although the latter band will be difficult to access for warm telescopes (either ground-based or actively heated space-based telescopes) dominated by thermal radiation in this spectral region. CO also absorbs near 2.35 and 4.6 μm, where a warm (room temperature) mirror will also preclude observation. In addition, these longer wavelengths will require a large telescope diameter to avoid falling within the IWA for observatories cold enough to see them, or an extremely large starshade to provide suppression at those longer wavelengths.

Transit transmission observations, however, from the ground and JWST may allow access to longer wavelengths in the near term, compared with direct imaging techniques, and ground-based observations may also be attempted for the 2.35 μm CO band (c.f. Snellen *et al.*, 2013).

5.5. Detailed planet characterization and the search for secondary biosignatures

If all known false positive mechanisms for the presence of O_2 have been eliminated, and if photochemical models and the presence of sinks such as CH_4 suggest a high O_2 flux into the environment, then this would make a biogenic source more likely. This conclusion can be bolstered not only by ruling out false positives, but also by searching for secondary confirmation of the dominant metabolism that is believed to have been discovered. In the case of oxygenic photosynthesis, this could come in the form of secondary biosignatures such as detection of a red edge or other pigment-associated feature in multi-wavelength, time-resolved photometric mapping (Lustig-Yaeger, 2017) or in seasonally varying concentrations of O_2, CO_2, or CH_4 (Meadows, 2008; Reinhard *et al.*, 2016), or the detection of other biosignatures such as N_2O (Schwieterman *et al.*, 2018). Eventually, other biosignatures and their false positives will be identified and sought, and the measurements obtained from any single planet will be placed in the broader context of similar measurements made on other worlds (Fujii *et al.*, 2018; Walker *et al.*, 2018), further informing our understanding of comparative planetology, and the prevalence of life in the Universe.

6. Discussion and Lessons Learned

The recent detailed study of O_2 has advanced the field of biosignatures by providing an in-depth exploration of the impact a planetary environment can have on our ability to detect and recognize biosignatures. O_2 can, therefore, serve as an exemplar for a more generalized framework for biosignature detection, and this concept is further developed for other biosignatures in the work of Catling *et al.* (2018).

O_2 has long been considered an excellent biosignature, in part, because of its characteristics in the modern Earth environment. O_2 is an abundant gas that is stable against photolysis, and so it is evenly mixed throughout the atmosphere. This increases its detectability even in the presence of clouds, or when using techniques such as transmission spectroscopy that do not probe deep into the planetary atmosphere (Meadows, 2017). In addition, for Earth, there are no known abiotic processes that would produce it in large abundance.

The study of O_2 as a biosignature draws heavily on our understanding of how Earth and life coevolved over time, and the planetary processes that may have suppressed or enabled oxygen's rise from a trace gas to one of the principal components of our planetary atmosphere (Lyons *et al.*, 2014). We have learned that a biosignature will not build up to detectable levels in a planetary atmosphere simply because life evolved, but rather as a result of the complex interactions of life with the planet and the host star, often for billions of years. The study of O_2 throughout Earth's history has introduced the concept of a false negative (*e.g.*, Reinhard *et al.*, 2017), wherein life is present, but its mark on the environment is unseen.

Similarly, the field of exoplanets has revealed stars and worlds, with evolutionary sequences that are likely very different to Earth's around the Sun. By modeling these environments and their interactions, researchers have opened up a possibility that was previously unthinkable for an Earth-like environment—that O_2 (or O_3) could be generated in a planetary environment without the action of life (*e.g.*, Hu *et al.*, 2012; Domagal-Goldman *et al.*, 2014; Wordsworth and Pierrehumbert, 2014; Gao *et al.*, 2015; Harman *et al.*, 2015; Luger and Barnes, 2015; Narita *et al.*, 2015; Tian, 2015).

Our improved understanding of false negatives for O_2 may help us optimize target selection for the search for life on exoplanets, and it points to a rich area for future work. Being able to assess a target's false negative potential could be an integral part of the search for life, and it is an important foundation for interpreting what we do (and do not) detect. To advance this area of research, we will need to develop an improved understanding of planetary and stellar characteristics that may lead to false negatives, and the observational discriminants that might reveal them.

As specific examples, O_2 may have only overwhelmed (or outlasted) its environmental sinks on Earth fairly recently, and so perhaps it would be prudent to prioritize older planets to allow time for a photosynthetic metabolism to develop and leave its footprint. The interior and crustal composition of the planet may make it more likely for reducing gases to be present. Understanding how observed stellar composition affects terrestrial planet composition (*e.g.*, Young *et al.*, 2014; Dorn *et al.*, 2015; Unterborn and Panero, 2017), how planetary orbit and star may affect tidal heating, interior structure, and surface heat flow (*e.g.*, Driscoll and Barnes, 2015), and searching for the presence of reducing gases or tectonic/volcanic activity through atmospheric gases or aerosols (*e.g.*, Kaltenegger and Sasselov, 2009; Kaltenegger *et al.*, 2010; Misra *et al.*, 2015), may all be important for constraining possible sinks for O_2. Similarly, understanding the incoming stellar UV spectrum and activity levels and the overall impact on atmospheric chemistry and photolysis rates would also help identify processes that may enhance or suppress the detectability of a biosignature (*e.g.*, Segura *et al.*, 2003, 2005; Grenfell *et al.*, 2007, 2014; Rugheimer *et al.*, 2013, 2015). In this example, young volcanically active planets with strongly reducing atmospheres may not represent good targets for the search for oxygenic photosynthesis.

Our improved understanding of the star–planet processes that may lead to false positives for O_2 has only strengthened the robustness of O_2 as a biosignature. This knowledge can also inform our target selection, and prepare us to observe planetary characteristics that will help discriminate whether observed O_2 has a biological or abiotic origin. We now know of several abiotic planetary processes that will generate O_2 or O_3 for planets orbiting M dwarfs (Wordsworth and Pierrehumbert, 2014; Domagal-Goldman *et al.*, 2014; Tian *et al.*, 2014; Harman *et al.*, 2015; Luger and Barnes, 2015; Tian, 2015). There are very likely more, and the search should continue for additional false positive mechanisms using modeling efforts or observations of exo-Venuses (Kane *et al.*, 2014; Berta-Thompson *et al.*, 2015; Gillon *et al.*, 2017), which may provide observational tests for some of the proposed mechanisms. In particular, planetary environmental modeling is critically needed to anticipate the challenges we will face in interpreting the spectra obtained by future observatories.

Identification of potential false positives helps guide recommendations for the wavelength ranges and spectral resolutions needed to discriminate them, and allows us to design a more sophisticated and robust observing sequence for the search for life to exoplanets. We now know that the detection of any potential biosignature gas in an exoplanet's atmosphere must be considered in the context of the complex web of interrelated processes that shape the broader planetary environment. For example: where is the planet relative to its star's habitable zone? What is the activity level of the star, and what types of photochemistry can it drive? Does the planet show other signs of habitability such as liquid surface water from water vapor or glint? What other gases are present? What fluxes are required to maintain the observed concentrations of the biosignatures gas? What false positive mechanisms may explain the observed possible biosignatures? Are there other potential biosignatures present?

If O_2 is detected, other characteristics of the planet can be observed to rule out false positive mechanisms, and to bolster the likelihood that the O_2 comes from a planetary biosphere. Choosing an older planet would again not only decrease the probability of a false negative but decrease the likelihood of a false positive as well, as an initially high atmospheric O_2 abundance from ocean loss becomes sequestered or lost to space (Chassefière, 1996; Schaefer *et al.*, 2016).

Searching for a combination of gases or planetary characteristics, and not finding some of them, could also be powerful. Detecting O_2 and water or ocean glint, without O_4, can be more robust than O_2 alone. Detecting O_2, CH_4, and water, or detecting O_2 and water without strong CO_2 or CO, are both stronger detections. Finally, searching for secondary biosignatures of photosynthesis such as the red edge (Gates *et al.*, 1965) and seasonal variability (Meadows, 2008; Reinhard *et al.*, 2016) also strengthens the case for O_2 as a biosignature. Searching for the multiple planetary characteristics that strengthen the likelihood that O_2 is a biosignature requires observations that span the broadest possible spectral range, and that are tailored for the strengths of the observing mode chosen, whether that is direct imaging, transmission, or high-resolution spectroscopy.

In closing, oxygenic photosynthesis evolved a metabolism that harvested light from the parent star to split water and fix carbon, and it ultimately rose to sculpt the history of our planet and produce the strongest biosignatures on Earth today. However, the absence of O_2 throughout much of Earth's history also encourages us to learn more about biosignatures that are not tied to oxygenic photosynthesis, to be better prepared for environments in which oxygenic photosynthesis has either not evolved or not yet overwhelmed sinks for O_2. Yet for any new biosignatures that are identified, the same process that has been developed for the study of O_2 should still be applied. Biosignatures cannot exist distinct from the environment that harbors them. Understanding the impact of the environment on the detectability of biosignatures, and the potential generation of false positives, will be an important activity for future biosignature research.

7. Conclusions

The study of O_2 has catalyzed the interdisciplinary synthesis of research in early Earth science with the modeling of star–planet interactions in exoplanet science, to greatly expand our understanding of biosignatures in the context of their environments. The early simplistic view that O_2 alone constituted the most robust biosignature for detection of life on exoplanets has given way to a more sophisticated understanding of the impact of a planetary environment on the detectability and interpretation of O_2 in a planetary spectrum. The delay between the advent of oxygenic photosynthesis on Earth and the rise of atmospheric O_2 to modern levels reveal a false negative process where life is present, but not detectable, due to suppression of the biosignature by the planetary environment. Future research into false negative processes may reveal planetary processes and observational discriminants that could help identify planets on which biosignatures are likely suppressed. This could potentially support exoplanet target selection for biosignature searches and inform the interpretation of observed planetary spectra. Similarly, the study of false positives has revealed stellar and planetary characteristics that may cause O_2 to build up abiotically in a planetary environment and identified observational discriminants for those processes. This allows observations of O_2 in a planetary spectrum to be more robustly interpreted as a biosignature by searching for and ruling out false positive mechanisms. The processes to identify false negatives and positives for O_2 serve as an exemplar for a more generalized process for biosignature detection that should be applied to other novel biosignatures.

Acknowledgments

We thank the NASA Astrobiology Program and the Nexus for Exoplanet System Science (NExSS) for their support for the NExSS Exoplanet Biosignatures Workshop. Conversations at this workshop, held in the northern hemisphere summer of 2016, formed the basis for the drafting of the five review articles in this issue. We thank Mary Voytek, the senior scientist for Astrobiology, for her leadership of NExSS, without whom this interdisciplinary community synthesis would not have been possible, and her feedback on our organization of the workshop and articles. We would like to thank Tanai Cardona and Mercedes Lopez-Morales who provided helpful comments on a draft of this article during the NExSS-hosted open community discussion forum. We thank two anonymous reviewers for thoughtful comments that helped us improve this article. V.S.M., G.N.A., M.N.P., S.D.-G., E.W.S., A.P.L., J.L.Y., and R.D. were supported by NASA Astrobiology Institute's Virtual Planetary Laboratory under Cooperative Agreement Number NNA13AA93A. C.T.R., E.W.S., and T.W.L. received support from the NASA Astrobiology Institute Alternative Earths team under Cooperative Agreement Number NNA15BB03A. S.D.S. acknowledges support from NASA Exobiology grant NNX15AM07G. E.W.S. is also grateful for support from the NASA Postdoctoral Program, administered by the Universities Space Research Association.

Author Disclosure Statement

No competing financial interests exist.

References

Airapetian, V.S., Glocer, A., Gronoff, G., Hébrard, E., and Danchi, W. (2016) Prebiotic chemistry and atmospheric warming of early Earth by an active young Sun. *Nat Geosci* 9:52.

Airapetian, V.S., Glocer, A., Khazanov, G.V., Loyd, R.O.P., France, K., Sojka, J., Danchi, W.C., and Liemohn, M.W. (2017) How hospitable are space weather affected habitable zones? The role of ion escape. *Astrophys J Lett* 836:L3.

Allen, J.P. and Williams, J.C. (1998) Photosynthetic reaction centers. *FEBS Lett* 438:5–9.

Anbar, A.D., Duan, Y., Lyons, T.W., Arnold, G.L., Kendall, B., Creaser, R.A., Kaufman, A.J., Gordon, G.W., Scott, C., Garvin, J., and Buick, R. (2007) A whiff of oxygen before the great oxidation event? *Science (New York, N.Y.)* 317:1903–1906.

Anglada-Escudé, G., Amado, P.J., Barnes, J., Berdiñas, Z.M., Butler, R.P., Coleman, G.A.L., de la Cueva, I., Dreizler, S., Endl, M., Giesers, B., Jeffers, S.V., Jenkins, J.S., Jones, H.R.A., Kiraga, M., Kürster, M., López-González, M.J., Marvin, C.J., Morales, N., Morin, J., Nelson, R.P., Ortiz, J.L., Ofir, A., Paardekooper, S.-J., Reiners, A., Rodríguez, E., Rodríguez-López, C., Sarmiento, L.F., Strachan, J.P., Tsapras, Y., Tuomi, M., and Zechmeister, M. (2016) A terrestrial planet candidate in a temperate orbit around Proxima Centauri. *Nature* 536:437–440.

Arney, G., Domagal-Goldman, S.D., Meadows, V.S., Wolf, E.T., Schwieterman, E., Charnay, B., Clare, M., Hébrard, E., and Trainer, M.G. (2016) The pale orange dot: the spectrum and habitability of hazy Archean earth. *Astrobiology* 16:873–899.

Arney, G.N., Meadows, V.S., Domagal-Goldman, S.D., Deming, D., Robinson, T.D., Tovar, G., Wolf, E.T., and Schwieterman, E. (2017) Pale orange dots: the impact of organic haze on the habitability and detectability of earthlike exoplanets. *Astrophys J* 836:49.

Baraffe, I., Chabrier, G., Allard, F., and Hauschildt, P. (1998) Evolutionary models for solar metallicity low-mass stars: mass-magnitude relationships and color-magnitude diagrams. *A&A* 337:403–412.

Barnes, R., Deitrick, R., Luger, R., Driscoll, P.E., Quinn, T.R., Fleming, D.P., Guyer, B., McDonald, D.V., Meadows, V.S., Arney, G., Crisp, D., Domagal-Goldman, S.D., Lincowski, A., Lustig-Yaeger, J., and Schwieterman, E. (2018) The habitability of Proxima Centauri b I: evolutionary scenarios. arXiv:1608.06919v2.

Barstow, J.K., Aigrain, S., Irwin, P.G., Fletcher, L.N., and Lee, J.M. (2013). Constraining the atmosphere of GJ 1214b using an optimal estimation technique. *MNRAS* 434:2616–2628.

Barstow, J.K., Aigrain, S., Irwin, P.G., Kendrew, S., and Fletcher, L.N. (2015) Transit spectroscopy with James Webb Space Telescope: systematics, starspots and stitching. *MNRAS* 448: 2546–2561. Chicago.

Bekker, A., Holland, H.D., Wang, P.-L., Rumble, D., Stein, H.J., Hannah, J.L., Coetzee, L.L., and Beukes, N.J. (2004) Dating the rise of atmospheric oxygen. *Nature* 427:117–120.

Bell, E.A., Boehnke, P., Hopkins-Wielicki, M.D., and Harrison, T.M. (2015) Distinguishing primary and secondary inclusion assemblages in Jack Hills zircons. *Lithos* 234:15–26.

Benneke, B. and Seager, S. (2012) Atmospheric retrieval for super-earths: uniquely constraining the atmospheric composition with transmission spectroscopy. *Astrophys J* 753:100.

Berner, R.A. (1982) Burial of organic carbon and pyrite sulfur in the modern ocean: its geochemical and environmental significance. *Am J Sci* 282:451–473.

Berner, R.A. (2004) *The Phanerozoic Carbon Cycle: CO_2 and O_2*. Oxford University Press, New York.

Berner, R.A. (2006) GEOCARBSULF: a combined model for Phanerozoic atmospheric O_2 and CO_2. *Geochim Cosmochim Acta* 70:5653–5664.

Berta-Thompson, Z.K., Irwin, J., Charbonneau, D., Newton, E.R., Dittmann, J.A., Astudillo-Defru, N., Bonfils X, Gillon M, Jehin E, Stark AA, Stalder B, Bouchy F, Delfosse X, Forveille T, Lovis C, Mayor M, Neves V, Pepe F, Santos NC, Udry S, and Wünsche, A. (2015) A rocky planet transiting a nearby low-mass star. *Nature* 527:204–207.

Bétrémieux, Y. and Kaltenegger, L. (2013) Transmission spectrum of earth as a transiting exoplanet from the ultraviolet to the near-infrared. *Astrophys J Lett* 772:L31.

Bétrémieux, Y. and Kaltenegger, L. (2014) Impact of atmospheric refraction: how deeply can we probe exo-earth's atmospheres during primary eclipse observations? *ApJ* 791:7.

Bolcar, M.R., Balasubramanian, K., Clampin, M., Crooke, J., Feinberg, L., Postman, M., Quijada, M., Rauscher, B., Redding, D., Rioux, N., Shaklan, S., Stahl, H.P., Stahle, C., and Thronson, H. (2015) Technology development for the Advanced Technology Large Aperture Space Telescope (ATLAST) as a candidate large UV-Optical-Infrared (LUVOIR) surveyor. In *UV/Optical/IR Space Telescopes: Innovative Technologies and Concepts VII, Proc. SPIE*, edited by H.A. MacEwen, and J.B. Breckinridge, p 960209. DOI: 10.1117/12.2188559

Brandl, B.R., Feldt, M., Glasse, A., Guedel, M., Heikamp, S., Kenworthy, M., Lenzen, R., Meyer, M.R., Molster, F., Paalvast, S., Pantin, E.J., Quanz, S.P., Schmalz, E., Stuik, R., Venema, L., and Waelkens, C. (2014) METIS: the mid-infrared E-ELT imager and spectrograph. In *Ground-Based and Airborne Instrumentation for Astronomy V,* Proc. SPIE 914721.

Buick, R., Dunlop, J.S.R., and Groves, D.I. (1981) Stromatolite recognition in ancient rocks: an appraisal of irregularly laminated structures in an Early Archaean chert-barite unit from North Pole, Western Australia. *Alcheringa* 5:161–181.

Bryant, D.A., Costas, A.M.G., Maresca, J.A., Chew, A.G.M., Klatt, C.G., Bateson, M.M., Tallon, L.J., Hostetler, J., Nelson, W.C., Heidelberg, J.F., and Ward, D.M. (2007) Candidatus Chloracidobacterium thermophilum: an aerobic phototrophic acidobacterium. *Science* 317:523–526.

Buick, R. (2007) Did the Proterozoic 'Canfield Ocean' cause a laughing gas greenhouse? *Geobiology* 5:97–100.

Canfield, D.E. (2005) The early history of atmospheric oxygen: homage to Robert M. Garrels. *Ann Rev Earth Planet Sci* 33: 1–36.

Canfield, D.E., Rosing, M.T., and Bjerrum, C. (2006) Early anaerobic metabolisms. *Phil Trans R Soc B* 361:1819–1836.

Cardona, T. (2015) A fresh look at the evolution and diversification of photochemical reaction centers. *Photosynth Res* 126:111–134.

Cardona, T. (2016) Reconstructing the origin of oxygenic photosynthesis: do assembly and photoactivation recapitulate evolution? *Front Plant Sci* 7:257.

Cardona, T. (2017) Photosystem II is a chimera of reaction centers. *J Mol Evol* 84:149–151.

Carroll, S.B. (2001) Chance and necessity: the evolution of morphological complexity and diversity. *Nature* 409:1102–1109.

Catling, D. and Kasting, J.F. (2007) Planetary atmospheres and life. In *Planets and Life: The Emerging Science of Astrobiology*, edited by W.T. Sullivan and J. Baross, Cambridge University Press, Cambridge, UK, pp 91–116.

Catling, D.C., Zahnle, K.J., and McKay, C.P. (2001) Biogenic methane, hydrogen escape, and the irreversible oxidation of early Earth. *Science* 293:839–843.

Catling, D.C., Glein, C.R., Zahnle, K.J., and McKay, C.P. (2005) Why O_2 is required by complex life on habitable planets and the concept of planetary ''oxygenation time.'' *Astrobiology* 5: 415–438.

Catling, D.C., J. Krissansen-Totton, J., Kiang, N.Y., Crisp, D., Robinson, T.D., DasSarma, S., Rushby, A.J., Del Genio, A., Bains, W., and Domagal-Goldman, S. (2018) Exoplanet biosignatures: a framework for their assessment. *Astrobiology* 18:709–738.

Chassefière, E. (1996) Hydrodynamic escape of hydrogen from a hot water-rich atmosphere: the case of Venus. *J Geophys Res Planets* 101:26039–26056.

Cole, D.B., Reinhard, C.T., Wang, X., Gueguen, B., Halverson, G.P., Gibson, T., Hodgskiss, M.S., McKenzie, N.R., Lyons, T.W., and Planavsky, N.J. (2016) A shale-hosted Cr isotope record of low atmospheric oxygen during the Proterozoic. *Geology* 44:555–558.

Collinson, G.A., Frahm, R.A., Glocer, A., Coates, A.J., Grebowsky, J.M., Barabash, S., Domagal-Goldman, S.D., Fedorov, A., Futaana, Y., Gilbert, L.K., and Khazanov, G. (2016) The electric wind of Venus: a global and persistent ''polar wind''-like ambipolar electric field sufficient for the direct escape of heavy ionospheric ions. *Geophys Res Lett* 43:5926–5934.

Cowan, N.B., Agol, E., Meadows, V.S., Robinson, T., Livengood, T.A., Deming, D., Lisse, C.M., A'Hearn, M.F., Wellnitz, D.D., Seager, S., and Charbonneau, D. (2009) Alien maps of an ocean-bearing world. *Astrophys J* 700:915.

Cowan, N.B., Greene, T., Angerhausen, D., Batalha, N.E., Clampin, M., Colón, K., Crossfield, I.J.M., Fortney, J.J., Gaudi, B.S., Harrington, J., and Iro, N. (2015) Characterizing transiting planet atmospheres through 2025. *Publ Astron Soc Pac* 127:311.

Cowan, N.B. and Strait, T.E. (2013) Determining reflectance spectra of surfaces and clouds on exoplanets. *ApJ* 765:L17.

Cox, C. and Munk, W. (1954) Measurement of the roughness of the sea surface from photographs of the sun's glitter. *JOSA* 44:838–850.

Crossfield, I.J. (2016) Exoplanet atmospheres and giant ground-based telescopes. arXiv preprint arXiv:1604.06458.

Crow, C.A., McFadden, L.A., Robinson, T., Meadows, V.S., Livengood, T.A., Hewagama, T., Barry, R.K., Deming, L.D., Lisse, C.M., and Wellnitz, D. (2011) Views from EPOXI: colors in our solar system as an analog for extrasolar planets. *Astrophys J* 729:130.

Crowe, S.A., Døssing, L.N., Beukes, N.J., Bau, M., Kruger, S.J., Frei, R., and Canfield, D.E. (2013) Atmospheric oxygenation three billion years ago. *Nature* 501:535–538.

Czaja, A.D., Johnson, C.M., Roden, E.E., Beard, B.L., Voegelin, A.R., Nägler, T.F., Beukes, N.J., and Wille, M. (2012) Evidence for free oxygen in the Neoarchean ocean based on coupled iron-molybdenum isotope fractionation. *Geochim Cosmochim Acta* 86:118–137.

Dalcanton, J., Seager, S., Aigrain, S., Hirata, C., Battel, S., Mather, J., Brandt, N., Postman, M., Conroy, C., Redding, D., Feinberg, L., Schiminiovich, D., Gezari, S., Stahl, H.P., Guyon, O., Tumilinson, J., and Harris, W. (2015) *From Cosmic Birth to Living Earths: the Future of UVOIR Space Astronomy. From Cosmic Births to Living Earths Report*. Association for Research in Astronomy, Washington, DC. www.hdstvision.org/report.

de Bergh, C., Bezard, B., Owen, T., Crisp, D., Maillard, J.P., and Lutz, B.L. (1991) Deuterium on venus: observations from earth. *Science* 251:547–549.

Deming, D., Seager, S., Winn, J., Miller-Ricci, E., Clampin, M., Lindler, D., Greene, T., Charbonneau, D., Laughlin, G., Ricker, G., Latham, D., and Ennico, K. (2009) Discovery and characterization of transiting super earths using an all-sky transit survey and follow-up by the James Webb Space Telescope. *PASP* 121:952–967.

Des Marais, D.J., Harwit, M.O., Jucks, K.W., Kasting, J.F., Lin, D.N.C., Lunine, J.I., Schneider, J., Seager, S., Traub, W.A., and Woolf, N.J. (2002) Remote sensing of planetary properties and biosignatures on extrasolar terrestrial planets. *Astrobiology* 2:153–181.

Des Marais, D.J., Strauss, H., Summons, R.E., and Hayes, J.M. (1992) Carbon isotope evidence for the stepwise oxidation of the Proterozoic environment. *Nature* v359:p605–p609.

de Wit, J., Wakeford, H.R., Gillon, M., Lewis, N.K., Valenti, J.A., Demory, B.-O., Burgasser, A.J., Burdanov, A., Delrez, L., Jehin, E., Lederer, S.M., Queloz, D., Triaud, A.H., and Van Grootel, V. (2016) A combined transmission spectrum of the Earth-sized exoplanets TRAPPIST-1 b and c. *Nature* 537: 69–72.

Dodd, M.S., Papineau, D., Grenne, T., Slack, J.F., Rittner, M., Pirajno, F., O'Neil, J., and Little, C.T. (2017) Evidence for early life in Earth's oldest hydrothermal vent precipitates. *Nature* 543:60–64.

Domagal-Goldman, S.D. and Meadows, V.S. (2010) Abiotic buildup of ozone. *Pathways Towards Habitable Planets, Astronomical Society of the Pacific Conference Series* 430: 152–157.

Domagal-Goldman, S.D., Meadows, V.S., Claire, M.W., and Kasting, J.F. (2011) Using biogenic sulfur gases as remotely detectable biosignatures on anoxic planets. *Astrobiology* 11: 419–441.

Domagal-Goldman, S.D., Segura, A., Claire, M.W., Robinson, T.D., and Meadows, V.S. (2014) Abiotic ozone and oxygen in atmospheres similar to prebiotic earth. *ApJ* 792:43.

Dong, C., Lingam, M., Ma, Y., and Cohen, O. (2017) Is Proxima Centauri b habitable? A study of atmospheric loss. *Astrophys J Lett* 837:L26.

Dorn, C., Khan, A., Heng, K., Connolly, J.A., Alibert, Y., Benz, W., and Tackley, P. (2015) Can we constrain the interior structure of rocky exoplanets from mass and radius measurements? *A&A* 577:A83.

Dressing, C.D. and Charbonneau, D. (2015) The occurrence of potentially habitable planets orbiting M dwarfs estimated from the full Kepler dataset and an empirical measurement of the detection sensitivity. *Astrophys J* 807:45.

Driese, S.G., Jirsa, M.A., Ren, M., Brantley, S.L., Sheldon, N.D., Parker, D., and Schmitz, M. (2011) Neoarchean paleoweathering of tonalite and metabasalt: implications for reconstructions of 2.69Ga early terrestrial ecosystems and paleoatmospheric chemistry. *Precambrian Res* 189:1–17.

Driscoll, P.E. and Barnes, R. (2015) Tidal heating of Earth-like exoplanets around M stars: thermal, magnetic, and orbital evolutions. *Astrobiology* 15:739–760.

Etiope, G. and Sherwood Lollar, B. (2013) Abiotic methane on Earth. *Rev Geophys* 51:276–299.

Falkowski, P., Scholes, R.J., Boyle, E., Canadell, J., Canfield, D., Elser, J., Gruber, N., Hibbard, K., Hogberg, P., Linder, S., Mackenzie, F.T., Moore, B., Pederson, T., Rosenthal, Y., Seitzinger, S., Smetacek, V., and Steffan, W. (2000) The global carbon cycle: a test of our knowledge of earth as a system. *Science* 290:291–296.

Farquhar, J. (2000) Atmospheric influence of earth's earliest sulfur cycle. *Science* 289:756–758.

Farquhar, J., Savarino, J., Airieau, S., and Thiemens, M.H. (2001) Observation of wavelength-sensitive mass-independent sulfur isotope effects during SO_2 photolysis: Implications for the early atmosphere. *J Geophys Res Planets* 106:829–839.

Feng, Y.K., Line, M.R., Fortney, J.J., Stevenson, K.B., Bean, J., Kreidberg, L., and Parmentier, V. (2016) The impact of non-uniform thermal structure on the interpretation of exoplanet emission spectra. *Astrophys J* 829:52.

Field, C.B., Behrenfeld, M.J., Randerson, J.T., and Falkowski, P. (1998) Primary production of the biosphere: integrating terrestrial and oceanic components. *Science* 281:237–240.

Fortney, J.J. (2005) The effect of condensates on the characterization of transiting planet atmospheres with transmission spectroscopy. *MNRAS* 364:649–653.

Fujii, Y., Angerhausen, D., Deitrick, R., Domagal-Goldman. S., Grenfell, J.L., Hori, Y., Kane, S.R., Palle, E., Rauer, H., Siegler, N., Stapelfeldt, K., and Stevenson, K.B. (2018) Exoplanet biosignatures: observational prospects. *Astrobiology* 18: 739–778.

Fulton, B.J., Petigura, E.A., Howard, A.W., Isaacson, H., Marcy, G.W., Cargile, P.A., Hebb, L., Weiss, L.M., Johnson, J.A., Morton, T.D., and Sinukoff, E. (2017) The California-Kepler Survey. III. A Gap in the Radius Distribution of Small Planets. arXiv preprint arXiv:1703.10375.

Gao, P., Hu, R., Robinson, T.D., Li, C., and Yung, Y.L. (2015) Stability of CO2 atmospheres on dessicated M dwarf exoplanets. *ApJ* 806:249.

Garcia-Sage, K., Glocer, A., Drake, J.J., Gronoff, G., and Cohen, O. (2017) On the magnetic protection of the atmosphere of Proxima Centauri b. *Astrophys J* 844:L13.

Gates, D.M., Keegan, H.J., Schleter, J.C. and Weidner, V.R. (1965) Spectral properties of plants. *Appl Opt* 4:11–20.

Gebauer, S., Grenfell, J.L., Stock, J.W., Lehmann, R., Godolt, M., von Paris, P., and Rauer, H. (2017) Evolution of earth-like extrasolar planetary atmospheres: assessing the atmospheres and biospheres of early earth analog planets with a coupled atmosphere biogeochemical model. *Astrobiology* 17:27–54.

Gillon, M., Jehin, E., Lederer, S.M., Delrez, L., de Wit, J., Burdanov, A., Van Grootel, V., Burgasser, A., Triaud, A.H.M.J., Opitom, C., Demory, B.-O., Sahu, D.K., Gagliuffi, D.B., Magain, P., Queloz, D., and Queloz, D. (2016) Temperate Earth-sized planets transiting a nearby ultracool dwarf star. *Nature* 533:221–224.

Gillon, M., Triaud, A.H.M.J., Demory, B.-O., Jehin, E., Agol, E., Deck, K.M., Lederer, S.M., de Wit, J., Burdanov, A., Ingalls, J.G., Bolmont, E., Leconte, J., Raymond, S.N., Selsis, F., Turbet, M., Barkaoui, K., Burgasser, A., Burleigh, M.R., Carey, S.J., Chaushev, A., Copperwheat, C.M., Delrez, L., Fernandes, C.S., Holdsworth, D.L., Kotze, E.J., Van Grootel, V., Almleaky, Y., Benkhaldoun, Z., Magain, P., and Queloz, D. (2017) Seven temperate terrestrial planets around the nearby ultracool dwarf star TRAPPIST-1. *Nature* 542:456–460.

Greenblatt, G.D., Orlando, J.J., Burkholder, J.B., and Ravishankara, A.R. (1990) Absorption measurements of oxygen between 330 and 1140 nm. *JGR* 95:18577.

Greene, T.P., Line, M.R., Montero, C., Fortney, J.J., Lustig-Yaeger, J., and Luther, K. (2016) Characterizing transiting exoplanet atmospheres with JWST. *Astrophys J* 817:17.

Grenfell, J.L., Gebauer, S., von Paris, P., Godolt, M., and Rauer, H. (2014) Sensitivity of biosignatures on Earth-like planets orbiting in the habitable zone of cool M-dwarf Stars to varying stellar UV radiation and surface biomass emissions. *P&SS* 98:66–76.

Grenfell, J.L., Stracke, B., von Paris, P., Patzer, B., Titz, R., Segura, A., and Rauer, H. (2007) The response of atmospheric chemistry on earthlike planets around F, G and K Stars to small variations in orbital distance. *P&SS* 55:661–671.

Grenfell, J.L., Grießmeier, J.M., von Paris, P., Patzer, A.B.C., Lammer, H., Stracke, B., Gebauer, S., Schreier, F., and Rauer, H. (2012) Response of atmospheric biomarkers to NOx-induced photochemistry generated by stellar cosmic rays for Earth-like planets in the habitable zone of M dwarf stars. *Astrobiology* 12:1109–1122.

Grundy, W.M. and Fink, U. (1991) A new spectrum of Triton near the time of the Voyager encounter. *Icarus* 93:379–385.

Hall, A.E., Schulze, E.D., and Lange, O.L. (1976) Current perspectives of steady-state stomatal responses to environment. In: *Water and Plant Life*. Springer, Berlin Heidelberg, pp 169–188.

Hamano, K., Abe, Y., and Genda, H. (2013) Emergence of two types of terrestrial planet on solidification of magma ocean. *Nature* 497:607–610.

Harman, C.E., Schwieterman, E.W., Schottelkotte, J.C., and Kasting, J.F. (2015) Abiotic O_2 levels on planets around F, G, K, and M stars: possible false positives for life? *ApJ* 812:137.

Harman, C.E., Felton, R.C., Domagal-Goldman, S., and Kasting, J.F. (2017) Oxygen false positives in terrestrial planetary atmospheres: an update from the front lines. In *Habitable Worlds 2017: A System Science Workshop*, November 13–17, 2017, Laramie Wyoming, LPI Contribution No. 2042.

Hazen, R.M., Papineau, D., Bleeker, W., Downs, R.T., Ferry, J.M., McCoy, T.J., Sverjensky, D.A. and Yang, H. (2008) Review Paper. Mineral evolution. *Am Mineral* 93:1693–1720.

Hegde, S. and Kaltenegger, L. (2013) Colors of extreme exo-Earth environments. *Astrobiology* 13:47–56.

Hegde, S., Paulino-Lima, I.G., Kent, R., Kaltenegger, L., and Rothschild, L. (2015) Surface biosignatures of exo-Earths: remote detection of extraterrestrial life. *PNAS* 112:3886–3891.

Heng, K. and Kitzmann, D. (2017) The theory of transmission spectra revisited: a semi-analytical method for interpreting WFC3 data and an unresolved challenge. *MNRAS* 470:2972.

Hermans, C., Vandaele, A.C., Carleer, M., Fally, S., Colin, R., Jenouvrier, A., Coquart, B., and Mérienne, M.-F. (1999) Absorption cross-sections of atmospheric constituents: NO2, O2, and H2O. *Environ Sci Pollut Res* 6:151–158.

Hitchcock, D.R. and Lovelock, J.E. (1967) Life detection by atmospheric analysis. *Icarus* 7:149–159.

Hu, R., Seager, S., and Bains, W. (2012) Photochemistry in terrestrial exoplanet atmospheres. I. Photochemistry model and benchmark cases. *ApJ* 761:166.

Hu, R., Seager, S., and Bains, W. (2013) Photochemistry in terrestrial exoplanet atmospheres. II. H2S and SO2 photochemistry in anoxic atmospheres. *Astrophys J* 769:6.

Hunten, D.M. (1973) The escape of light gases from planetary atmospheres. *J Atmos Sci* 30:1481–1494.

Igamberdiev, A.U. and Lea, P.J. (2006) Land plants equilibrate O_2 and CO_2 concentrations in the atmosphere. *Photosynth Res* 87:177–194.

Irwin, P.G.J., Teanby, N.A., De Kok, R., Fletcher, L.N., Howett, C.J.A., Tsang, C.C.C., Wilson, C.F., Calcutt, S.B., Nixon, C.A., and Parrish, P.D. (2008) The NEMESIS planetary atmosphere radiative transfer and retrieval tool. *J Quant Spectrosc Radiat Transfer* 109:1136–1150.

Izon, G., Zerkle, A.L., Williford, K.H., Farquhar, J., Poulton, S.W., and Claire, M.W. (2017) Biological regulation of at-

mospheric chemistry en route to planetary oxygenation. *Proc Natl Acad Sci U S A* 114:E2571–E2579.

Johnson, B. and Goldblatt, C. (2015) The nitrogen budget of Earth. *Earth Sci Rev* 148:150–173.

Kaltenegger, L., Henning, W.G., and Sasselov, D.D. (2010) Detecting volcanism on extrasolar planets. *Astron J* 140: 1370.

Kaltenegger, L. and Sasselov, D. (2009) Detecting planetary geochemical cycles on exoplanets: atmospheric signatures and the case of SO2. *Astrophys J* 708:1162.

Kane, S.R., Kopparapu, R.K., and Domagal-Goldman, S.D. (2014) On the frequency of potential Venus analogs from Kepler data. *Astrophys J Lett* 794:L5.

Kasper, M.E., Beuzit, J.-L., Verinaud, C., Yaitskova, N., Baudoz, P., Boccaletti, A., Gratton, R.G., Hubin, N., Kerber, F., Roelfsema, R., Schmid, H.M., Thatte, N.A., Dohlen, K., Feldt, M., Venema, L., and Wolf, S. (2008) EPICS: the exoplanet imager for the E-ELT. In *Adaptive Optics Systems*, edited by N. Hubin, C.E. Max, and P.L. Wizinowich. Proceedings of the SPIE, Volume 7015, Article Id. 70151S, 12 pp. p. 70151S. DOI:10.1117/12.789047

Kasting, J.F. (1997) Habitable zones around low mass stars and the search for extraterrestrial life. *Orig Life Evol Biosphere* 27:291–3107.

Kasting, J.F. (2001) Earth history: the rise of atmospheric oxygen. *Science* 293:819–820.

Kasting, J.F. (2013) What caused the rise of atmospheric O2? *Chem Geol* v362:13–25.

Kasting, J.F. and Canfield, D.E. (2012) The global oxygen cycle. *Fundam Geobiol* 93–104.

Kasting, J.F. and Donahue, T.M. (1980) The evolution of atmospheric ozone. *J Geophys Res* 85:3255–3263.

Kasting, J.F., Whitmire, D.P., and Reynolds, R.T. (1993) Habitable zones around main sequence stars. *Icarus* 101:108–128.

Kasting, J.F., Kopparapu, R., Ramirez, R.M., and Harman, C.E. (2013) Remote life-detection criteria, habitable zone boundaries, and the frequency of Earth-like planets around M and late K stars. *Proc Natl Acad Sci U S A* 111:1–6.

Kawahara, H. and Fujii, Y. (2010) Global mapping of Earth-like exoplanets from scattered light curves. *Astrophys J* 720: 1333.

Keeling, C.D. (1960) The concentration and isotopic abundances of carbon dioxide in the atmosphere. *Tellus* 12:200–203.

Keeling, C.D., Bacastow, R.B., Bainbridge, A.E., Ekdahl, Jr., C.A., Guenther, P.R., Waterman, L.S., and Chin, J.F.S. (1976) Atmospheric carbon dioxide variations at Mauna Loa Observatory, Hawaii. *Tellus A* 28:538–551.

Kendall, B., Reinhard, C.T., Lyons, T.W., Kaufman, A.J., Poulton, S.W., and Anbar, A.D. (2010) Pervasive oxygenation along late Archaean ocean margins. *Nat Geosci* 3:647–652.

Kiang, N.Y., Segura, A., Tinetti, G., Govindjee, Blankenship, R.E., Cohen, M., Siefert, J., Crisp, D., and Meadows, V.S. (2007a). Spectral signatures of photosynthesis. II. Coevolution with other stars and the atmosphere on extrasolar worlds. *Astrobiology* 7:252–274.

Kiang, N.Y., Siefert, J., Govindjee, Blankenship, R.E. (2007b). Spectral signatures of photosynthesis. I. Review of earth organisms. *Astrobiology* 7:222–251.

Knoll, A.H., Javaux, E.J., Hewitt, D., and Cohen, P. (2006) Eukaryotic organisms in Proterozoic oceans. *Philos Trans R Soc B Biol Sci* 361:1023–1038.

Kopparapu, R.K., Ramirez, R., Kasting, J.F., Eymet, V., Robinson, T.D., Mahadevan, S., Terrien, R.C., Domagal-Goldman, S., Meadows, V., and Deshpande, R. (2013) Habitable zones around main-sequence stars: new estimates. *Astrophys J* 765(2):131.

Kopparapu, R.K., Ramirez, R.M., SchottelKotte, J., Kasting, J.F., Domagal-Goldman, S., and Eymet, V. (2014) Habitable zones around main-sequence stars: dependence on planetary mass. *Astrophys J Lett* 787:L29.

Kreidberg, L. and Loeb, A. (2016) Prospects for characterizing the atmosphere of Proxima Centauri b. *Astrophys J Lett* 832: L12.

Kreidberg, L., Bean, J.L., Désert, J.M., Benneke, B., Deming, D., Stevenson, K.B., Seager, S., Berta-Thompson, Z., Seifahrt, A., and Homeier, D. (2014) Clouds in the atmosphere of the super-Earth exoplanet GJ 1214b. *Nature* 505:69–72.

Krissansen-Totton, J., Buick, R., and Catling, D.C. (2015) A statistical analysis of the carbon isotope record from the Archean to Phanerozoic and implications for the rise of oxygen. *Am J Sci* 315:275–316.

Krissansen-Totton, J., Bergsman, D., and Catling, D.C. (2016a) On detecting biospheres from chemical thermodynamic disequilibrium in planetary atmospheres. *Astrobiology* 16:39–67.

Krissansen-Totton, J., Schwieterman, E.W., Charnay, B., Arney, G., Robinson, T.D., Meadows, V., and Catling, D.C. (2016b) Is the pale blue dot unique? Optimized photometric bands for identifying earth-like exoplanets. *ApJ* 817:31.

Kump, L.R. and Barley, M.E. (2007) Increased subaerial volcanism and the rise of atmospheric oxygen 2.5 billion years ago. *Nature* 448:1033–1036.

Lafferty, W.J., Solodov, A.M., Weber, A., Olson, W.B., and Hartmann, J.M. (1996) Infrared collision-induced absorption by N(2) near 4.3 μm for atmospheric applications: measurements and empirical modeling. *Appl Opt* 35:5911–5917.

Lederberg, J. (1965) Signs of life: criterion-system of exobiology. *Nature* 207:9–13.

Lee, C.T., Yeung, L.Y., McKenzie, N.R., Yokoyama, Y., Ozaki, K., and Lenardic, A. (2016) Two-step rise of atmospheric oxygen linked to the growth of continents. *Nat Geosci* 9:417–424.

Léger, A., Fontecave, M., Labeyrie, A., Samuel, B., Demangeon, O., and Valencia, D. (2011) Is the presence of oxygen on an exoplanet a reliable biosignature? *Astrobiology* 11:335–341.

Lepland, A., Arrhenius, G., and Cornell, D. (2002) Apatite in early Archean Isua supracrustal rocks, southern West Greenland: its origin, association with graphite and potential as a biomarker. *Precambrian Res* 118:221–241.

Line, M.R., Knutson, H., Wolf, A.S., and Yung, Y.L. (2014) A systematic retrieval analysis of secondary eclipse spectra. II. A uniform analysis of nine planets and their C to O Ratios. *Astrophys J* 783:70.

Line, M.R. and Parmentier, V. (2016) The influence of nonuniform cloud cover on transit transmission spectra. *Astrophys J* 820:78.

Lissauer, J.J. (2007) Planets formed in habitable zones of M dwarf stars probably are deficient in volatiles. *ApJ* 660:L149–L152.

Livengood, T.A., Deming, L.D., A'Hearn, M.F., Charbonneau, D., Hewagama, T., Lisse, C.M., McFadden, L.A., Meadows, V.S., Robinson, T.D., Seager, S., and Wellnitz, D.D. (2011) Properties of an Earth-like planet orbiting a Sun-like star: earth observed by the EPOXI mission. *Astrobiology* 11:907–930.

Lovelock, J.E. (1965) A physical basis for life detection experiments. *Nature* 207:568–570.

Lovelock, J.E. and Kaplan, I.R. (1975) Thermodynamics and the recognition of alien biospheres [and Discussion]. *Proc R Soc B Biol Sci* 189:167–181.

Lovis, C., Snellen, I., Mouillet, D., Pepe, F., Wildi, F., Astudillo-Defru, N., Beuzit, J.L., Bonfils, X., Cheetham, A., Conod, U., and Delfosse, X. (2017) Atmospheric characterization of Proxima b by coupling the SPHERE high-contrast imager to the ESPRESSO spectrograph. *A&A* 599:A16.

Luger, R. and Barnes, R. (2015) Extreme water loss and abiotic O2 buildup on planets throughout the habitable zones of M dwarfs. *Astrobiology* 15:119–143.

Luger, R., Lustig-Yaeger, J., Fleming, D.P., Tilley, M.A., Agol, E., Meadows, V.S., Deitrick, R., and Barnes, R. (2017) The pale green dot: a method to characterize Proxima Centauri b using Exo-Aurorae. *Astrophys J* 837:63.

Luo, G., Ono, S., Beukes, N.J., Wang, D.T., Xie, S., and Summons, R.E. (2016) Rapid oxygenation of Earths atmosphere 2.33 billion years ago. *Science Adv* 2:e1600134.

Lustig-Yaeger, J., Tovar, G., Schwieterman, E.W., Fujii, Y., and Meadows, V.S., Meadows (2017) Detecting oceans on exoplanets using phase-dependent mapping with next generation coronagraph-equipped telescopes, Habitable Worlds 2017, LPI Contribution No. 2042. Available online at www.hou.usra.edu/meetings/habitableworlds2017/pdf/4110.pdf

Lyons, T.W., Reinhard, C.T., and Planavsky, N.J. (2014) The rise of oxygen in Earth's early ocean and atmosphere. *Nature* 506:307–315.

Madhusudhan, N. and Seager, S. (2009) A temperature and abundance retrieval method for exoplanet atmospheres. *Astrophys J* 707:24.

Maté, B., Lugez, C., Fraser, G.T., and Lafferty, W.J. (1999) Absolute intensities for the O2 1.27 continuum absorption. *J Geophys Res* 104:585–590.

Maté, B., Lugez, C.L., Solodov, A.M., Fraser, G.T., and Lafferty, W.J. (2000) Investigation of the collision-induced absorption by O_2 near 6.4 μm in pure O_2 and O_2/N_2 mixtures. *J Geophys Res* 105:222–225, 230.

McCollom, T.M. and Seewald, J.S. (2006) Carbon isotope composition of organic compounds produced by abiotic synthesis under hydrothermal conditions. *Earth Planet Sci Lett* 243:74–84.

Meadows, V.S. (2008) Planetary environmental signatures of habitability and life. In: *Exoplanets: Detection, Formation, Properties, Habitability*, edited by J. Mason. Springer Praxis Books. ISBN 978-3-540-74007-0. Chichester, UK: Praxis Publishing Ltd, p 259.

Meadows, V.S. (2017) Reflections on O_2 as a biosignature in exoplanetary atmospheres. *Astrobiology* 17:1022–1052.

Meadows, V.S., Arney, G.N., Schwieterman, E.W., Lustig-Yaeger, J., Lincowski, A.P., Robinson, T., Domagal-Goldman, S.D., Barnes, R.K., Fleming, D.P., Deitrick, R., Luger, R., Driscoll, P.E., Quinn, T.R., and Crisp, D. (2018) The habitability of Proxima Centauri b: environmental states and observational discriminants. *Astrobiology* 18:133–189.

Mennesson, B., Gaudi, S., Seager, S., Cahoy, K., Domagal-Goldman, S., Feinberg, L., Guyon, O., Kasdin, J., Marois, C., Mawet, D., Tamura, M., Mouillet, D., Prusti, T., Quirrenbach, A., Robinson, T., Rogers, L., Scowen, P., Somerville, R., Stapelfeldt, K., Stern, D., Still, M., Turnbull, M., Booth, J., Kiessling, A., Kuan, G., and Warfield, K. (2016) The Habitable Exoplanet (HabEx) Imaging Mission: preliminary science drivers and technical requirements. In *Proc. SPIE 9904, Space Telescopes and Instrumentation 2016: Optical, Infrared, and Millimeter Wave*, edited by H.A. MacEwen, G.G. Fazio, M. Lystrup, N. Batalha, N. Siegler, and E.C. Tong. International Society for Optics and Photonics, p 99040L. DOI:10.1117/12.2240457

Misra, A.K. and Meadows, V.S. (2014). Discriminating between cloudy, hazy, and clear sky exoplanets using refraction. *Astrophys J Lett* 795:L14.

Misra, A., Meadows, V., Claire, M., and Crisp, D. (2014a). Using dimers to measure biosignatures and atmospheric pressure for terrestrial exoplanets. *Astrobiology* 14:67–86.

Misra, A., Meadows, V., and Crisp, D. (2014b). The Effects of refraction on transit transmission spectroscopy: application to Earth-like exoplanets. *ApJ* 792:61–72.

Misra, A., Krissansen-Totton, J., Koehler, M.C., and Sholes, S. (2015) Transient sulfate aerosols as a signature of exoplanet volcanism. *Astrobiology* 15:462–477.

Mojzsis, S.J., Arrhenius, G., McKeegan, K.D., Harrison, T.M., Nutman, A.P., and Friend, C.R.L. (1996) Evidence for life on Earth before 3,800 million years ago. *Nature* 384:55.

Morley, C.V., Fortney, J.J., Marley, M.S., Zahnle, K., Line, M., Kempton, E., Lewis, N., and Cahoy, K. (2015) Thermal emission and reflected light spectra of super Earths with flat transmission spectra. *Astrophys J* 815:110.

Murata, N., Takahashi, S., Nishiyama, Y., and Allakhverdiev, S.I. (2007) Photoinhibition of photosystem II under environmental stress. *Biochim Biophys Acta* 1767:414–421.

Narita, N., Enomoto, T., Masaoka, S., and Kusakabe, N. (2015) Titania may produce abiotic oxygen atmospheres on habitable exoplanets. *Sci Rep* 5:13977.

Nutman, A.P., Bennett, V.C., Friend, C.R., Van Kranendonk, M.J., and Chivas, A.R. (2016) Rapid emergence of life shown by discovery of 3,700-million-year-old microbial structures. *Nature* 537:535–538.

Olson, J.M. (1970) The evolution of photosynthesis. *Science (New York, NY)* 168:438.

Olson, J.M. (1978) Precambrian evolution of photosynthetic and respiratory organisms. In *Evolutionary Biology,* Springer, Boston, pp 1–37.

Olson, J.M. (1980) Chlorophyll organization in green photosynthetic bacteria. *Biochim Biophys Acta* 594:33–51.

Olson, J.M. (2006) Photosynthesis in the Archean era. *Photosynth Res* 88:109–117.

Olson, J.M. and Pierson, B.K. (1986) Origin and evolution of photosynthetic reaction centers. *Orig Life Evol Biosph* 16: 361–362.

Olson, S.L., Reinhard, C.T., and Lyons, T.W. (2016) Limited role for methane in the mid-Proterozoic greenhouse. *PNAS* 113:11447–11452.

Pallé, E., Osorio, M.R.Z., Barrena, R., Montañés-Rodríguez, P., and Martín, E.L. (2009) Earth's transmission spectrum from lunar eclipse observations. *Nature* 459:814–816.

Pavlov, A.A., Hurtgen, M.T., Kasting, J.F., and Arthur, M.A. (2003) Methane-rich Proterozoic atmosphere?. *Geology* 31:87–90.

Pavlov, A.A. and Kasting, J.F. (2002) Mass-independent fractionation of sulfur isotopes in Archean sediments: strong evidence for an anoxic Archean atmosphere. *Astrobiology* 2: 27–41.

Pierson, B.K. and Olson, J.M. (1989) Evolution of photosynthesis in anoxygenic photosynthetic procaryotes. In *Microbial Mats, Physiological Ecology of Benthic Communities,* edited by Y. Cohen and E. Rosenberg, American Society of Microbiology, Washington, DC, pp 402–427.

Pierson, B.K., Mitchell, H.K., and Ruff-Roberts, A.L. (1993) Chloroflexus aurantiacus and ultraviolet radiation: implica-

tions for archean shallow-water stromatolites. *Orig Life Evol Biosph* 23:243–260.

Pilcher, C.B. (2003) Biosignatures of early earths. *Astrobiology* 3:471–486.

Planavsky, N.J., Asael, D., Hofmann, A., Reinhard, C.T., Lalonde, S.V, Knudsen, A., Wang, X., Ossa Ossa, F., Pecoits, E., Smith, A.J.B., Beukes, N.J., Bekker, A., Johnson, T.M., Konhauser, K.O., Lyons, T.W., and Rouxel, O.J. (2014a). Evidence for oxygenic photosynthesis half a billion years before the Great Oxidation Event. *Nat Geosci* 7:283–286.

Planavsky, N.J., Reinhard, C.T., Wang, X., Thomson, D., Mcgoldrick, P., Rainbird, R.H., Johnson, T., Fischer, W.W., and Lyons, T.W. (2014b). Low mid-proterozoic atmospheric oxygen levels and the delayed rise of animals. *Science* 346:635–638.

Postman, M., Brown, T., Sembach, K., Giavalisco, M., Traub, W., Stapelfeldt, K., Calzetti, D., Oegerle, W., Rich, R.M., Stahl, H.P., Tumlinson, J., Mountain, M., Soummer, R., and Hyde, T. (2010) Science drivers and requirements for an Advanced Technology Large Aperture Space Telescope (ATLAST): implications for technology development and synergies with other future facilities. *SPIE* 7731:12.

Quanz, S.P., Crossfield, I., Meyer, M.R., Schmalzl, E., and Held, J. (2015) Direct detection of exoplanets in the 3–10 μm range with E-ELT/METIS. *Int J Astrobiol* 14:279–289.

Ratner, M.I. and Walker, J.C.G. (1972) Atmospheric ozone and the history of life. *J Atmos Sci* 29:803–808.

Rauer, H., Catala, C., Aerts, C., Appourchaux, T., Benz, W., Brandeker, A., Christensen-Dalsgaard, J., Deleuil, M., Gizon, L., Goupil, M.J., and Güdel, M. (2014) The PLATO 2.0 mission. *Exp Astron* 38:249–330.

Rauer, H., Gebauer, S.V., Paris, P.V., Cabrera, J., Godolt, M., Grenfell, J.L., Belu, A., Selsis, F., Hedelt, P., and Schreier, F. (2011) Potential biosignatures in super-Earth atmospheres-I. Spectral appearance of super-Earths around M dwarfs. *A&A* 529:A8.

Rauscher, B.J., Bolcar, M.R., Clampin, M., Domagal-Goldman, S.D., McElwain, M.W., Moseley, S.H., Stahle, C., Stark, C.C., and Thronson, H.A. (2015) ATLAST detector needs for direct spectroscopic biosignature characterization in the visible and near-IR. SPIE 9602–9612. ArXiv: 1508.06661.

Raymond, S.N., Scalo, J., and Meadows, V.S. (2007) A decreased probability of habitable planet formation around low-mass stars. *Astrophys J* 669:606; arXiv:0707.1711v1.

Reinhard, C.T., Olson, S.L., Schwieterman, E.W., and Lyons, T.W. (2017) False negatives for remote life detection on ocean-bearing planets: lessons from the early Earth. *Astrobiology* 17:287–297.

Reinhard, C.T., Planavsky, N.J., Olson, S.L., Lyons, T.W., and Erwin, D.H. (2016) Earth's oxygen cycle and the evolution of animal life. *PNAS* 113:8933–8938.

Ribas, I., Bolmont, E., Selsis, F., Reiners, A., Leconte, J., Raymond, S.N., Engle, S.G., Guinan, E.F., Morin, J., Turbet, M., Forget, F., and Anglada-Escude, G. (2016) The habitability of Proxima Centauri b. I. Irradiation, rotation and volatile inventory from formation to the present. *A&A* 596: A111.

Richard, C., Gordon, I.E., Rothman, L.S., Abel, M., Frommhold, L., Gustafsson, M., Hartmann, J.M., Hermans, C., Lafferty, W.J., Orton, G.S., Smith, K.M., and Tran, H. (2012) New section of the HITRAN database: collision-induced absorption (CIA). *JQSRT* 113:1276–1285.

Ricker, G.R., Winn, J.N., Vanderspek, R., Latham, D.W., Bakos, G.Á., Bean, J.L., Berta-Thompson, Z.K., Brown, T.M., Buchhave, L., Butler, N.R. and Butler, R.P. (2015) Transiting exoplanet survey satellite. *J Astron Telesc Instrum Syst* 1, 014003.

Riding, R., Fralick, P., and Liang, L. (2014) Identification of an Archean marine oxygen oasis. *Precambrian Res* 251:232–237.

Roberson, A.L., Roadt, J., Halevy, I., and Kasting, J.F. (2011) Greenhouse warming by nitrous oxide and methane in the Proterozoic Eon. *Geobiology* 9:313–320.

Robinson, T.D., Ennico, K., Meadows, V.S., Sparks, W., Bussey, D.B.J., Schwieterman, E.W., and Breiner, J. (2014) Detection of ocean glint and ozone absorption using LCROSS Earth observations. *Astrophys J* 787:171.

Robinson, T.D., Meadows, V.S., and Crisp, D. (2010) Detecting oceans on extrasolar planets using the glint effect. *ApJ* 721: L67–L71.

Robinson, T.D., Stapelfeldt, K.R., and Marley, M.S. (2016) Characterizing rocky and gaseous exoplanets with 2 m class space-based coronagraphs. *Publ Astron Soc Pac* 128:025003.

Rodler, F. and López-Morales, M. (2014) Feasibility studies for the detection of O2 in an Earth-like exoplanet. *Astrophys J* 781:54.

Rogers, L.A. (2015) Most 1.6 Earth-radius planets are not rocky. *Astrophys J* 801:41.

Rosenqvist, J. and Chassefière, E. (1995) Inorganic chemistry of O_2 in a dense primitive atmosphere. *P&SS* 43:3–10.

Rosing, MT. (1999) ^{13}C-depleted carbon microparticles in >3700-Ma sea-floor sedimentary rocks from West Greenland. *Science* 283:674–676.

Rosing, M.T. and Frei, R. (2004) U-rich Archaean sea-floor sediments from Greenland–indications of >3700 Ma oxygenic photosynthesis. *Earth Planet Sci Lett* 217:237–244.

Rothman, L.S., Gordon, I.E., Babikov, Y., Barbe, A., Chris Benner, D., Bernath, P.F., Birk, M., Bizzocchi, L., Boudon, V., Brown, L.R., Campargue, A., Chance, K., Cohen, E.A., Coudert, L.H., Devi, V.M., Drouin, B.J., Fayt, A., Flaud, J.-M., Gamache, R.R., Harrison, J.J., Hartmann, J.-M., Hill, C., Hodges, J.T., Jacquemart, D., Jolly, A., Lamouroux, J., Le Roy, R.J., Li, G., Long, D.A., Lyulin, O.M., Mackie, C.J., Massie, S.T., Mikhailenko, S., Müller, H.S.P., Naumenko, O.V., Nikitin, A.V., Orphal, J., Perevalov, V., Perrin, A., Polovtseva, E.R., Richard, C., Smith, M.A.H., Starikova, E., Sung, K., Tashkun, S., Tennyson, J., Toon, G.C., Tyuterev, V.G., and Wagner, G. (2013) The HITRAN2012 molecular spectroscopic database. *JQSRT* 130: 4–50.

Rugheimer, S., Kaltenegger, L., Zsom, A., Segura, A., and Sasselov, D. (2013) Spectral fingerprints of Earth-like planets around FGK stars. *Astrobiology* 13:251–269.

Rugheimer, S., Kaltenegger, L., Segura, A., Linsky, J., and Mohanty, S. (2015) Effect of UV radiation on the spectral fingerprints of earth-like planets orbiting M stars. *ApJ* 809:57.

Schaefer, L., Wordsworth, R., Berta-Thompson, Z., Sasselov, D., Blamey, N.J.F., Brand, U., Parnell, J., Spear, N., Lécuyer, C., and Benison, K. (2016) Predictions of the atmospheric composition of GJ 1132b 651–654. DOI:10.1130/G37937.1

Schindler, T.L. and Kasting, J.F. (2000) Synthetic spectra of simulated terrestrial atmospheres containing possible biomarker gases. *Icarus* 145:262–271.

Schwieterman, E.W., Cockell, C.S., and Meadows, V.S. (2015a). Nonphotosynthetic pigments as potential biosignatures. *Astrobiology* 15:341–361.

Schwieterman, E.W., Robinson, T.D., Meadows, V.S., Misra, A., and Domagal-Goldman, S. (2015b). Detecting and constraining

N2 abundances in planetary atmospheres using collisional pairs. *ApJ* 810:57.

Schwieterman, E.W., Meadows, V.S., Domagal-Goldman, S.D., Deming, D., Arney, G.N., Luger, R., Harman, C.E., Misra, A., and Barnes, R. (2016) Identifying planetary biosignature impostors: spectral features of CO And O4 resulting from abiotic O_2/O_3 production. *ApJ* 819:L13.

Schwieterman, E.W., Kiang, N.Y., Parenteau, M.N., Harman, C.E., DasSarma, S., Fisher, T.M., Arney, G.N., Hartnett, H.E., Reinhard, C.T., Olson, S.L., Meadows, V.S., Cockell, C.S., Walker, S.I., Grenfell, J.L., Hegde, S., Rugheimer, S., Hu, R., and Lyons, T.W. (2018). Exoplanet biosignatures: a review of remotely detectable signs of life. *Astrobiology* 18:663–708.

Seager, S. and Bains, W. (2015) The search for signs of life on exoplanets at the interface of chemistry and planetary science. *Sci Adv* 1:e1500047.

Seager, S., Schrenk, M., and Bains, W. (2012) An astrophysical view of Earth-based metabolic biosignature gases. *Astrobiology* 12:61–82.

Seager, S., Cash, W., Domagal-Goldman, S., Kasdin, N.J., Kuchner, M., Roberge, A., Shaklan, S., Sparks, W., Thomson, M., Turnbull, M., and Warfield, K. (2015) Exo-S: starshade probe-class exoplanet direct imaging mission concept Final Report. Available online at exep.jpl.nasa.gov/stdt

Segura, A., Krelove, K., Kasting, J.F., Sommerlatt, D., Meadows, V., Crisp, D., Cohen, M., and Mlawer, E. (2003) Ozone concentrations and ultraviolet fluxes on Earth-like planets around other stars. *Astrobiology* 3:689–708.

Segura, A., Kasting, J.F., Meadows, V., Cohen, M., Scalo, J., Crisp, D., Butler, R.A.H., and Tinetti, G. (2005) Biosignatures from Earth-like planets around M dwarfs. *Astrobiology* 5:706–725.

Segura, A., Walkowicz, L.M., Meadows, V., Kasting, J., and Hawley, S. (2010) The effect of a strong stellar flare on the atmospheric chemistry of an earth-like planet orbiting an M dwarf. *Astrobiology* 10:751–771.

Selsis, F., Despois, D., and Parisot, J.P. (2002) Signature of life on exoplanets: can Darwin produce false positive detections?. *A&A* 388:985–1003.

Senge, M.O. and Smith, K.M. (1995) Biosynthesis and structure of the bacteriochlorophylls. In *Anoxygenic Photosynthetic Bacteria*, edited by R.E. Blankenship, M.T. Madigan, and C.E. Bauer. Springer, Netherlands, pp 137–151.

Shapiro, M.M. and Gush, H.P. (1966) The collision-induced fundamental and first overtone bands of oxygen and nitrogen. *Can J Phys* 44:949–963.

Sheldon, N.D. (2006) Precambrian paleosols and atmospheric CO_2 levels. *Precambrian Res* 147:148–155.

Shen, Y., Buick, R., and Canfield, D.E. (2001) Isotopic evidence for microbial sulphate reduction in the early Archaean era. *Nature* 410:77–81.

Sleep, N.H. (2010) The Hadean-Archaean environment. *Cold Spring Harb Perspect Biol* 2:a002527.

Snellen, I.A.G., de Kok, R., Birkby, J.L., Brandl, B., Brogi, M., Keller, C.U., Kenworthy, M., Schwarz, H., and Stuik, R. (2015) Combining high-dispersion spectroscopy with high contrast imaging: probing rocky planets around our nearest neighbors. *A&A* 576:A59.

Snellen, I.A.G., de Kok, R.J., Le Poole, R., Brogi, M., and Birkby, J. (2013) Finding extraterrestrial life using ground-based high-dispersion spectroscopy. *Astrophys J* 764:182.

Soo, R.M., Hemp, J., Parks, D.H., Fischer, W.W., and Hugenholtz, P. (2017) On the origins of oxygenic photosynthesis and aerobic respiration in Cyanobacteria. *Science* 355:1436–1440.

Sozzetti, A. (2014) Exoplanets with Gaia: synergies in the Making. *Eur Astron Soc Publ Ser* 68:93–99.

Stapelfeldt, K.R., Belikov, R., Bryden, G., Cahoy, K., Chakrabarti, S., Marley, M. McElwain, M., Meadows, V., Serabyn, E., Trauger, J., Dekens, F., Brenner, M., Brugarolas, P. Dubovitsky, S., Effinger, R., Heeg, C., Hirsch, B., Kissel, A., Krist, J., Lange, J., Nissen, J., Oseas, J., Pong, C., Rubio, M., Sunada, E., Warfield, K., Domagal-Goldman, S., Kuchner, M., Lawson, P., Morley, C., Menati, B., Roberge, A., Robinson, T., Sandhu, J., Seager, S., and Unwin, S. (2015) Exo-C Mission Study Final Report, NASA Exoplanet Exploration Program internal document, available at https://exoplanets.nasa.gov/exep/stdt/Exo-C_Final_Report_for_Unlimited_Release_150323.pdf

Stephan, K., Jaumann, R., Brown, R.H., Soderblom, J.M., Soderblom, L.A., Barnes, J.W., Sotin, C., Griffith, C.A., Kirk, R.L., Baines, K.H., and Buratti, B.J. (2010) Specular reflection on Titan: liquids in Kraken Mare. *Geophys Res Lett* 37: L07104.

Stock, J.W., Blaszczak-Boxe, C.S., Lehmann, R., Grenfell, J.L., Patzer, A.B.C., Rauer, H., and Yung, Y.L. (2017) A detailed pathway analysis of the chemical reaction system generating the Martian vertical ozone profile. *Icarus* 291: 192–202.

Sullivan, P.W., Winn, J.N., Berta-Thompson, Z.K., Charbonneau, D., Deming, D., Dressing, C.D., Latham, D.W., Levine, A.M., McCullough, P.R., Morton, T., and Ricker, G.R. (2015) The Transiting Exoplanet Survey Satellite: simulations of planet detections and astrophysical false positives. *Astrophys J* 809:77.

Szentgyorgyi, A., Baldwin, D., Barnes, S., Bean, J., Ben-Ami, S., Brennan, P., Budynkiewicz, J., Chun, M.Y., Conroy, C., Crane, J.D., Epps, H., Evans, I., Evans, J., Foster, J., Frebel, A., Gauron, T., Guzmán, D., Hare, T., Jang, B.H., Jang, J.G., Jordan, A., Kim, J., Kim, K.M., de Oliveira, C.M., Lopez-Morales, M., McCracken, K., McMuldroch, S., Miller, J., Mueller, M., Oh, J.S., Onyuksel, C., Ordway, M., Park, B.G., Park, C., Park, S.J., Paxson, C., Phillips, D., Plummer, D., Podgorski, W., Seifahrt, A., Stark, D., Steiner, J., Uomoto, A., Walsworth, R., and Yu, Y.S. (2016) The GMT-Consortium Large Earth Finder (G-CLEF): an optical Echelle spectrograph for the Giant Magellan Telescope (GMT). In *Ground-Based and Airborne Instrumentation for Astronomy VI*. Proc. SPIE 990822.

Tang, D., Shi, X., Wang, X., and Jiang, G. (2016) Extremely low oxygen concentration in mid-Proterozoic shallow seawaters. *Precambrian Res* 276:145–157.

Tian, F. (2015) History of water loss and atmospheric O_2 buildup on rocky exoplanets near M dwarfs. *Earth Planet Sci Lett* 432:126–132.

Tian, F., France, K., Linsky, J.L., Mauas, P.J.D., and Vieytes, M.C. (2014) High stellar FUV/NUV ratio and oxygen contents in the atmospheres of potentially habitable planets. *Earth Planet Sci Lett* 385:22–27.

Tinetti, G., Meadows, V.S., Crisp, D., Kiang, N.Y., Kahn, B.H., Bosc, E., Fishbein, E., Velusamy, T., and Turnbull, M. (2006) Detectability of planetary characteristics in disk-averaged spectra II: synthetic spectra and light-curves of earth. *Astrobiology* 6:881–900.

Thalman, R. and Volkamer, R. (2013) Temperature dependent absorption cross-sections of O_2-O_2 collision pairs between 340 and 630 nm and at atmospherically relevant pressure. *Phys chem chem phys* 15:15371–15381.

Trouwborst, R.E., Johnston, A., Koch, G., Luther, III G.W., and Pierson, B.K. (2007) Fe(II) oxidation mediated by photo-

synthetic activity of Yellowstone hot spring microbial mats: model for Precambrian Fe(II) oxidation. *Geochim Cosmochim Acta* 71:4629–4643.

Turbet, M., Leconte, J., Selsis, F., Bolmont, E., Forget, F., Ribas, I., Raymond, S.N., and Anglada-Escudé, G. (2016) The habitability of Proxima Centauri b-II. Possible climates and observability. *A&A* 596:A112.

Ueno, Y., Yamada, K., Yoshida, N., Maruyama, S., and Isozaki, Y. (2006) Evidence from fluid inclusions for microbial methanogenesis in the early Archaean era. *Nature* 440:516–519.

Ueno, Y., Johnson, M.S., Danielache, S.O., Eskebjerg, C., Pandey, A., and Yoshida, N. (2009) Geological sulfur isotopes indicate elevated OCS in the Archean atmosphere, solving faint young sun paradox. Proc Natl Acad Sci U S A 106:14784–14789.

Unterborn, C.T. and Panero, W.R. (2017) The effects of Mg/Si on the exoplanetary refractory oxygen budget. *Astrophys J* 845:61.

Van Zuilen, M.A., Lepland, A., and Arrhenius, G. (2002) Reassessing the evidence for the earliest traces of life. *Nature* 418:627–630.

von Paris, P., Grenfell, J.L., Rauer, H., and Stock, J.W. (2013a). N_2-associated surface warming on early Mars. *Planet Space Sci* 82:149–154.

von Paris, P., Hedelt, P., Selsis, F., Schreier, F., and Trautmann, T. (2013b). Characterization of potentially habitable planets: retrieval of atmospheric and planetary properties from emission spectra. *A&A* 551:A120.

Waldmann, I.P., Tinetti, G., Rocchetto, M., Barton, E.J., Yurchenko, S.N., and Tennyson, J. (2015) Tau-REx I: a next generation retrieval code for exoplanetary atmospheres. *Astrophys J* 802:107.

Walker, J.C.G. (1977) *Evolution of the Atmosphere*. Macmillan, New York.

Walker, J.C.G., Hays, P.B., and Kasting, J.F. (1981) A negative feedback mechanism for the long-term stabilization of Earth's surface temperature. *J Geophys Res* 86:9776–9782.

Walker, S.I., Bains, W., Cronin, L., DasSarma, S., Danielache, S., Domagal-Goldman, S., Kacar, B., Kiang, N.Y., Lenardic, A., Reinhard, C.T., Moore, W., Schwieterman, E.W., Shkolnik, E.L., and Smith, H.B. (2018) Exoplanet biosignatures: future directions. *Astrobiology* 18:779–824.

Weiss, L.M. and Marcy, G.W. (2014) The mass-radius relation for 65 exoplanets smaller than 4 Earth radii. *Astrophys J Lett* 783:L6.

Westall, F., Cavalazzi, B., Lemelle, L., Marrocchi, Y., Rouzaud, J.N., Simionovici, A., Salomé, M., Mostefaoui, S., Andreazza, C., Foucher, F., and Toporski, J. (2011) Implications of in situ calcification for photosynthesis in a ~3.3 Ga-old microbial biofilm from the Barberton greenstone belt, South Africa. *Earth Planet Sci Lett* 310:468–479.

Winn, J.N. (2010) Exoplanet transits and occultations. *Exoplanets* 1:55–77.

Wordsworth, R.D. (2016) Atmospheric nitrogen evolution on Earth and Venus. *Earth Planet Sci Lett* 447:103–111.

Wordsworth, R. and Pierrehumbert, R. (2014) Abiotic oxygen-dominated atmospheres on terrestrial habitable zone planets. *ApJ* 785:L20.

Young, P.A., Desch, S.J., Anbar, A.D., Barnes, R., Hinkel, N.R., Kopparapu, R., Madhusudhan, N., Monga, N., Pagano, M.D., Riner, M.A., and Scannapieco, E. (2014) Astrobiological stoichiometry. *Astrobiology* 14:603–626.

Yung, Y.L. and DeMore, W.B. (1999) *Photochemistry of Planetary Atmospheres*. New York: Oxford University Press.

Zahnle, K., Claire, M., and Catling, D. (2006) The loss of mass-independent fractionation in sulfur due to a Palaeoproterozoic collapse of atmospheric methane. *Geobiology* 4:271–283.

Address correspondence to:
Victoria S. Meadows
Department of Astronomy
University of Washington
PO Box 351580
Seattle, WA 98195

E-mail: vsm@astro.washington.edu

Submitted 12 December 2017
Accepted 15 December 2017

Abbreviations Used

ELTs = extremely large telescopes
HabEx = Habitable Exoplanet Imaging Mission
IWA = inner-working angles
JWST = James Webb Space Telescope
LUVOIR = Large UltraViolet Optical Infrared Surveyor
MIR = mid-infrared
NIR = near-infrared
OWAs = outer-working angles
PAL = present atmospheric level
PSI = photosystem I
PSII = photosystem II
RV = radial velocity
S/N = signal-to-noise
WFIRST = Wide Field Infrared Survey Telescope